NTNU

Norwegian University of
Science and Technology

Kinetic Modelling of Dynamic Contrast-Enhanced MR Images: Impact of the Arterial Input Function

Tina Sandø Evensen

Master of Science in Physics and Mathematics
Submission date: June 2018
Supervisor: Kathrine Røe Redalen, IFY

Norwegian University of Science and Technology
Department of Physics

Preface

This report is my master thesis, written as a conclusion to the study programme Biophysics and Medical Technology at the Norwegian University of Science and Technology. The majority of the work has been performed during the spring of 2018, and is based on a specialisation project carried out during the autumn of 2017.

The study was performed on image data acquired during the period 2014 to 2017 by the Oxytarget study, which aims to uncover how to use functional MRI to better detect tumour aggressiveness in rectal cancer patients in order to better adapt treatment.

I would like to thank my supervisor Kathrine Røe Redalen, for valuable guidance, advice and encouragement throughout the semester. I would also like to thank Kine Mari Bakke, for contributing a script for sorting MR image data, which was of great help in getting started on the project. Finally, I would like to thank Endre Sandø Evensen, for his encouragement throughout the semester, and for proof-reading this thesis.

Tina Sandø Evensen
June 2018, Trondheim

Abstract

The standard treatment of rectal cancer is surgery, and in locally advanced cases, neoadjuvant chemoradiotherapy (CRT). By obtaining knowledge about the aggressiveness of tumours prior to treatment, the treatment can be adapted individually, which may contribute to an improved quality of life and survival for the patients. In this thesis, the potential of using parametric models in dynamic contrast enhanced (DCE) magnetic resonance imaging (MRI) for this purpose has been explored.

DCE-MRI data of 91 rectal cancer patients were analysed in Matlab using two parametric analysis models: the Tofts and Kermode (TK) model and the Brix model. In order to explore the potential of the models for assessing treatment response and aggressiveness, and determine the significance of the arterial input function (AIF), both a population-based AIF and individual AIFs were applied to the TK model, and compared to the (AIF-independent) Brix model. The TK model parameters K^{trans} (min^{-1}), v_e (%), v_p (%), and k_{ep} (min^{-1}), and the Brix model parameters A_{Brix}, k_{el} (min^{-1}) and k_{ep} (min^{-1}) were estimated within the tumour volumes of the patients. Pretreatment and post-CRT parameter medians and median parameter changes were tested for associations with aggressiveness and treatment response using a Mann-Whitney U test. For the statistically significant pretreatment associations, statistical analysis was additionally performed on percentile parameter values and histogram quantities.

For the pretreatment medians, associations were found for v_e in the individual AIF-based TK model, for A_{Brix} and k_{ep} in the Brix model, and for the histogram analysis in the relative peak height of k_{ep} in the Brix model. For the post-CRT medians, associations were found for K^{trans} and v_p in both versions of the TK model, and for k_{ep} in the Brix model and individual AIF-based TK model. For median parameter changes, associations were found for Δv_e in both versions of the TK model, and for Δk_{ep} in the Brix model.

This study showed that parametric modelling can be used to identify patients who require either no surgery or less advanced surgery, which may improve the expected quality of life, and patients in need of more advanced CRT regimes, which may improve the overall survival.

Sammendrag

Standardbehandling for rektalkreft er kirurgisk fjerning av tumoren, og i lokalavanserte tilfeller, neoadjuvant kjemo- og stråleterapi. Ved å tilegne seg mer kunnskap om tumoraggressivitet før behandling, kan behandlingen tilpasses individuelt, hvilket kan bidra til bedre livskvalitet og overlevelse for pasientene. I denne studien ble potensialet til parametriske modeller i dynamisk kontrastbasert (DCE) magnetresonanstomografi (MRI) til denne typen arbeid undersøkt.

DCE-MRI data fra 91 pasienter med rektalkreft ble analysert i Matlab med to parametriske analysemodeller: Tofts og Kermode (TK)-modellen og Brix-modellen. For å utforske potensialet til modellene til prediksjon av aggressivitet og behandlingsrespons, og betydningen av den arterielle inputfunksjonen (AIF), ble både en populasjonsbasert AIF og individuelle AIF-er brukt i TK-modellen, og sammenlignet med (den AIF-uavhengige) Brix-modellen. De følgende parametrene fra TK-modellen, K^{trans} (min^{-1}), v_e (%), v_p (%), og k_{ep} (min^{-1}), og Brix-modellen A_{Brix}, k_{el} (min^{-1}) og k_{ep} (min^{-1}) ble beregnet i tumorvolumene. Medianparametre før og etter behandling, og forskjeller mellom dem, ble testet for assosiasjoner med behandlingsrespons og aggressivitet med en Mann-Whitney U-test. For de statistisk signifikante assosiasjonene funnet før CRT, ble en statistisk analyse i tillegg utført på persentilverdier og histogramverdier.

For medianene før behandling ble det funnet assosiasjoner for v_e i TK-modellen med individuelle AIF-er, for A_{Brix} og k_{ep} i Brix-modellen, og i histogramanalysen for relativ maksimum søylehøyde av k_{ep} i Brix-modellen. For medianene etter behandling ble assosiasjoner funnet for K^{trans} og v_p i begge varianter av TK-modellen, og for k_{ep} i Brix-modellen og TK-modellen med individuelle AIF-er. Assosiasjoner med medianendringer ble funnet for Δv_e i begge versjoner av TK-modellen, og for Δk_{ep} i Brix-modellen.

Denne studien indikerer at parametrisk modellering kan brukes til å identifisere pasienter som enten ikke har behov for, eller kan få en mindre avansert kirurgisk fjerning av tumoren, som kan forbedre livskvalitet, og pasienter som trenger mer aggressiv kjemo- og stråleterapi, som kan forbedre overlevelse.

Contents

Abbreviations

AIF Arterial Input Function

AUC Area Under Curve

CRT Chemoradiotherapy

DCE Dynamic Contrast-Enhanced

EES Extracellular Extravascular Space

HIF-1α Hypoxia-Inducible Factor-1α

LARC Locally Advanced Rectal Cancer

MRI Magnetic Resonance Imaging

PK Pharmacokinetic

RF Radiofrequency

ROI Region Of Interest

RPH Relative Peak Height

RSI Relative Signal Intensity

SD Standard Deviation

SNR Signal to Noise Ratio

TE Echo Time

TK Tofts and Kermode

TNM Tumour Node Metastasis

TR Repetition Time

TRG Tumour Regression Grade

TTP Time To Peak

Chapter 1

Introduction

The standard treatment for rectal cancer patients is a surgical resection of the primary tumour and nearby lymph nodes [1]. If the tumour has grown through the rectal wall and invaded adjacent organs it is considered locally advanced, and in these cases the patient also receives chemoradiotherapy (CRT) in order to shrink the tumour prior to surgery. This treatment protocol gives a five-year survival of 68 % for rectal cancer [2].

Medical imaging at the time of diagnosis provides relevant information about how advanced the disease is, but does not directly assess the aggressiveness of the tumour, which is an important factor for treatment response and long term survival [3]. Tumour biopsies assess aggressiveness, but only a small sample is extracted and tumour tissue can be highly heterogeneous, resulting in a considerable margin of error. Patients in need of a more aggressive treatment may therefore go unnoticed if their tumours have not yet reached an advanced stage. A procedure for better evaluating the aggressiveness of tumours could thus increase the overall survival for rectal cancer.

Functional MRI is able to obtain information about the tissue properties within the entire tumour volume [4]. Dynamic contrast-enhanced (DCE) magnetic resonance imaging (MRI) is a functional MRI technique that injects a contrast agent into the patient and maps its distribution. Extracted signal intensity curves describe the time-dependent variations of contrast agent

concentration within each pixel, and the shapes of these curves depend on properties that are known to be associated with tumour aggressiveness.

To effectively assess tumour aggressiveness from DCE-MRI it is necessary to determine how to best analyse the signal intensity curves in order to extract reliable and useful information. Parametric analysis fits the curves to a model that describes the distribution of a contrast agent in tissue, and thus extracts parameters that describe the tissue properties [5]. Two well-known parametric models are the Tofts and Kermode (TK) model and the Brix model [6] [7]. Both models consider the interactions between the intravascular space and the extravascular extracellular space (EES), but differ in that the TK model requires the arterial input function (AIF), defined as the contrast agent concentration in the bloodstream, to be known, while the Brix model does not. The AIF has a sharp peak that can be difficult and time consuming to measure accurately. Consequently, to save time and acquire a stable AIF it is common to use a population-based AIF calculated from a group of patients, rather than using individual AIFs for all patients. This does, however, result in the loss of variations between the AIFs of different patients.

In rectal cancer, associations between TK model parameters and treatment response have been found by Gollub et al. [8] and Intven et al. [9] using a population-based AIF, and by Tong et al. [10] using individual AIFs. Lollert et al. [11] found associations between Brix model parameters and nodal metastases. Due to the sensitivity of compartmental models to the variation of MRI input parameters, a systematic comparison of the two approaches to AIF estimation is necessary to determine which method has the most potential. Furthermore, a comparison of the potential of the Brix model and the TK model could provide insight about the importance of the AIF.

The aims of this study were to:

1. Investigate the potential of DCE-MRI analysis for assessing tumour aggressiveness and predicting treatment response in rectal cancer.
2. Investigate the potential of using an individual AIF compared to a population-based AIF in the TK model.
3. Investigate the significance of an AIF by comparing the TK model and the Brix model.

Chapter 2

Theory

Some sections in the following chapter are either completely taken or adapted from a specialisation project report written by the author during the fall of 2017: "Analysis of DCE-MRI for Chemoradiotherapy Response Prediction in Rectal Cancer" [12]. These sections are marked with an asterix (*).

2.1 Cancer*

Cancer is caused by a series of genetic mutations resulting in a malignant but durable cell population [3]. Accelerated angiogenesis is a consequence of one such mutation, and is a well known cancer trait [13]. Tumour cells are dependent on oxygen and energy to grow, and thus when the tumour radius approaches the maximum diffusion length of blood in tissue, the tumour needs a vascular system. This is achieved by emitting growth factors that will cause the nearby arteries to build new vessels growing towards and into the tumour [14]. Tumour cells often have an overexpression of these growth factors, and therefore do not follow the controlled routine used by normal cells. Illustrated in figure 2.1, a consequence of this is that the vascular system of the tumour is often disorganised, which in combination with the rapid tumour growth, can result in areas deficient in oxygen, defined as hypoxic.

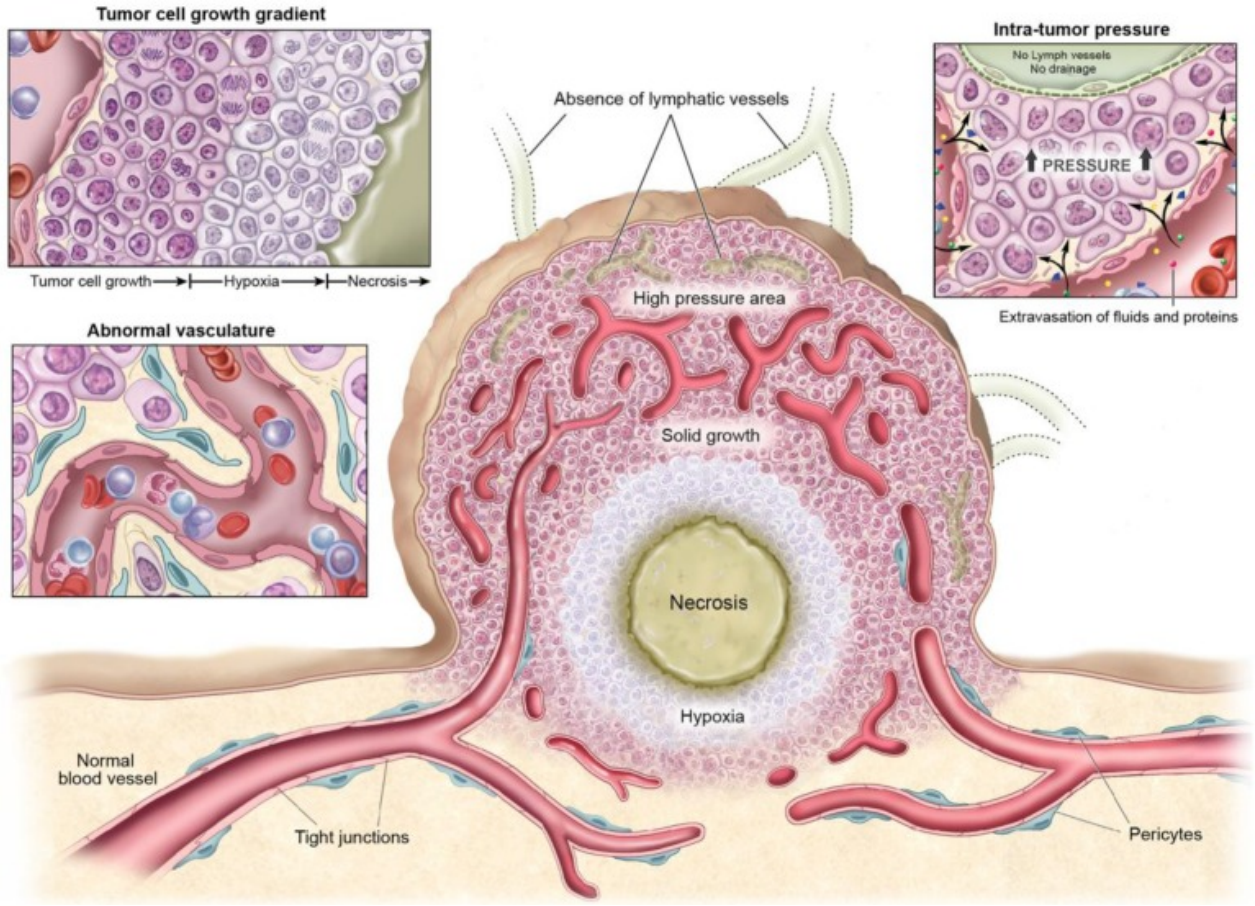

Figure 2.1: Properties of cancer. Accelerated angiogenesis in tumour tissue cause a disorganised vascular system, resulting in hypoxic areas and necrosis. The accelerated angiogenesis additionally results in leaky blood vessels. Combined with a lack of a lymphatic system in tumour tissue, this leads to an accumulation of particles in the tumour tissue, defined as the enhanced permeability and retention effect. Reproduced with permission from [15].

Hypoxia can be divided into two categories: acute hypoxia and chronic hypoxia [14]. Acute hypoxia occurs when a blood vessel is temporarily blocked. Often, blood vessels alternate between being blocked and being open, causing the connected tumour areas to periodically alternate between hypoxic and normoxic conditions. Chronic hypoxia occurs at a distance from the blood vessel equal to the limit of the diffusion length of blood in the tissue.

Cancer cells often have an increased ability to survive in hypoxic conditions relative to normal cells, among several factors caused by the upregulation of hypoxia-inducible factor-1α (HIF-1α) [16]. HIF-1α is degenerated under normoxic conditions, but under hypoxic conditions it is stabilised and in a chain of reactions induces the expression of genes related to angiogenesis, glycolysis and metastasis. Thus, patients with hypoxic tumours may experience a more rapid tumour growth and are more likely to develop metastasis, which is the main cause of death from cancer.

Hypoxic tumour tissue is a problem in cancer treatment for two reasons. First, chemotherapeutic drugs travel through the blood stream, and the amount of drug that is able to diffuse from the closest blood vessel to the hypoxic area is therefore limited [14]. Second, the effect of radiotherapy is reduced in hypoxic cells, explained by the oxygen effect. This makes it challenging to provide a high enough dose to kill the hypoxic cancer cells while at the same time sparing healthy tissue.

Another effect of the accelerated angiogenesis is that the disorganised vascular system results in leaky blood vessels in cancer tissue [14] [17]. This leads to an increased amount of particles leaking out into the extravascular space of a tumour. In addition, the abnormal growth of the tumour results in a nonexistent or underdeveloped lymphatic system, which in turn leads to a reduced wash-out of particles from the tumour. Together these two tumour characteristics lead to an accumulation of particles in the tumour, a phenomenon known as the enhanced permeability and retention effect, illustrated in figure 2.1.

2.2 Rectal Cancer

Rectal cancer is a colorectal cancer of the lower bowel. The main treatment is a surgical removal of the primary tumour and nearby lymph nodes [3]. At the time of diagnosis, approximately 30 % of rectal cancer cases have evolved to locally advanced rectal cancer (LARC), which means that the primary tumour has grown into or through the rectal wall and invades adjacent organs [1]. For this group, combined radiation therapy and chemotherapy is performed in order to shrink and downstage the tumour prior to surgery: neoadjuvant CRT.

The surgery results in good local control when successful, but may reduce the patient's quality of life [1]. The amount of unsuccessful surgeries has been found to increase for tumours with low vascularity or high amounts of fibrotic tissue, because these tumours to a greater extent adhere to healthy tissue, making it challenging to achieve a clear surgical resection [8]. In 2005, Theodoropoulos et al. found that an overexpression of HIF-1α and vascular endothelial growth factor (VEGF) occurred for about 44 % of LARC patients [18]. Studies have found strong associations between these biological markers and nodal metastases, poor treatment response and poor survival [19] [20]. This suggests that the poor treatment response in LARC is highly associated with hypoxia and accelerated angiogenesis in the tumour.

2.2.1 Staging and Response Evaluation in Rectal Cancer*

Rectal cancer is commonly staged using the tumour node metastasis (TNM) system, presented in table 2.1 [3]. It defines the stage of the primary tumour T from 0-4, the invasion of regional lymph nodes N from 0-2, and the existence of distant metastases M from 0-1. In addition, prefixes are used to indicate when and how the stage has been determined, where 'r' and 'mr' denote respectively radiological (MRI and/or CT) and MR-based assessment, 'p' signifies pathological assessment, and 'y' signifies that the assessment occurred after CRT [21]. The TNM system has been found useful for assessing treatment response, as the probability for survival has been found to decrease for advanced tumours, tumours with nodal metastases, and tumours with distant metastases.

Primary tumour (T)		Regional lymph nodes (N)		Distant metastasis (M)	
TX	Primary tumour cannot be assessed	NX	Regional lymph nodes cannot be assessed	MX	Distant metastasis cannot be assessed
T0	No evidence of primary tumour	N0	No regional lymph node metastasis	M0	No metastasis
Tis	Carcinoma in situ: intraepithelial or invasion of lamina propria	N1	Metastasis in 1-3 regional lymph nodes	M1	Distant metastasis
T1	Tumour invades submucosa	N1a	Metastasis in one regional lymph node	M1a	Metastasis confined to one organ or site
T2	Tumour invades muscularis propria	N1b	Metastasis in 2-3 regional lymph nodes	M1b	Metastasis in more than one organ/site or the peritonium
T3	Tumour invades through the muscularis propria into the pericolorectal tissues	N1c	Tumour deposit(s) in the subserosa, mesentery, or nonperitonealised pericolic or perirectal tissues without regional nodal metastasis		
T4a	Tumour penetrates to the surface of the visceral peritoneum	N2	Metastasis in 4 or more regional lymph nodes		
T4b	Tumour directly invades or is adherent to other organs or structures	N2a	Metastasis in 4-6 regional lymph nodes		
		N2b	Metastasis in 7 or more regional lymph nodes		

Table 2.1: Explanation of the different stages in rectal cancer according to the TNM system. The table is reproduced from [21].

The tumour regression grade (TRG) has been found to be predictive of overall survival in rectal cancer patients after neoadjuvant CRT, and is therefore often used to evaluate CRT response [22]. It is determined histomorphologically according to the TRG scale of 0 to 3, explained in table 2.2.

Tumour regression grade	
TRG 0	No viable cancer cells.
TRG 1	Single cells or small groups of cancer cells.
TRG 2	Residual cancer outgrown by fibrosis.
TRG 3	Minimal or no tumour regression. Extensive residual cancer.

Table 2.2: Explanation of the different levels of TRG. The table is reproduced from [23].

2.3 MRI*

MRI is a noninvasive imaging technique that exploits the magnetic properties of protons to acquire images [4]. The signal detected from a proton is obtained by applying an external magnetic field, $\mathbf{B_0}$, that the proton will precess around with a bulk frequency dependent on the molecule the proton belongs to. A visual interpretation of the precession frequency of a proton is shown in figure 2.2, where the axis of the proton oscillates around the net magnetic field with a precession angular frequency

$$\omega_0 = \gamma B_0 \tag{2.1}$$

where $\gamma \approx 2.68 \times 10^8$ rad s^{-1} T^{-1} is the gyromagnetic ratio for protons, also called the Larmor frequency [24]. The spin, which is either spin-up or spin-down, can also be visualised in this way, where the spins with spin-down will align themselves antiparallel to the external field axis as opposed parallel, which is the orientation of the nuclei in state spin-up. The number of spins in spin-up exceeding the number of spins in spin-down, is called the spin excess and is given by

$$SE \simeq N\frac{\hbar\omega_0}{2kT} \tag{2.2}$$

where N is the number of spins, $\hbar$ is the reduced Planck's constant, T is the temperature and k is Boltzmann's constant. The ratio will be very small for body temperatures, because the thermal energy is much higher than the spin energy. The sum of all spin axes, the net magnetisation vector $\mathbf{M}$, will thus be small and parallel to the applied magnetic field. By applying a second magnetic field $\mathbf{B_1}$, one may excite and resonate the spins so that $\mathbf{M}$ gets a component in the

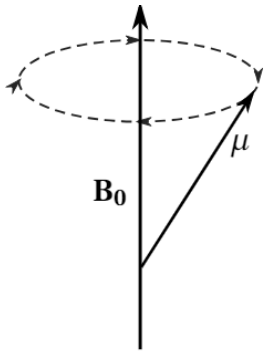

Figure 2.2: Precession of the magnetic moment μ around a static magnetic field $\mathbf{B_0}$.

transverse plane. The decay from the transverse plane when $\mathbf{B_1}$ is switched off, produces a measurable signal which lays the foundation for MRI.

2.3.1 The Bloch Equation*

The Bloch equation describes the motion of the magnetisation vector $\mathbf{M}$ as a function of time, and in its general form is given by

$$\frac{d\mathbf{M}}{dt} = \gamma \mathbf{M} \times \mathbf{B} \tag{2.3}$$

where $\mathbf{B}$ is the external magnetic field [4].

The concept of MRI is to observe the relaxation of the magnetisation vector $\mathbf{M}$ from the transverse state back to equilibrium after excitation by $\mathbf{B_1}$ [25]. This makes it possible to measure the relaxation times, longitudinal T_1, and transverse T_2 and T_2^*. The relaxation times will vary for different molecules, thus providing contrast in the image, dependent on three factors. First, the inherent energy of the tissue, where a low inherent energy will allow the tissue to absorb energy from the proton. Second, on the density of the molecules, where a higher density allows for a more efficient interaction between the magnetic fields. Last, on the molecular tumbling rate, where those with rates close to the Larmor frequency will interact better with the proton, leading to a fast relaxation. The longitudinal relaxation can be described by

$$\frac{d\mathbf{M_z}}{dt} = \frac{1}{T_1}(\mathbf{M_0} - \mathbf{M_z}) \tag{2.4}$$

and the transverse relaxation by

$$\frac{d\mathbf{M_{xy}}}{dt} = -\frac{1}{T_2}\mathbf{M_{xy}}[4]. \tag{2.5}$$

Thus, for relaxation from resonance equation 2.3 becomes

$$\frac{d\mathbf{M}}{dt} = \gamma\mathbf{M}\times\mathbf{B} + \frac{1}{T_1}(\mathbf{M_0} - \mathbf{M_z})\hat{z} - \frac{1}{T_2}\mathbf{M_{xy}}. \tag{2.6}$$

2.3.2 Image Acquisition*

MR images are acquired by applying a pulse which produces a signal by pulling some or all spins away from equilibrium and into phase in the transverse plane [25]. Often a gradient or second pulse is applied to rephase the dephasing signal, and the rephased signal is measured. Gradients are applied to determine spatial settings where a slice gradient decides the slice location of the image. The measured signals are stored in K space, which is the Fourier transform of the acquired image. One line in K space chosen by the phase gradient (y-direction) is measured per acquisition, the content of which is controlled by the readout gradient (x-direction).

One achieves contrast in MRI by weighting a certain parameter and looking at how this varies for different types of tissue. Commonly used weightings are T_1 relaxation time, caused by spin lattice energy transfer to the surrounding environment, T_2 decay time, caused by spin-spin interactions, and proton density, decided by the density of mobile hydrogen protons in the voxel [25]. In a T_1-weighted image the contrast in the image is based on the different degrees of longitudinal relaxation for different types of tissue. Molecules that relax quickly, for example water, therefore appear to be bright, while molecules that take a long time to relax, for example fat, appear dark. For T_2-weighted images the opposite is true, because the contrast in the image is based on the amount of transverse decay: molecules that decay quickly, like water, will cause there to be little signal in the image, and thus appear dark, whilst molecules that take longer to relax appear bright. An example of a T_2-weighted MR image is shown in figure 2.3.

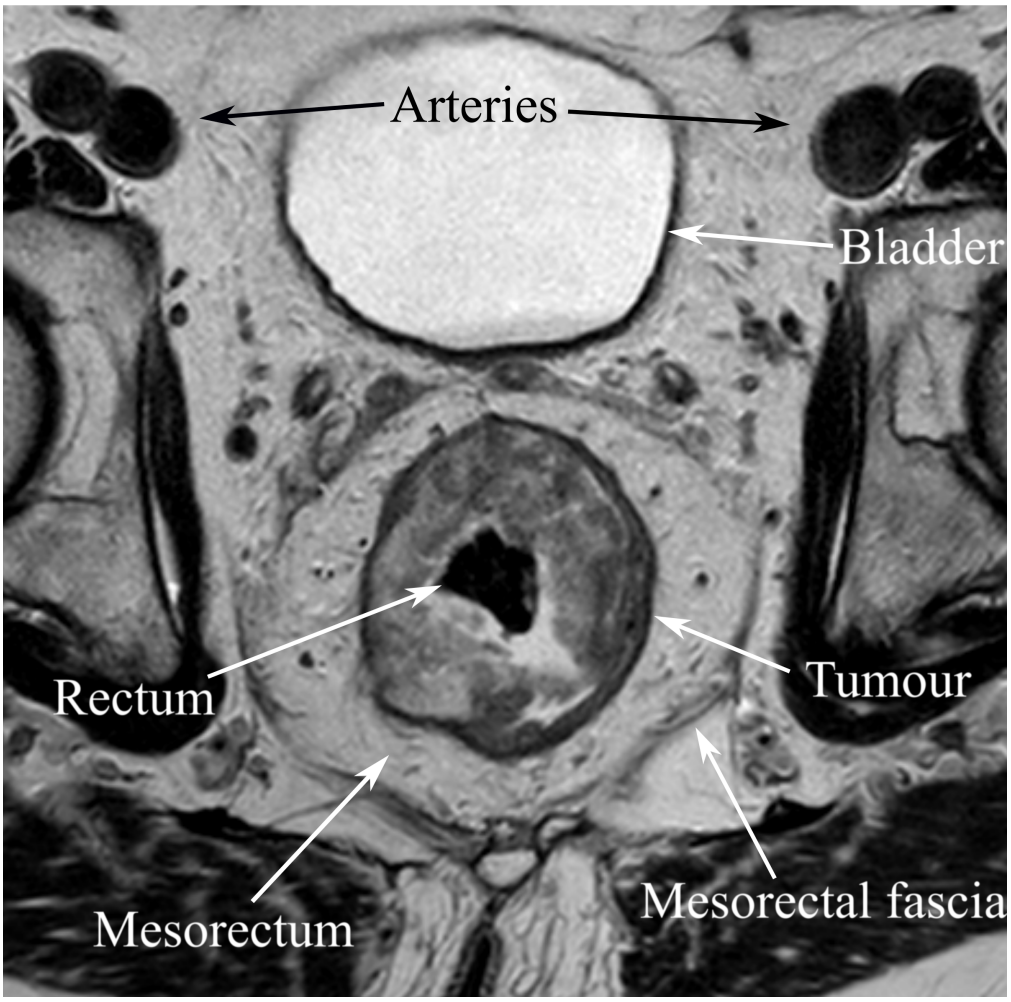

Figure 2.3: A T_2-weighted MR image of the axial plane of the pelvic area and rectum, acquired using a fast spin echo sequence. The T_2-weighting causes the fatty tissue to appear bright due to its long relaxation time, and the tissue with high concentrations of water to appear dark. Arrows indicate the tumour, mesorectum, mesorectal fascia, rectum, bladder and four artery cross sections. The image shows a patient from the Oxytarget study.

2.3.3 The Spin Echo Sequence*

One example of an MRI pulse sequence is the spin echo sequence, illustrated in figure 2.4. An initial radiofrequency (RF) pulse of 90° is used, followed by a second rephasing pulse of 180° [25]. The rephased signal then appears at the echo time (TE) after the initial signal, and the pulse sequence is repeated at the repetition time (TR). A spin echo sequence gives the following

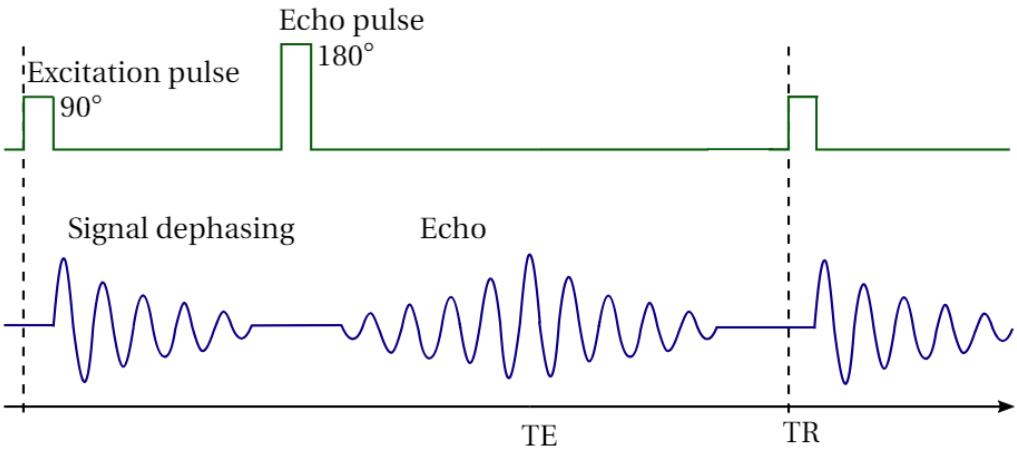

Figure 2.4: A spin echo sequence. An initial 90° RF pulse creates a dephasing signal, which is then rephased by adding a 180° RF pulse at TE/2. This results in an echo signal at the TE. At the TR the sequence is repeated.

equation for the transverse magnetisation vector,

$$M_{\perp}(TE) = M_0(1 - e^{-TR/T_1})e^{-TE/T_2} \tag{2.7}$$

where M_0 is the initial magnetisation [24]. For a T_1-weighted image, the signal in a voxel is decided by the amount of T_1 relaxation at the TR. From equation 2.7 it is apparent that the TR needs to be short to maximise the effects from the T_1-dependent exponential. The differences in relaxation time for different tissues thus create contrast in the image. In the same way, in a T_2-weighted image the TE needs to be long to maximise the effects of the transverse relaxation, because it decides the amount of T_2 decay that has occurred before the signal is measured. In a proton density weighted image, one seeks to minimise these two effects, which is achieved by using a long TR and a short TE. A spin echo sequence optimises the signal to noise ratio (SNR) and consequently provides excellent soft tissue contrast.

2.3.4 The Gradient Echo Sequence

In a gradient echo sequence the initial pulse has a flip angle α, commonly between 0° and 90° [4]. As illustrated in figure 2.5, after the α pulse has excited the spins, a gradient is applied in order to dephase the decaying spins, followed by a readout gradient of the opposite polarity to

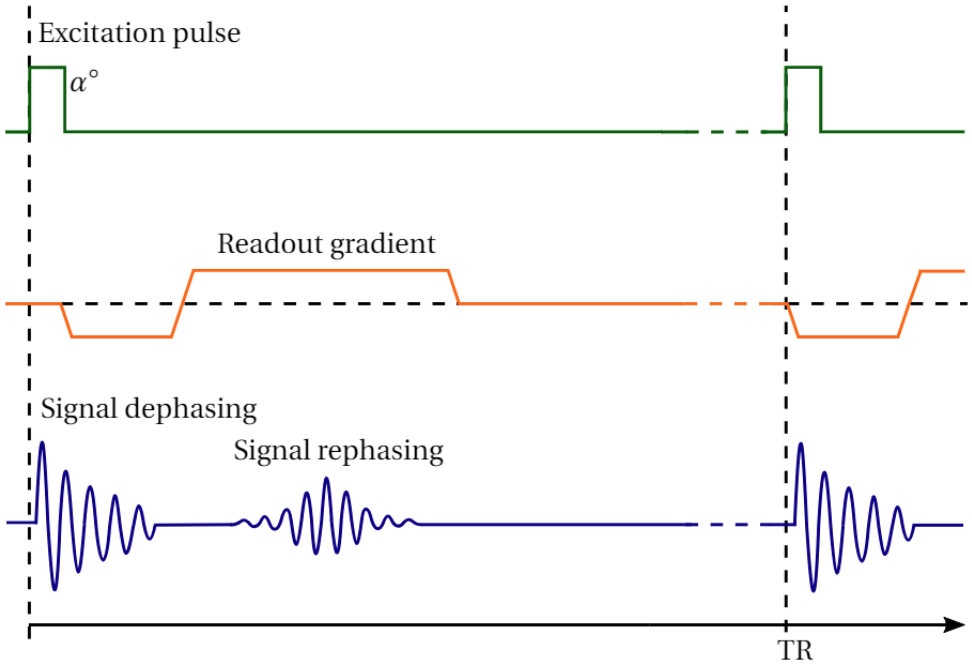

Figure 2.5: An example of a spoiled gradient echo sequence. An initial RF pulse α excites the spins, which are then dephased by a dephasing gradient. A readout gradient then causes the spins to rephase, and the rephased signal is measured. The sequence repeats at the TR.

rephase them [24]. The gradient echo sequence does not compensate for magnetic field inhomogeneities [25]. This results in T_2^*-weighting in the images.

The application of the gradients results in a quicker dephasing and rephasing, which allows for a faster image acquisition [25]. In addition, a small flip angle α can further reduce the time of decay to equilibrium. However, these features come at the cost of the SNR, which is lower in a gradient echo sequence than in a spin echo sequence. The SNR decreases further with a decreasing flip angle, and can therefore in general be considered to decrease with an increasing speed of image acquisition.

A short TR may prevent the transverse spins from dephasing properly before a new excitation pulse, which may lead to artefacts in the image [4]. The spoiled gradient echo sequence solves this by utilising additional RF-pulses and gradients to eliminate remaining transverse magnetisation. The signal intensity for a spoiled gradient echo sequence is given by

$$S_{SPGR} = S_0 \frac{\sin(\alpha)(1-e^{-TR/T_1})}{1-\cos(\alpha)\cdot e^{-TR/T_1}} e^{-TE/T_2^*} \tag{2.8}$$

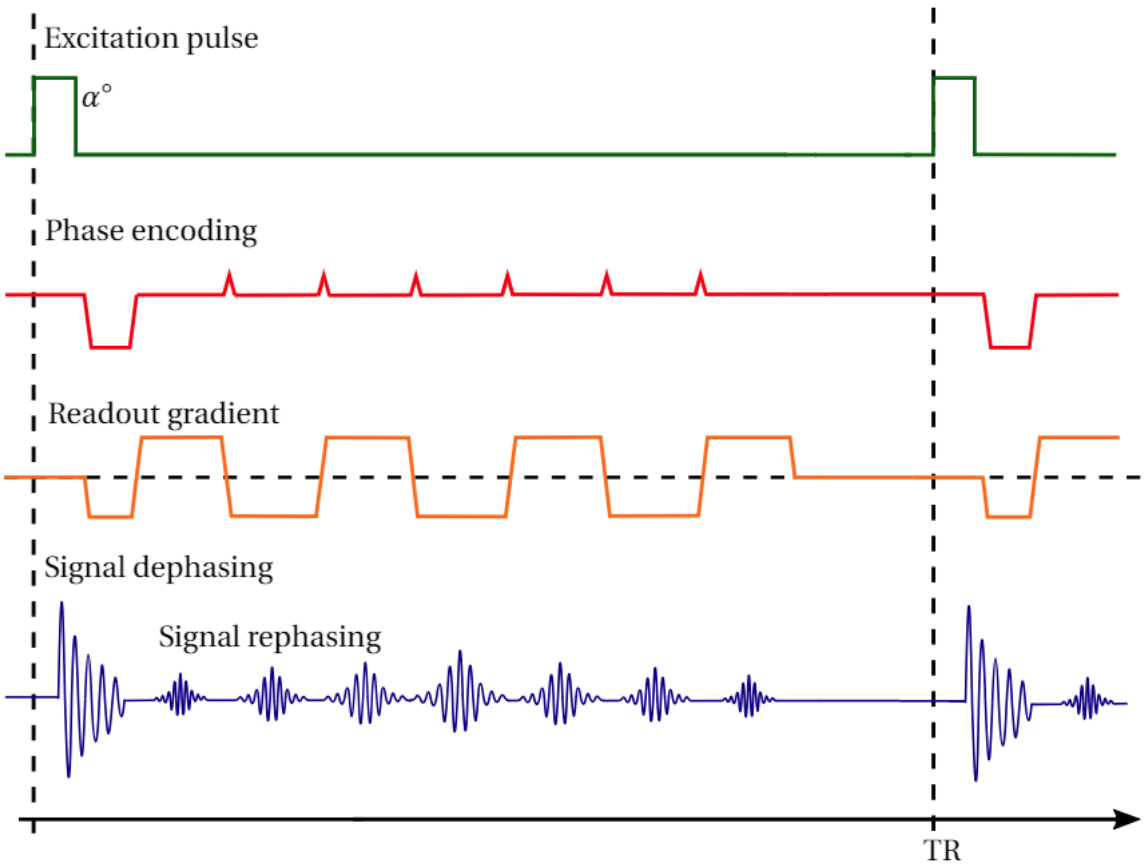

Figure 2.6: An example of an EPI sequence. An initial pulse α excites the spins, that are then dephased by a dephasing gradient. At the same time, the initial phase is encoded. A readout gradient follows to rephase the spins and simultaneously read the signal. Several lines in K-space are read during one TR by applying blips for phase encoding whenever the polarity of the readout gradient is reversed. After a TR the sequence can be repeated.

where S_0 is proportional to the proton density, and α is the flip angle [26].

Fast imaging techniques make it possible to avoid and reduce motion artefacts and study physiological properties of tissue [25]. A variant of the spoiled gradient echo sequence that is particularly popular for fast imaging is the echo planar imaging (EPI) sequence. By alternating the polarity of the readout gradients and using multiple so-called blips for phase encoding, acquisitions of entire images during only one repetition (single-shot EPI) or during a few repetitions (multi-shot EPI) become possible [27]. The workings of an EPI sequence are shown in figure 2.6.

2.3.5 Functional MRI*

In morphological MRI, the goal is to acquire images that accurately describe the morphology of the tissue. These have good tissue contrast and are therefore optimal to use for the T- and N-staging of the tumour and to delineate a region of interest (ROI) [25]. In functional MRI this is no longer the case, the aim is instead to learn about the processes that occur within the tissue. For example, diffusion of water molecules and the distribution of a contrast agent over a period time offer information about the cellular density and the vascularity within a ROI [28] [5].

The high temporal resolution of fast imaging techniques makes them ideal for observing functional properties of the tissue. Due to the low SNR and poor spatial resolution of high speed-imaging techniques, the tissue contrast is often poor in these images, but the functional information they provide is useful [4]. For example, diffusion weighted MRI provides contrast between tissues of different cellular densities, because dense tissues will allow for less diffusion than areas where water is allowed to flow freely [28]. In DCE-MRI a paramagnetic contrast agent is injected into the blood stream, which leads to a significant reduction in T_1 relaxation time for the nearby protons. It thereby leads to a significant increase in signal intensity which can easily be detected in the acquired images. Therefore, if one wishes to observe the flow and diffusion of blood, DCE-MRI is a valuable tool. Functional and morphological MRI are often used in combination in order to acquire both functional and morphological information on the tissue of interest.

2.4 DCE-MRI*

In DCE-MRI a contrast agent is injected into the bloodstream to enhance contrast in the tumour, as seen in the example in figure 2.7 [4]. The contrast agent contains paramagnetic ions (often gadolineum), which are known to have large magnetic moments. Spins of water molecules that interact with the local magnetic field of the contrast agent, result in magnetic field fluctuations that reduce the precession frequency of the protons to one close to the Larmor frequency. Thus, both the T_1 relaxation and T_2 decay of water will be reduced [25]. For DCE-MRI, which is T_1-

weighted, this results in a significant enhancement of the original signal. The relationship between the reduced T_1 from the contrast agent and the original T_1 is given by,

$$\frac{1}{T_{1,c}} = \frac{1}{T_{1,0}} + c\frac{1}{t_1} \tag{2.9}$$

where $T_{1,c}$ is the relaxation time for the tissue with contrast agent, $T_{1,0}$ is the original relaxation time of the tissue, c is the contrast agent concentration, and t_1 is the ability of the contrast agent to reduce the relaxation time of the surrounding tissue.

The contrast agent is administered during an acquisition of a series of T_1-weighted images over a period of time with fast imaging techniques [5]. This makes it possible to observe the distribution of a contrast agent as a function of time, where the amount of signal enhancement represents the contrast agent concentration. From equation 2.9, the relaxation rate $R_1(t)$ for a contrast agent concentration that varies over a period of time is

$$R_1(t) = \frac{1}{T_1(t)} = \frac{1}{T_{1,0}} + r_1 C(t), \tag{2.10}$$

where $r_1 = 1/t_1$ is the relaxivity of the contrast agent.

The contrast agent concentration in a particular area depends on the proximity of the tissue to blood vessels and of blood vessel properties [5]. This is because the contrast agent first enters the bloodstream, and must diffuse through the vessel walls to reach other parts of the tissue. Hypoxic areas will have a low signal enhancement because only small amounts of contrast agent is able to diffuse far from the blood vessels [14]. The leakiness of blood vessels in tumours further affects the signal enhancement: first the leaky vessels cause a high contrast agent concentration in the surrounding tissue, and secondly the increase to maximum signal enhancement in tumours is often steeper than in normal tissue. Leaky vessel walls increase the contrast agent wash-out rate in the same way, causing the signal enhancement curves to have a quick time to peak (TTP) followed by a steady decrease. Thus, DCE-MRI makes it possible not only to distinguish tumour tissue from normal tissue, but also to detect a tumour's hypoxic and vascular properties.

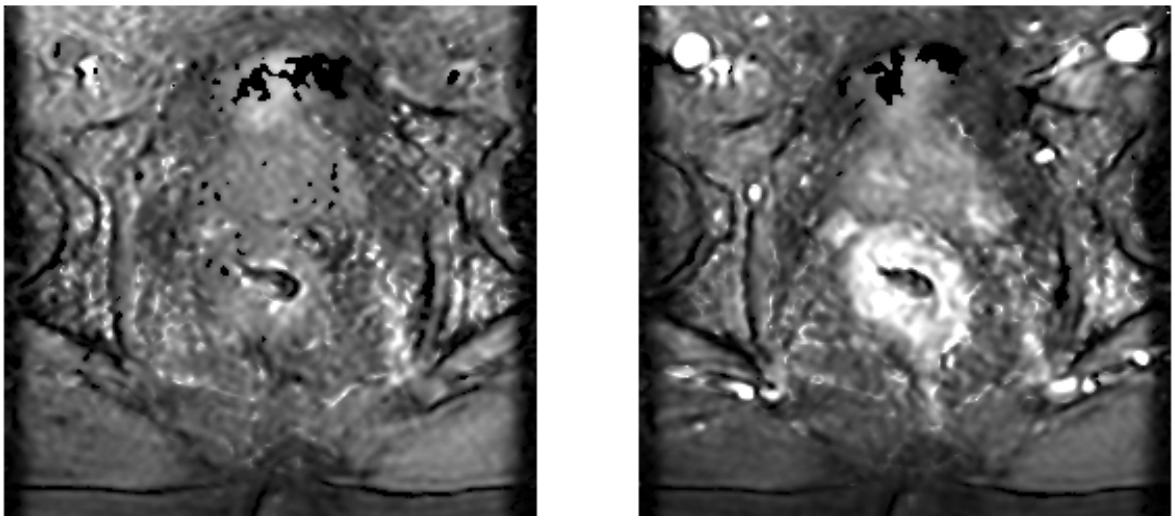

(a) (b)

Figure 2.7: An example of a DCE-MR image, before (**a**) and after (**b**) injection of contrast agent. In the centre of the second image the tumour can be seen, enlightened due to an increased uptake of contrast agent in the tumour compared to the normal tissue. The bright circular shapes in the upper corners are arteries, which appear bright because there is a high concentration of contrast agent in the blood. The images are from the Oxytarget study.

2.4.1 Estimation of Contrast Agent Concentration

Equation 2.8 represents the signal intensity of a spoiled gradient echo sequence. By assuming that $TE << T_2^*$, making T_2^*-effects negligible, the expression can be reduced to

$$S_{SPGR} = M_0 \frac{\sin(\alpha)(1-e^{-TR/T_1})}{1-\cos(\alpha)\cdot e^{-TR/T_1}}[4]. \tag{2.11}$$

From this expression an estimate for the variation in the longitudinal relaxation time $T_1(t)$ as the contrast agent is injected can be derived

$$\frac{1}{T_1(t)} = -\frac{1}{TR}\ln\left(\frac{1-K(t)}{1-\cos(\alpha)K(t)}\right) \tag{2.12}$$

where

$$K(t) = \frac{S(t)}{S_0}\cdot\frac{1-e^{-TR/T_{1,0}}}{1-\cos(\alpha)e^{-TR/T_{1,0}}} \tag{2.13}$$

and $T_{1,0}$ is the initial relaxation time when no contrast agent is present, $S(t)$ is the signal intensity at time t, and S_0 is the average initial signal intensity before the contrast agent is injected.

By applying this expression for T_1 to equation 2.10, an expression for the contrast agent concentration $C(t)$ is obtained.

Problems can occur during the calculation of $T_1(t)$ if the SNR is low [4]. Therefore it can be advantageous to further simplify the expression. If it is assumed that $TR << T_1$ and that the flip angle α is large, equation 2.11 can be reduced to

$$S \approx \frac{M_0 TR}{T_1} \tag{2.14}$$

which gives a relative signal intensity (RSI)

$$RSI(t) = \frac{S(t) - S_0}{S_0} \approx r_1 T_{1,0} C(t). \tag{2.15}$$

which from equation 2.10 gives the contrast agent concentration given by

$$C(t) = \frac{RSI(t)}{r_1 T_{1,0}}. \tag{2.16}$$

This equation is generally true for soft tissue, but may cause errors for blood vessels, because the contrast agent concentration can become too high for the assumption $TR << T_1$ to be reasonable.

2.4.2 Analysis of DCE-MRI*

DCE-MRI provides images that show the distribution of contrast agent in the tissue for a relevant time period, usually starting when the contrast agent is injected. Illustrated in figure 2.8, it is possible to plot signal intensity curves describing the varying signal intensity for a pixel during the chosen period from these images. These curves have a characteristic shape depending on the type of tissue the pixel represents, and constitute the basis for the different methods of analysis for DCE-MRI [5].

Semi-quantitative DCE-MRI analysis is considered to be the simplest method of analysis [5].

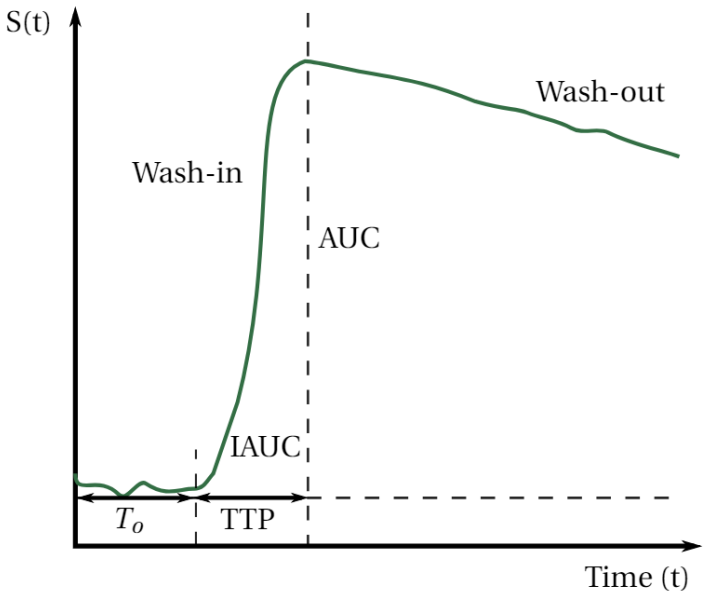

Figure 2.8: An example of how the signal intensity S(t) curve in solid tissue may look when a contrast agent is injected. The type of tissue determines the parameters TTP, AUC, IAUC, wash-in and wash-out. Cancerous tissue is known to have a short TTP and a wash-out as illustrated, due to the EPR effect described in section 2.1 [28]. Normal tissue will have a slower TTP, and the signal may plateau or continue to increase in the wash-out phase illustrated.

Figure 2.8 indicates the descriptive parameters TTP, area under curve (AUC), and initial area under curve (IAUC). These parameters do not directly describe physiological properties in the tissue, but are related to them. For example, a short TTP can indicate a high vascularity and leakiness of the blood vessels. While some studies have found these relations to be strong, there is often a significant uncertainty involved. Parameters that more accurately represent the physiological properties in question, can be calculated with by using parametric analysis. Parametric analysis relates the signal intensity curves, which are proportional to contrast agent concentration curves according to equations 2.10 and 2.15, to parameters describing the permeability of the vascular wall and retention abilities of the tissue in question. These parameters will thus give a more accurate image of the functional properties of the tissue in question.

Parametric modelling is divided into two categories: compartmental pharmacokinetic (PK) models and spatially distributed kinetic models [5]. In compartmental PK models, the system is divided into different compartments according to tissue type, and the contrast agent flow between these is described. The contrast agent concentration is assumed to be uniform within each

compartment. In spatially distributed kinetic models the tissue is divided into a high number of infinitesimal compartments that only interact with nearby compartments [5]. This is a more accurate method, but it is also a lot more time-consuming.

For many compartmental PK models it is necessary to estimate the contrast agent concentration in the blood plasma, called the AIF, which will reach a peak shortly after contrast agent injection, and then decrease [5]. Accounting for the AIF is believed to provide a more accurate interpretation of the measured DCE-MRI signal.

2.4.3 The Arterial Input Function

The AIF describes the contrast agent concentration in the blood plasma for a period of time that starts upon injection of the contrast agent, illustrated in figure 2.9a. Acquiring an acceptable approximation is often a requirement in compartmental models and can be one of the major obstacles it is necessary to overcome for a good estimation of the model parameters to be achieved [5]. It can be difficult because the peak of the AIF is often sharp, particularly for bolus (short time) injections, so that an insufficient spatial resolution may prevent accurate sampling of this area.

The AIF is often described by an equation where constants are adjusted according to a given patient. Tofts and Kermode suggest an equation of two exponentials to approximate the AIF,

$$C_p(t) = D(a_1 e^{-m_1 t} + a_2 e^{-m_2 t}) \tag{2.17}$$

where $D(\text{mmol}\,\text{kg}^{-1})$ is the contrast agent dose, a_1 and a_2 $(\text{kg}\,\text{l}^{-1})$ are amplitudes of the exponentials, and m_1 and m_2 (min^{-1}) are rate constants [6]. This equation gives an approximation of the AIF that relates to the true case as illustrated in figure 2.9 b), and is the best-established function for AIF modelling [29]. It has the advantage of being simple, with only four unknown parameters. Its main weakness is that it does not account for the second peak, which may make the fitting process challenging in cases where it is evident, as its data points then may disturb the fitting to the simplified function. However, the SNR is often too low for the second peak to be

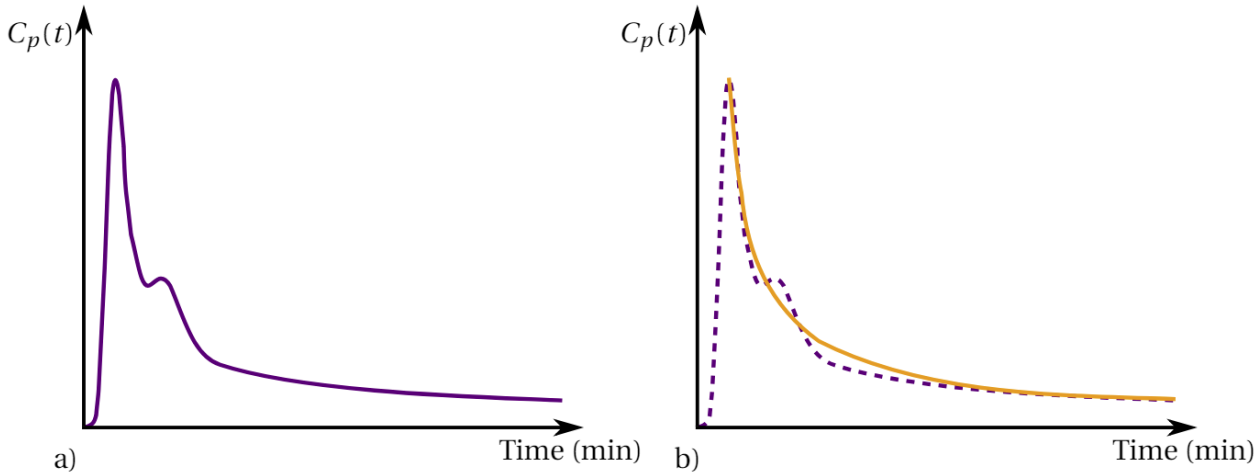

Figure 2.9: **a)** The contrast agent concentration during the first three to five minutes after the contrast agent is injected. The concentration $C_p(t)$ will first increase rapidly to a sharp peak, and then decrease quickly from the peak before increasing slightly for a second peak, caused by recirculation of the contrast agent in the arterial system [5] [29]. The contrast agent further decreases as the contrast agent is both absorbed by the tissue and cleared out through the renal system, and stabilise at a slowly decaying plateau. **b)** The approximated AIF (orange) obtained when equation 2.17 is fitted to the measured concentration curve $C_p(t)$. As seen the approximation starts at the time of the peak.

sufficiently evident for accurate estimation in the contrast agent concentrations curves, making it advantageous to use a model that does not account for its presence.

It is common to estimate an average AIF from a few representative patients and apply this to a larger group [5]. Increasing the number of patients the AIF is measured for will then increase the stability of the population-based AIF. A potential weakness with using a population-based AIF is that it does not account for individual differences between patients, for example blood flow velocity, heart rate, and renal function, that affect the shape of the peak [29] [30]. A potential solution can be to measure individual AIFs for and use them directly in the TK model, instead of calculating a population-based AIF. Individual differences will then be accounted for, but less stable AIFs may occur for some patients if the SNR is low or if image artefacts or errors affect the individual measurement.

The AIF can be determined by measuring the contrast agent concentrations at different time points by using an arterial catheter in the patient [5]. If the temporal resolution is adequate, an accurate approximation will be achieved using this approach. The procedure can however be

uncomfortable for the patient, and less invasive methods are therefore often sought out.

A promising alternative is to measure the AIF from the DCE-MRI data [5]. This approach has the advantage that it requires no additional contribution from the patient, which facilitates the measurement of large numbers of individual AIFs. The AIFs are instead calculated from the measured signal intensity within an artery over a period of time, and the contrast agent concentration in the blood, $C_b(t)$, is calculated using the procedure described in section 2.4.1. To find the contrast agent concentration in the blood plasma, $C_p(t)$, it is necessary to correct for the hematocrit value Hct using:

$$C_p(t) = \frac{C_b(t)}{1 - Hct} \text{[29]}. \tag{2.18}$$

The hematocrit value is defined as the fraction of red blood cell volume to total blood volume in a centrifuged blood sample and is normally between 0.36 and 0.46 for women and 0.41 and 0.53 for men [31].

2.4.4 The Tofts and Kermode Model

Presented by Tofts and Kermode in 1989, the TK model is the best-established compartmental PK analysis model for DCE-MRI [6] [5]. It divides the system into two compartments: the intravascular space and the EES, which are thought to represent a capillary and the extravascular space the contrast agent is able to leak into, respectively [32]. Illustrated in figure 2.10, the contrast agent concentrations in the intravascular space and the EES are given by $C_p(t)$ and $C_e(t)$, and the contrast agent travels between the intravascular space to the EES with rates K^{trans} (min^{-1}) and k_{ep} (min^{-1}). The volume fraction of tissue that consists of intravascular space is given by v_p (%) and the volume fraction of tissue consisting of EES is given by v_e (%).

The TK model can be described by

$$\frac{dC_t}{dt} = K^{trans} C_p(t) - k_{ep} C_t(t) \tag{2.19}$$

where $C_t(t) = v_e C_e(t)$ is the contrast agent concentration in the tissue, and $C_p(t)$ is given by

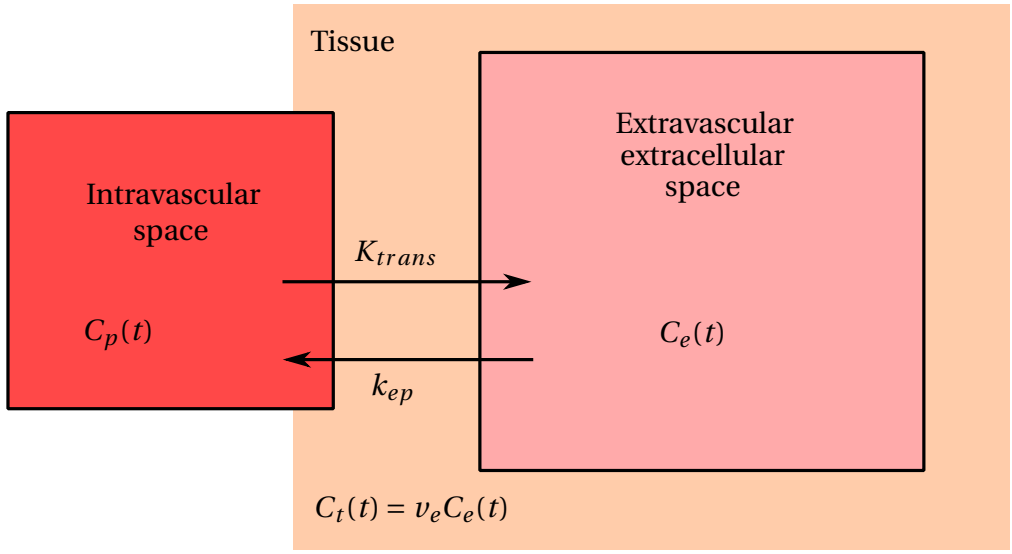

Figure 2.10: Illustration of the system described in the TK model. The contrast agent travels from the intravascular space to the EES with a volume transfer rate, K^{trans}, and back from the EES to the intravascular space at a rate k_{ep}. The contrast agent concentration in the intravascular space is given by $C_p(t)$ (the AIF), and the contrast agent concentration in the EES is given by $C_e(t)$. The contrast agent concentration in the tissue is then given by $C_t(t) = v_e C_e(t)$ where v_e is the fraction of the tissue that consists of EES. The figure is based on [33].

an AIF, and $k_{ep} = K^{trans}/v_e$ (min^{-1}). Solving equation 2.19 gives an expression for the contrast agent concentration in the tissue given by

$$C_t(t) = \int_0^t C_p(t') e^{-(K^{trans}/v_e)(t-t')} dt'. \tag{2.20}$$

The vascularity of the tissue is thought to be negligible. This is a reasonable assumption in healthy tissue, but in tumour tissue the vascularity is often significantly higher due to accelerated angiogenesis in tumour tissue [34]. In 1997, Tofts therefore introduced a second term to the TK model to account for the vascularity: $v_p C_p(t)$ [34]. Equation 2.20 then becomes

$$C_t(t) = v_p C_p(t) + \int_0^t C_p(t') e^{-(K^{trans}/v_e)(t-t')} dt', \tag{2.21}$$

giving a more realistic model often termed the extended TK model.

The relevant parameters from the extended TK model that are commonly interpreted for further analysis are K^{trans}, v_e, v_p, and k_{ep}. K^{trans} has been found to be influenced by blood flow

and vessel permeability [26]. In 1999, Tofts et al. determined that K^{trans} describes the blood plasma flow per unit volume of tissue under flow-limited conditions, while under permeability-limited conditions it is equivalent to the permeability surface area product per unit volume of tissue [32]. For rectal cancer it has been found by Gollub et al. that a high K^{trans} was associated with a clear resection margin, while Intven et al. found that a decrease in K^{trans} after CRT was associated with a good treatment response [8] [9]. Tong et al. similarly found a significantly higher K^{trans} for patients who achieved complete pathological response, and found that for these patients there was a significant decrease in the parameter value after treatment [10]. v_e is the volume of EES per unit volume of tissue, and can therefore be associated with the cellular density in the tissue. Tong et al. found that v_e was significantly higher for patients who achieved complete pathological response than for those who did not. v_p is the volume fraction of tissue consisting of capillaries. This is commonly very small in normal tissue: below 1 %, but in tumours the vascularity is often increased. An association with progression free survival was found for a low v_p in renal cancer metastases. Finally, k_{ep} is the rate transfer constant from the EES to the intravascular space, and is known to be associated with leakiness of blood vessels [4]. Gollub et al. found a high k_{ep} to be associated with a clear resection margin, and Tong et al. found a high k_{ep} for patients with complete pathological response, as well as a decrease in the parameter value for this group after treatment [8] [10].

2.4.5 The Brix Model*

Proposed by Brix et al. in 1991, the Brix model is a compartmental PK analysis model that is not dependent on the AIF [7]. Instead, a particular AIF is assumed known from the infusion rate of the contrast agent entering the body. This makes for a simpler implementation than that of the TK model, with less required variables, but may also provide results with a higher uncertainty.

As in the TK model, two compartments are used in the Brix model: the intravascular space and the EES, illustrated in figure 2.11 [5] [7]. The contrast agent enters the system through the intravascular space at a rate k_{in} during a time period τ, and leaves the system at a rate k_{el}. In the system the contrast agent travels between the intravascular space and EES at rates k_{pe} and k_{ep},

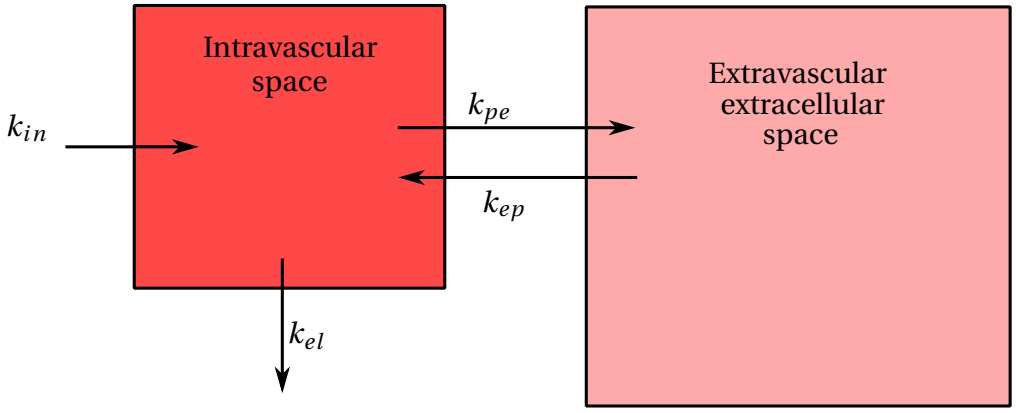

Figure 2.11: Illustration of the compartments of the Brix model. The contrast agent enters the system at a rate k_{in} during a time period, τ, and leaves the system at a rate k_{el}. The contrast agent travels between the intravascular space and EES at rates k_{pe} and k_{ep}, where $k_{pe} = -k_{ep}$.

where $k_{pe} = -k_{ep}$.

The relationship between the intravascular space and the EES is given by the mass conservation principle,

$$\frac{dC_p}{dt} = \frac{k_{in}}{V_p}(u(t) - u(t-\tau)) - k_{el}C_p(t) \tag{2.22}$$

$$\frac{dC_t}{dt} = k_{pe}\frac{V_p}{V_e}C_p - k_{ep}C_p(t) \tag{2.23}$$

where $u(t)$ is the Heaviside step function, τ is the time span for which the contrast agent is injected, V_p is the intravascular plasma volume, and V_e is the extravascular extracellular volume [7]. The relationship between the signal intensity $S(t)$ and the concentration of contrast agent in the image is given by

$$\frac{S(t)}{S_0} = 1 + \frac{A_{Brix}}{k_{ep} - k_{el}}\left[\frac{e^{k_{el}t}}{k_{el}}\left(e^{k_{el}t'} - 1\right) - \frac{e^{-k_{ep}t}}{k_{ep}}\left(e^{k_{ep}t'} - 1\right)\right] \tag{2.24}$$

where $t' = t$ for $0 \leq t \leq \tau$ and $t' = \tau$ for $t \geq \tau$ [5]. Here, k_{ep} can be put into relation to the leakiness of blood vessels, and k_{el} to the vascularity of the system. The amplitude A_{Brix} is a constant that depends on the tissue properties (two tissue and frequency dependent constants, k_{ep}, relaxation times in absence of contrast agents, the volume of the EES compartment, and the fraction of the extracellular volume), the infusion rate of the contrast agent k_{in}, and the MRI sequence parameters (TR and TE) [7]. It can be associated with the amplitude parameter K^{trans}

in the TK model. Since a lot of variables affect A_{Brix}, looking at the parameter alone may not always be enough to get a full idea of its physiological indications. It can instead be useful to also take some of the image acquisition settings into account.

The Brix model was developed using a slow infusion rate leading to a τ of around four minutes [7]. By assuming τ is one minute, equation 2.24 is simplified to

$$\frac{S(t)}{S_0} = 1 + \frac{A_{Brix}}{k_{ep} - k_{el}}\left(e^{-k_{el}t} - e^{-k_{ep}t}\right)[35]. \tag{2.25}$$

This approximation was suggested by Hoffman et al. and is the most commonly used version of the Brix model [35] [5]. It provides a fairly simple implementation, but does not account for bolus contrast agent injections.

Even though many factors affect it, an association between A_{Brix} and treatment response has been found in several studies. For breast cancer, a significant decrease from the initial A_{Brix} value was found after treatment by Thukral et al. in 2007 [36]. In cervical cancer, Halle et al. found that a low A_{Brix} was associated with an upregulation of HIF-1α expression, known to negatively impact treatment response [37]. Lollert et al. found associations between high A_{Brix} and nodal involvement in rectal cancer, which is associated with a decreased treatment response [11]. Similarly, for k_{ep} Torheim et al. found an association for parameter heterogeneity and treatment response in cervical cancer, and for rectal cancer Lollert et al. found significantly higher k_{ep} for patients with distant metastases, which is usually associated with aggressive treatment resistant disease [38]. Little focus has been put on the washout rate k_{el} in previous studies, but associations with treatment response was found for its heterogeneity by Torheim et al [38].

Chapter 3

Method

3.1 Clinical Data

The clinical data were obtained from the Oxytarget study. The Oxytarget study aims to learn how to more effectively identify patients at risk of metastasis and poor treatment response in rectal cancer through the use of functional MRI, and to utilise this to better adapt treatment [39].

3.2 Patients

169 patients diagnosed with rectal cancer in the period 2014-2017 were initially included in this study. 60 of the patients were excluded because of insufficient data: 20 patients because all MR data were absent, 23 patients because dynamic MR data were absent, and 17 patients because any or suitable tumour delineations were absent. Additionally 18 patients were excluded due to differing treatment regimes: 16 patients who did not receive surgery and two patients who received palliative chemotherapy prior to surgery. Thus, the sample size was reduced to 91 patients. 43 of the patients received neoadjuvant CRT. Furthermore, for 18 out of these 43 patients, images were acquired both before and after neoadjuvant CRT was given.

Regime	Number of patients	Description
		Chemotherapy
Xeloda	29	Radiosensitiser. Metabolises into 5-Fluorouracil, an antimetabolite which inhibits thymidylate synthase, giving a radiosensitising effect [14].
FLOX	4	Multidrug consisting of 5-Fluorouracil, oxaliplatin, and folinic acid [3] [40]. Works as a neurotoxic and radiosensitiser. Given in combination with 5 fractions of 5 Gy radiation therapy.
FLV	5	Multidrug consisting of 5-Fluorouracil and folinic acid. Works as a radiosensitiser [40].
None	5	For some elderly or sick patients, only radiotherapy was given.
		Radiotherapy
2 Gy x 25	35	25 dose fractions of 2 Gy. Gives a total dose of 50 Gy, normally over a period of five weeks.
5 Gy x 5	8	5 dose fractions of 5 Gy, over a period of 5 days, a total dose of 25 Gy. Normally used for elderly or sick patients deemed unlikely to manage a more advanced treatment.

Table 3.1: Description of the different treatments received by the patients with LARC in the Oxytarget study.

Diagnosis and pretreatment staging were determined using standard diagnostic tools for rectal cancer, which include rigid rectoscopy with biopsy, CT imaging of the thorax and abdomen, and MRI of the rectum [3]. All patients received pelvic surgery to remove the tumour and nearby lymph nodes. The cancer of 43 patients was locally advanced, and these patients therefore received neoadjuvant CRT prior to surgery, while the rest of the patients received surgery without any prior treatment. The technique used for all the radiotherapy treatments was volumetric modulated arc therapy. Further details about the CRT regimes are described in table 3.1.

After tumour resection, TRG and TNM stages were determined for each tumour by an experienced pathologist. Tumour and patient characteristics are displayed in table 3.2.

Patient Characteristics	**n** (%)	**Median age (range)**
Total number of patients	91	64 (41-88)
Male	61 (67 %)	66 (41-88)
Female	30 (33 %)	62 (47-80)
Patients that received CRT	43 (47 %)	63 (41-79)
Male	31 (72 %)	63 (41-78)
Female	12 (28 %)	62 (49-79)
Patients that did not receive CRT	48 (53 %)	66 (47-88)
Male	30 (63 %)	67 (47-88)
Female	18 (38 %)	62 (47-48)

CRT	**n** (%)	**No CRT**	**n** (%)
rTNM stage		**rTNM stage**	
mrT2	3 (6 %)	mrT2	19 (40 %)
mrT3	21 (49 %)	mrT3	22 (46 %)
mrT4	19 (44 %)	mrT4	7 (15 %)
mrN0	13 (30 %)	mrN0	33 (69 %)
mrN1	16 (37 %)	mrN1	12 (25 %)
mrN2	14 (33 %)	mrN2	3 (6 %)
rM0	36 (84 %)	rM0	44 (92 %)
rM1	7 (16 %)	rM1	4 (9 %)
ypTN stage		**pTN stage**	
ypT0	6 (14 %)	pT1	4 (8 %)
ypT1	5 (12 %)	pT2	20 (42 %)
ypT2	4 (9 %)	pT3	21 (44 %)
ypT3	25 (58 %)	pT4	3 (6 %)
ypT4	3 (7 %)	pN0	29 (60 %)
ypN0	25 (58 %)	pN1	15 (31 %)
ypN1	12 (28 %)	pN2	4 (8 %)
ypN2	6 (14 %)		
TRG stage			
TRG0	5 (12 %)		
TRG1	11 (26 %)		
TRG2	17 (40 %)		
TRG3	10 (23 %)		

Table 3.2: Patient and tumour characteristics. The left column displays the tumour characteristics of the patients that received CRT, and the right column displays the tumour characteristics of the patients that did not receive CRT. The prefixes 'r' and 'mr' denote respectively radiologically (MR and/or CT) and MRI-assessed staging, the prefix 'p' denotes assessment by pathologist, and 'y' denotes that the assessment took place after CRT [26].

3.3 MRI Acquisition

MR images were obtained using a Philips Achieva 1.5 Tesla system (Philips Healthcare, The Netherlands) with NOVA Dual HP gradients (maximum gradient amplitude 33 $\mathrm{mT\,m^{-1}}$ and slew rate 180 $\mathrm{T\,m^{-1}\,s^{-1}}$), and a five-channel cardiac coil with parallel imaging capabilities [26]. Prior to imaging, the patients received glucagon and buscopan in order to reduce bowel peristalsis.

High quality morphological images were acquired by performing a T_2-weighted spin-echo sequence (figure 3.1) [26]. Additionally a diffusion weighted sequence was performed, using a fat-saturated single-shot spin-echo EPI sequence. Using the T_2-weighted and diffusion weighted images, ROIs delineating the tumours were drawn by two radiologists with respectively 7 and 14 years of experience.

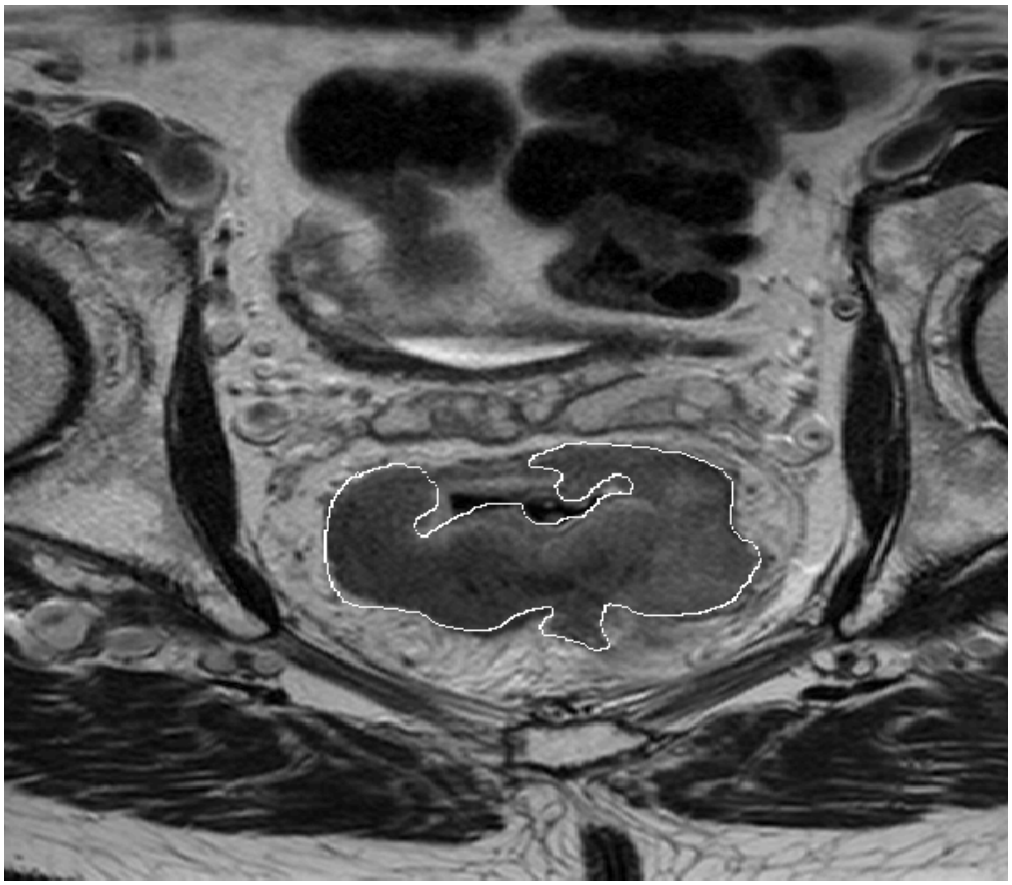

Figure 3.1: A high quality (526 x 526) T_2-weighted axial MR image of one of the patients in the Oxytarget study. Drawn by an experienced radiologist, the delineated area indicates the tumour.

The T_1-weighted DCE-MR images (figure 3.2) were acquired by performing a multi-echo three-dimensional T_1-weighted EPI sequence with three echoes [26]. The sequence had TR = 39 ms with the first echo at TE = 4.6 ms, time between echoes of 9.3 ms, a flip angle of 28° and an EPI factor of 9. To enhance contrast in the images, the gadolineum-based contrast agent Dotarem (279 mg ml^{-1}) was used [4]. A dose of 0.2 ml kg^{-1} (0.1 mmol kg^{-1}) was administered at a rate of 3 ml s^{-1}, followed by 20 ml of saline solution. Images were acquired in 60 time steps, with an average of 15 images taken prior to contrast agent administration, followed by an average of 45 images after contrast agent administration. The temporal resolution was around 2.6 seconds. The sequence was interleaved with a 3D T_1 weighted turbo field echo sequence (THRIVE) in order to obtain images of high spatial resolution during the same acquisition, starting after 1-2 minutes. After this, the dynamic images were acquired in bulks of four, with pauses of 67 seconds each, where the THRIVE images were acquired. Only the DCE-MR images were used in this study.

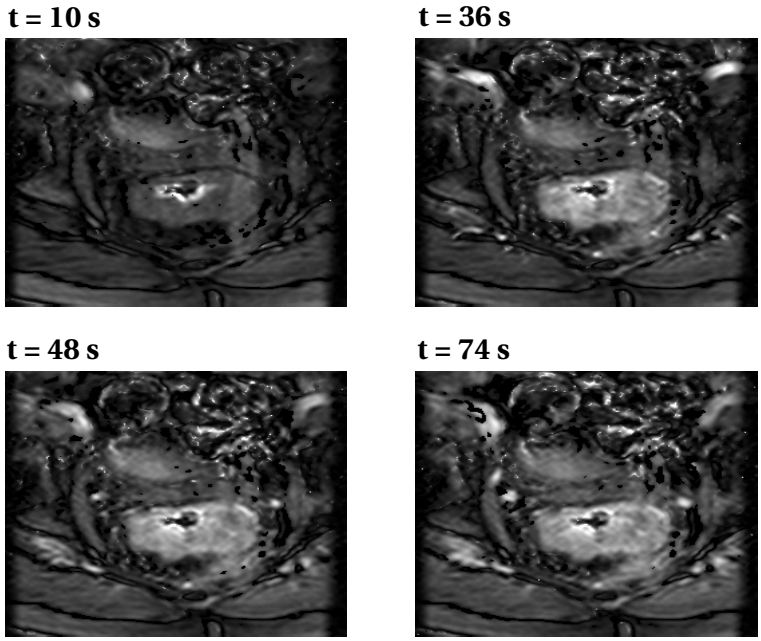

Figure 3.2: DCE-MR images of one of the patients in the Oxytarget study, showing the distribution of contrast agent after 10 s, 36 s, 48 s, and 74 s. The axes indicate the pixel locations. There is little contrast in the first image, which is before any contrast agent has entered the blood stream. In the second image, the signal in the tumour (in the centre of the image) and the two arteries in the upper corners is enhanced. In the last image the signal enhancement in the arteries has decreased, but the signal enhancement in the tumour is still present.

3.4 Image Analysis

The images were first sorted into four-dimensional matrices, using the script found in appendix A.1, with three spatial dimensions (sagittal, coronal, and axial) and one temporal. Thus signal intensity curves for each pixel in the images were available from the matrix, from which RSI curves could be calculated using

$$RSI(t) = \frac{S(t) - S_0}{S_0}. \tag{3.1}$$

An example of an RSI curve compared to a signal intensity curve can be seen in figure 3.3.

Curve fitting was performed to estimate the model parameters described in table 3.3, scripts for which are attached in appendix A.2.3 for the Brix model and appendix A.2.2 for the two versions of the TK model. The Matlab function *fit* was used, and in all cases, the maximum number of evaluations of model allowed (*MaxFunEvals*) was set to 2000 and the maximum number of iterations allowed for fit (*MaxIter*) was set to 800, with method set to *NonLinearLeastSquares* [41]. Further details about the different curve fits are presented in table 3.4.

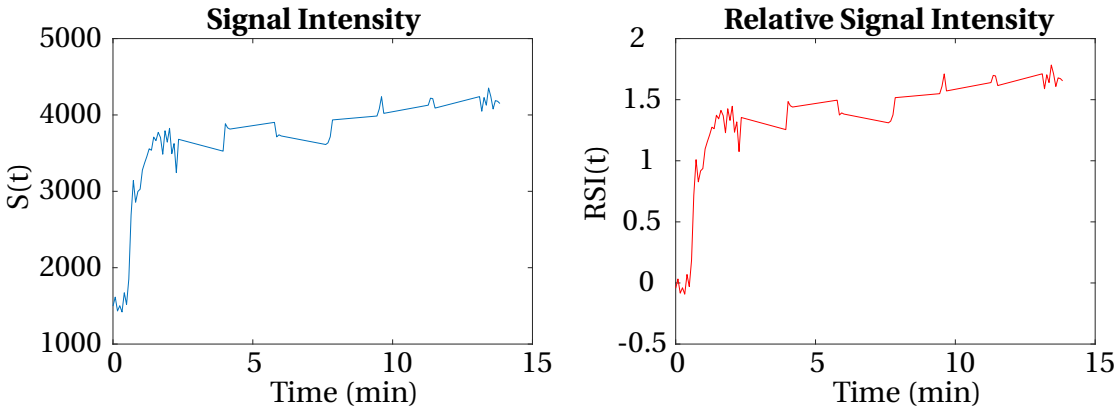

Figure 3.3: Example of the measured signal intensity in one pixel, and the RSI calculated from equation 3.1. The curves are disjointed due to the alternation between acquisition of dynamic and morphological images, described in section 3.3 [42].

Parameter	Description	Unit
	The AIF	
a_1	Amplitude of the fast exponential decay, which describes leakage into the interstitium [43].	kgl^{-1}
m_1	Rate constant of fast exponential decay.	min^{-1}
a_2	Amplitude of slow exponential decay, which describes excretion through the kidneys [43].	kgl^{-1}
m_2	Rate constant of slow exponential decay.	min^{-1}
	The TK model	
K^{trans}	Contrast agent volume transfer constant from intravascular space to EES.	min^{-1}
v_e	EES volume per unit volume of tissue	%
v_p	Intravascular space volume per unit volume of tissue	%
k_{ep}	Contrast agent rate constant from EES to intravascular space.	min^{-1}
	The Brix model	
A_{Brix}	Decides magnitude of enhancement in curve. Dependent on perfusion, EES volume, intravascular volume permeability and contrast agent dose [44].	None
k_{ep}	Contrast agent rate constant from EES to intravascular space.	min^{-1}
k_{el}	Contrast agent clearance rate constant from intravascular space.	min^{-1}

Table 3.3: The following parameters were estimated for the AIF, TK model, and the Brix model. The parameters for the TK model were estimated in two different ways: from a population-based AIF and from individual AIFs.

Model	Algorithm	Robust	Limits	
AIF	Levenberg-Marquadt	None	None	
TK	Trust-Region	Bisquare	K^{trans}:	(0 , 10)
			v_e:	(0 , 1)
			v_p:	(0 , 1)
Brix	Trust-Region	Bisquare	A_{Brix}:	(0 , 500)
			k_{el}:	(0 , 500)
			k_{ep}:	(0 , 500)

Table 3.4: Algorithms and limits used for the different curve fits. The settings for the TK model analysis with the population-based AIF and individual AIFs were identical. During the curve fitting v_e and v_p were fractions with no units. After estimation both fractions were multiplied with 100 % so that both parameters had unit %.

The AIF

The AIF was estimated for all patients using the scripts in appendix A.2.1. Arteries were located by inspecting the images at the time of peak and chosen based on the amount of noise in the image and size of the vessel. An ROI was drawn around the chosen artery for each patient, and signal intensity curves were measured within the ROI. An estimation of the contrast agent concentration in the blood $C_p(t)$ was calculated from the signal intensity curves by applying equations 2.16 and 2.18, and fitted to equation 2.17, with $D = 0.1\,\text{mmol}\,\text{kg}^{-1}$, and the hematocrit value set to 0.41 for women and 0.47 for men. The median of the fitted AIF parameters within the ROIs were calculated for each patient.

All fitted AIFs were examined, and those that did not obviously deviate from the measured data, and had a visible peak, were deemed suitable. An example can be seen in figure 3.4. A population-based AIF was calculated from the suitable AIFs, and the deviations from the population-based AIF parameters were examined for each patient. The unsuccessful individual AIFs were replaced with the population-based AIF prior to further analyses.

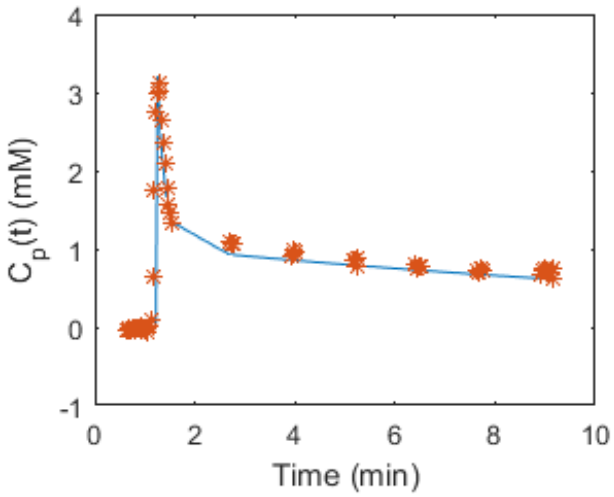

Figure 3.4: **a)** An example of a successful AIF approximation. The red dots indicate the measured data, and the blue line the fitted function. In the time prior to contrast agent injection, the contrast agent concentration was considered to be 0 mM.

The TK model

The TK model parameters K^{trans}, v_e, v_p, and k_{ep} were estimated using the scripts found in appendix A.2.2. Based on the maximum thresholds used by Grøvik in 2017, pixels where either $K^{trans} > 3$, $v_e > 80$ or $v_p > 20$, were considered to be nonphysiological and were thus omitted from further analysis [4]. k_{ep} was calculated from $k_{ep} = K^{trans}/v_e$. Because sometimes $v_e = 0$, a significant amount of NaN-values occurred in the k_{ep} matrices. These were removed prior to calculation of the k_{ep} medians.

The equation used for fitting the measured data to the TK model, was derived by inserting equation 2.17 into equation 2.21:

$$C_t(t) = v_p C_p(t) + K^{trans} D e^{-k_{ep}t}\left[a_1 \frac{1 - e^{(k_{ep}-m_1)t}}{m_1 - k_{ep}} + a_2 \frac{1 - e^{(k_{ep}-m_2)t}}{m_2 - k_{ep}}\right] \tag{3.2}$$

where $k_{ep} = K^{trans}/v_e$ and $C_p(t)$ is the AIF. Estimated tissue contrast agent concentration curves were calculated by applying equation 2.15 to the signal intensity curves. The TK model parameters were estimated by fitting the tissue contrast agent concentration curves to equation 3.2. The TK model was applied for all image data using the population-based AIF, and additionally using individual AIFs whenever successful individual AIFs were available.

The Brix Model

The Brix model parameters A_{Brix}, k_{el}, and k_{ep} were estimated using the script found in appendix A.2.3. For each patient, the RSI curves within the tumour ROI were fitted to equation 2.25. Values for the parameters were thus found for all pixels within the tumours. Pixels where either $A_{Brix} > 7$, $k_{el} > 2$ or $k_{ep} > 40$ were considered as nonphysiological values resulting from poor curve fits, and were therefore removed prior to further analysis.

3.5 Data Analysis

All statistical analyses of associations between the parameter values described in table 3.3 and treatment response or tumour aggressiveness were performed using the Mann-Whitney U test [45]. Presented by Mann and Whitney in 1947, the test is nonparametric and compares two groups, returning a p-value that indicates how likely it is that the groups originate from the same distribution. It does not require the test parameters to be from a normal distribution, and thus works well for the median and percentile values estimated in this study. Analyses on median parameter values and heterogeneity were performed using the scripts in appendix A.3.

3.5.1 Pretreatment Data

The different pretreatment median parameters of the patients were divided into groups based on TRG and TNM-stages that were considered positive or negative with regard to treatment response or aggressiveness. For example, separating patients with TRG 0 and TRG 1-3 into different groups to separate a good and poor histomorphological tumour response to CRT. The endpoints and the number of patients in the endpoint based groups are presented in table 3.5. When testing for decrease in N-stage, patients with mrN 0 were excluded, as a decrease for these patients would not be possible. Box plots were created for statistically significant results to illustrate the differences between the groups.

Heterogeneity analysis was performed for the parameters and endpoints where analysis on the median parameters gave statistically significant ($p < 0.05$) results. This included p-values plotted for the different parameter percentiles, in order to examine the stability of the statistical significance found for the parameter medians, and histogram analysis.

The histogram analysis was performed by creating parameter histograms for each patient using Matlab. From the histograms, values of the following quantities were calculated:

- **Standard deviation (SD):** Indicator of variation in bin heights. Increases for a high variation, which occurs if most parameter values are closely centered around a value [46].

Endpoint	CRT		Endpoint	No CRT	
	Group 1	Group 2		Group 1	Group 2
ypT 0-2 versus 3-4	15	28	pT 0-2 versus 3-4	24	24
ypN 0 versus 1-2	25	18	pN 0 versus 1-2	29	19
TRG 0 versus 1-3	5	38			
ΔT 0-2 versus 3-4	37	6			
ΔN 0 versus 1-2	10	20			

Table 3.5: The endpoints used in the Mann-Whitney U test and the number of patients in the endpoint based groups for the pretreatment data. Respectively Group 1 and Group 2 contain the first and second class mentioned in the endpoint. ΔT 0-2 versus 3-4 represents the magnitude of decrease in T-stage between mrT- and ypT-stage. ΔN 0 versus 1-2 describes the decrease in N-stage from mrN to ypN, where ΔN 0 represents no decrease, and patients with mrN 0, who would be unable to achieve a decrease, were not included.

- **Kurtosis:** Indicates the amount of extreme outliers. The value of kurtosis increases with the number of outliers [47].
- **Relative peak height (RPH):** Peak height divided by the mean bin height.
- **Skewness:** Asymmetry around the peak of a histogram. Positive skewness indicates that there are more bins on the right side of the peak than on the left [48].

The quantities were then divided into groups based on the endpoints in table 3.5, and box plots were created for the statistically significant results.

3.5.2 Post-CRT Data

For the 18 patients where both pretreatment and post-CRT data were available, the medians of the post-CRT model parameters, and the change in the median model parameters during CRT were calculated. Using the Mann-Whitney U test, they were compared to treatment response using the endpoints presented in table 3.6. Box plots were created for statistically significant results.

Endpoint	Group 1	Group 2
ypT 0-2 versus 3-4	8	10
ypN 0 versus 1-2	11	7
TRG 0 versus 1-3	3	15
ΔT 0-2 versus 3-4	15	3
ΔN 0 versus 1-2	10	8

Table 3.6: The endpoints used in the Mann-Whitney U test and the number of patients in the endpoint based groups for the post-CRT data. Respectively Group 1 and Group 2 contain the first and second class mentioned in the endpoint. ΔT 0-2 versus 3-4 represents the decrease in T-stage from mrT- to ypT-stage, and ΔN 0 versus 1-2 describes the decrease between mrN and ypN, where ΔN 0 represents no decrease, and patients with mrN 0 were not included.

Chapter 4

Results

4.1 The AIF

In total, 90 individual AIFs were estimated successfully: 41 for the group that did not receive CRT, and in the group that received CRT: 36 pretreatment images (15 of which were for the patients where post-CRT images were also available) and 13 for the image data acquired post-CRT. The value and range of the population-based AIF parameters are displayed in table 4.1. Deviations from the population-based parameters for the different individual AIFs are shown in figure 4.1.

	Mean (range)
a1 (kgl^{-1})	10.54 (1.95 , 42.07)
a2 (kgl^{-1})	6.84 (1.14 , 26.30)
m1 (min^{-1})	8.87 (0.06 , 40.42)
m2 (min^{-1})	0.50 (0.00 , 8.33)

Table 4.1: The population-based AIF parameters, calculated by taking the mean of the medians for the different patients. The minimum and maximum values of the parameter medians indicate the range.

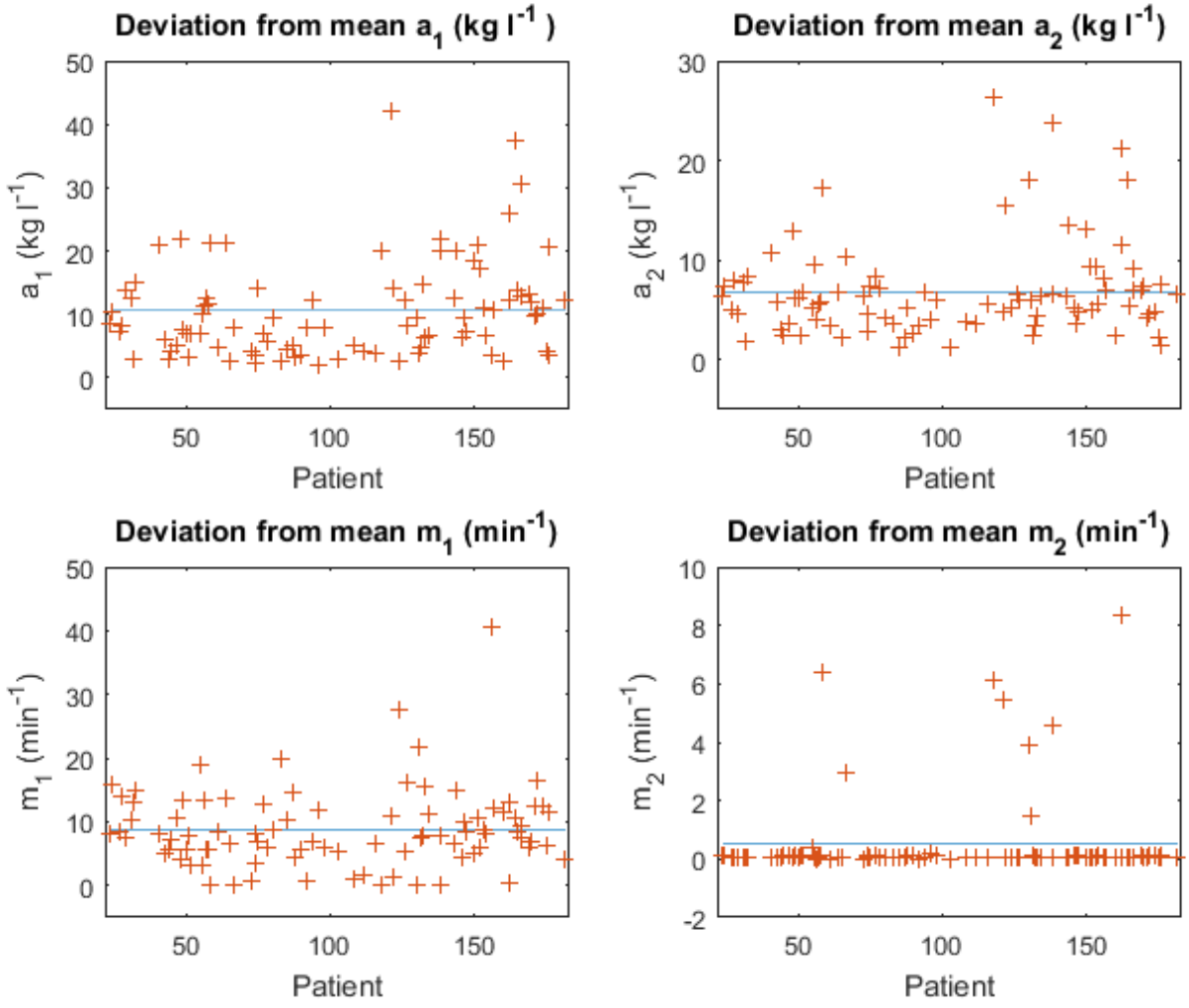

Figure 4.1: Deviations from the population-based AIF parameters for the different patients. The blue line indicates the mean value of the parameter. The y-axis indicates the parameter and the x-axis indicates the patient identification number from the Oxytarget study.

4.2 Analysis of Pretreatment Data

The results from the Mann-Whitney U test from the TK model with the population-based AIF, along with parameter medians and ranges in the different endpoints, are presented in table 4.2. No statistically significant associations with treatment response were found.

The results from the Mann-Whitney U test from the TK model with individual AIFs, along with parameter medians and ranges in the different endpoints, are presented in table 4.3. v_e signif-

Parameter		Median (range)		p-value
		Group 1	Group 2	
		Patients that received CRT		
K^{trans} (min^{-1})	ypT 0-2 versus 3-4	0.49 (0.00 , 2.20)	0.20 (0.00 , 1.29)	0.150
	ypN 0 versus 1-2	0.28 (0.00 , 2.20)	0.16 (0.00 , 0.89)	0.059
	TRG 0 versus 1-3	0.40 (0.00 , 2.20)	0.23 (0.00 , 1.32)	0.415
	ΔT 0-2 versus 3-4	0.23 (0.00 , 1.32)	0.30 (0.00 , 2.20)	0.739
	ΔN 0 versus 1-2	0.14 (0.00 , 0.50)	0.29 (0.00 , 2.20)	0.113
v_e (%)	ypT 0-2 versus 3-4	33.68 (0.05 , 50.37)	27.34 (0.00 , 64.90)	0.549
	ypN 0 versus 1-2	31.56 (0.00 , 64.90)	21.57 (0.00 , 58.54)	0.273
	TRG 0 versus 1-3	15.05 (0.05 , 48.13)	30.64 (0.00 , 64.90)	0.636
	ΔT 0-2 versus 3-4	31.56 (0.00 , 64.90)	14.82 (0.05 , 48.13)	0.371
	ΔN 0 versus 1-2	26.69 (0.00 , 54.57)	24.06 (0.00 , 64.90)	0.965
v_p (%)	ypT 0-2 versus 3-4	1.14 (0.00 , 4.10)	0.58 (0.00 , 10.09)	0.929
	ypN 0 versus 1-2	1.16 (0.00 , 10.09)	0.23 (0.00 , 8.69)	0.563
	TRG 0 versus 1-3	1.16 (0.00 , 2.43)	0.89 (0.00 , 10.09)	0.747
	ΔT 0-2 versus 3-4	0.72 (0.00 , 10.09)	1.11 (0.00 , 2.43)	0.766
	ΔN 0 versus 1-2	0.22 (0.00 , 8.69)	1.58 (0.00 , 10.09)	0.509
k_{ep} (min^{-1})	ypT 0-2 versus 3-4	1.98 (0.21 , 15.17)	1.83 (0.62 , 4.29)	0.566
	ypN 0 versus 1-2	1.98 (0.21 , 15.17)	1.80 (0.62 , 4.29)	0.777
	TRG 0 versus 1-3	1.98 (1.53 , 15.17)	1.82 (0.21 , 4.29)	0.179
	ΔT 0-2 versus 3-4	1.83 (0.21 , 4.29)	1.98 (0.24 , 15.17)	0.587
	ΔN 0 versus 1-2	1.48 (0.62 , 4.29)	1.87 (0.24 , 15.17)	0.391
		Patients that did not receive CRT		
K^{trans} (min^{-1})	pT 0-2 versus 3-4	0.59 (0.00 , 1.33)	0.17 (0.00 , 1.32)	0.190
	pN 0 versus 1-2	0.29 (0.00 , 1.33)	0.26 (0.00 , 1.32)	0.983
v_e (%)	pT 0-2 versus 3-4	36.42 (0.00 , 65.69)	27.04 (0.00 , 57.42)	0.197
	pN 0 versus 1-2	32.63 (0.00 , 65.69)	35.39 (0.00 , 57.45)	0.966
v_p (%)	pT 0-2 versus 3-4	0.01 (0.00 , 4.05)	0.18 (0.00 , 2.37)	0.556
	pN 0 versus 1-2	0.00 (0.00 , 2.60)	0.35 (0.00 , 4.05)	0.598
k_{ep} (min^{-1})	pT 0-2 versus 3-4	1.94 (0.28 , 4.77)	1.63 (0.19 , 3.79)	0.703
	pN 0 versus 1-2	1.80 (0.28 , 3.65)	1.59 (0.19 , 4.77)	0.850

Table 4.2: Results of the Mann-Whitney U test for different endpoints on the median pretreatment parameters from the TK model with the population-based AIF. The group of patients that received neoadjuvant CRT is presented first, followed by the group that did not receive CRT. p-values < 0.05 were considered statistically significant. The groups are presented with median values and ranges of the median parameters for the different patients.

icantly differentiated patients with good treatment response (ypT 0-2, TRG 0, and ΔT 3-4) from patients with poor treatment response (ypT 3-4, TRG 1-3, and ΔT 0-2) in the group of patients that received CRT. Box plots illustrating the median values of v_e for the patients in the different

Parameter		**Median (range)**		**p-value**
		Group 1	**Group 2**	
		Patients that received CRT		
K^{trans} (min^{-1})	ypT 0-2 versus 3-4	0.44 (0.00 , 1.96)	0.38 (0.00 , 2.00)	0.656
	ypN 0 versus 1-2	0.33 (0.00 , 2.00)	0.53 (0.00 , 1.64)	0.721
	TRG 0 versus 1-3	0.33 (0.00 , 1.96)	0.47 (0.00 , 2.00)	0.507
	ΔT 0-2 versus 3-4	0.49 (0.00 , 2.00)	0.27 (0.00 , 1.96)	0.301
	ΔN 0 versus 1-2	0.49 (0.02 , 1.64)	0.50 (0.00 , 2.00)	0.741
v_e (%)	ypT 0-2 versus 3-4	28.18 (0.00 , 51.44)	44.46 (0.00 , 66.26)	**0.045**
	ypN 0 versus 1-2	34.39 (0.00 , 65.98)	42.87 (0.00 , 66.26)	0.438
	TRG 0 versus 1-3	14.34 (0.00 , 34.39)	42.44 (0.00 , 66.26)	**0.022**
	ΔT 0-2 versus 3-4	42.96 (0.00 , 66.26)	14.52 (0.00 , 34.39)	**0.009**
	ΔN 0 versus 1-2	46.97 (1.71 , 66.26)	34.30 (0.00 , 65.98)	0.153
v_p (%)	ypT 0-2 versus 3-4	0.54 (0.00 , 5.18)	1.75 (0.00 , 14.82)	0.221
	ypN 0 versus 1-2	0.54 (0.00 , 14.82)	2.52 (0.00 , 9.00)	0.614
	TRG 0 versus 1-3	0.00 (0.00 , 2.55)	1.75 (0.00 , 14.82)	0.069
	ΔT 0-2 versus 3-4	1.17 (0.00 , 14.82)	0.27 (0.00 , 5.12)	0.220
	ΔN 0 versus 1-2	1.38 (0.00 , 9.00)	0.58 (0.00 , 14.82)	0.895
k_{ep} (min^{-1})	ypT 0-2 versus 3-4	2.42 (0.82 , 16.10)	1.89 (0.33 , 5.01)	0.136
	ypN 0 versus 1-2	1.87 (0.33 , 16.10)	2.16 (0.37 , 5.01)	0.530
	TRG 0 versus 1-3	1.75 (0.99 , 16.10)	2.16 (0.33 , 5.01)	0.691
	ΔT 0-2 versus 3-4	2.10 (0.33 , 5.01)	2.24 (0.99 , 16.10)	0.540
	ΔN 0 versus 1-2	1.81 (0.37 , 3.15)	2.56 (0.33 , 16.10)	0.194
		Patients that did not receive CRT		
K^{trans} (min^{-1})	pT 0-2 versus 3-4	0.75 (0.00 , 1.76)	0.75 (0.00 , 1.97)	0.934
	pN 0 versus 1-2	0.72 (0.00 , 1.97)	0.78 (0.00 , 1.41)	0.584
v_e (%)	pT 0-2 versus 3-4	35.01 (0.00 , 64.03)	31.46 (0.00 , 60.82)	0.711
	pN 0 versus 1-2	32.40 (0.00 , 64.03)	33.41 (0.00 , 60.82)	0.736
v_p (%)	pT 0-2 versus 3-4	0.10 (0.00 , 2.37)	0.00 (0.00 , 4.92)	0.757
	pN 0 versus 1-2	0.05 (0.00 , 2.72)	0.00 (0.00 , 4.92)	0.673
k_{ep} (min^{-1})	pT 0-2 versus 3-4	2.29 (0.28 , 4.77)	2.78 (0.73 , 4.22)	0.703
	pN 0 versus 1-2	2.70 (0.28 , 4.22)	2.33 (0.73 , 4.77)	0.866

Table 4.3: Results of the Mann-Whitney U test for different endpoints on the pretreatment median parameters from the TK model with individual AIFs. The group of patients that received neoadjuvant CRT is presented first, followed by the group that did not receive CRT. Emphasised in bold, p-values < 0.05 were considered statistically significant. The groups are presented with median values and ranges of the median parameters for the different patients.

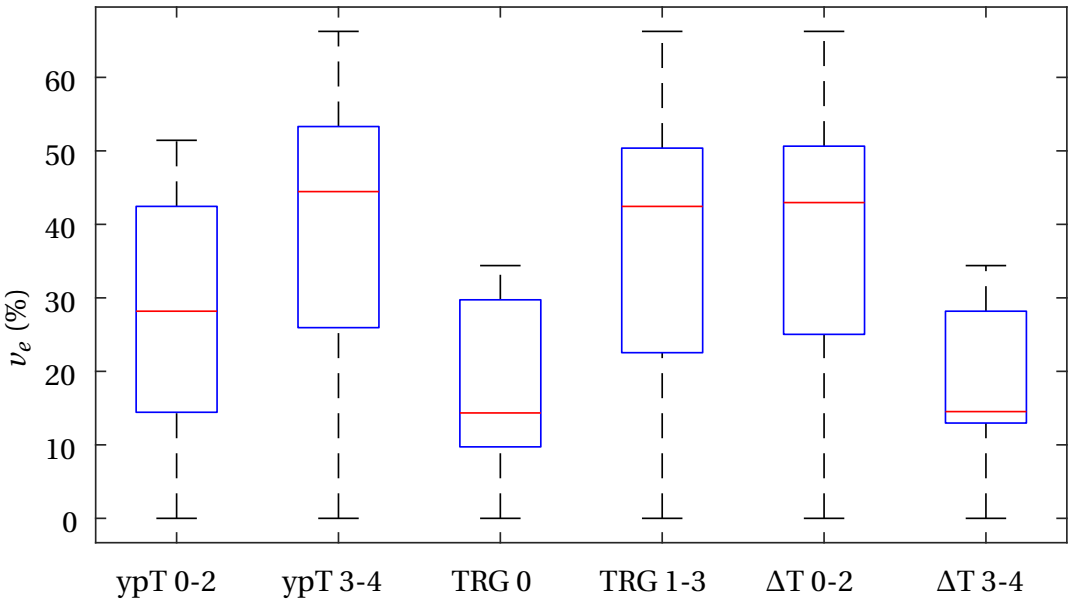

Figure 4.2: Box plots for the median pretreatment v_e from the TK model with individual AIFs, for patients with ypT 0-2, TRG 0, and ΔT 3-4 (good treatment response) compared to patients with ypT 3-4, TRG 1-3, and ΔT 0-2 (poor treatment response). The central mark, bottom and top of the boxes respectively indicate the median, 25th and 75th percentile, and the whiskers indicate the most extreme values not considered outliers. Outliers are plotted individually using the '+' symbol. Patients with good treatment response generally had the lowest median v_e.

groups are shown in figure 4.2, and it can be seen that v_e was generally higher for patients with poor treatment response than for patients with good treatment response.

The results of the Mann-Whitney U test on the Brix model parameters, along with parameter medians and ranges in the different endpoints, are presented in table 4.4. The medians of A_{Brix} significantly differentiated patients with ypT 0-2 (good treatment response) from patients with ypT 3-4 (poor treatment response), and k_{ep} significantly differentiated patients with ΔT 3-4 (good treatment response) from ΔT 0-2 (poor treatment response). Box plots illustrating the values of the parameter medians in the different groups are presented in figure 4.3. It can be seen that both the median A_{Brix} and k_{ep} were higher for the poor treatment response groups than for the good treatment response groups.

Parameter	Endpoint	Median (range)		p-value
		Group 1	Group 2	
		Patients that received CRT		
A_{Brix}	ypT 0-2 versus 3-4	1.40 (0.89 , 2.90)	1.57 (1.03 , 2.09)	**0.018**
	ypN 0 versus 1-2	1.44 (1.03 , 2.90)	1.55 (0.89 , 2.09)	0.468
	TRG 0 versus 1-3	1.49 (1.32 , 2.90)	1.51 (0.89 , 2.09)	0.865
	ΔT 0-2 versus 3-4	1.52 (0.89 , 2.09)	1.46 (1.32 , 2.90)	0.986
	ΔN 0 versus 1-2	1.62 (0.89 , 2.09)	1.43 (1.03 , 2.90)	0.210
k_{el} (min^{-1})	ypT 0-2 versus 3-4	0.04 (0.00 , 1.57)	0.02 (0.00 , 0.08)	0.085
	ypN 0 versus 1-2	0.03 (0.00 , 1.57)	0.02 (0.00 , 0.08)	0.514
	TRG 0 versus 1-3	0.04 (0.01 , 1.57)	0.03 (0.00 , 0.08)	0.233
	ΔT 0-2 versus 3-4	0.03 (0.00 , 0.08)	0.03 (0.00 , 1.57)	0.661
	ΔN 0 versus 1-2	0.01 (0.00 , 0.05)	0.04 (0.00 , 1.57)	0.090
k_{ep} (min^{-1})	ypT 0-2 versus 3-4	5.69 (1.79 , 13.42)	5.04 (1.54 , 21.49)	0.750
	ypN 0 versus 1-2	4.97 (1.54 , 21.49)	5.68 (2.15 , 13.42)	0.597
	TRG 0 versus 1-3	4.06 (1.81 , 5.69)	5.68 (1.54 , 21.49)	0.155
	ΔT 0-2 versus 3-4	5.69 (1.54 , 21.49)	3.71 (1.79 , 5.69)	**0.044**
	ΔN 0 versus 1-2	4.37 (2.15 , 10.91)	5.94 (1.54 , 21.49)	0.226
		Patients that did not receive CRT		
A_{Brix}	pT 0-2 versus 3-4	1.37 (0.55 , 2.40)	1.37 (0.48 , 1.82)	0.658
	pN 0 versus 1-2	1.39 (0.99 , 2.40)	1.31 (0.48 , 1.72)	0.061
k_{el} (min^{-1})	pT 0-2 versus 3-4	0.03 (0.01 , 0.09)	0.03 (0.00 , 0.05)	0.197
	pN 0 versus 1-2	0.03 (0.01 , 0.09)	0.03 (0.00 , 0.05)	0.146
k_{ep} (min^{-1})	pT 0-2 versus 3-4	6.44 (1.70 , 9.91)	6.69 (0.88 , 12.75)	0.439
	pN 0 versus 1-2	6.87 (2.46 , 12.75)	6.06 (0.88 , 9.91)	0.264

Table 4.4: Results of the Mann-Whitney U test for different endpoints on the median pretreatment Brix model parameters. The group of patients that received neoadjuvant CRT is presented first, followed by the group that did not receive CRT. Emphasised in bold, p-values < 0.05 were considered statistically significant. The groups are presented with median values and ranges of the median parameters for the different patients.

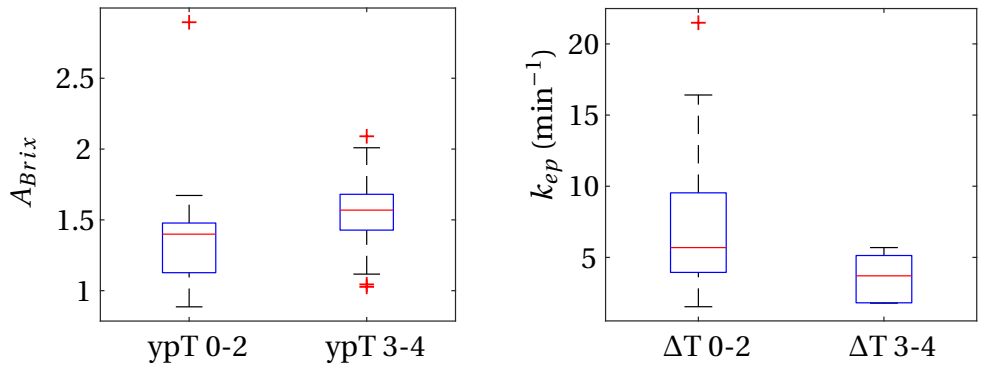

(a) (b)

Figure 4.3: Box plots showing the Brix model pretreatment medians of (**a**) A_{Brix} for the patients with ypT 0-2 (good treatment response) and ypT 3-4 (poor treatment response), and of (**b**) k_{ep} for the patients with ΔT 3-4 (good treatment response), and ΔT 0-2 (poor treatment response). The central mark, bottom and top of the boxes respectively indicate the median, 25th and 75th percentile, and the whiskers indicate the most extreme values not considered outliers. Outliers are plotted individually using the '+' symbol. Patients with good treatment response generally had a low median A_{Brix} and k_{ep}.

4.2.1 Tumour Heterogeneity

Results of the Mann-Whitney U test on the histogram quantities from the significant pretreatment associations are presented in table 4.5. The RPH of k_{ep} from the Brix model significantly

Parameter	**Endpoint**	**p-value**			
		Kurtosis	**RPH**	**Skewness**	**SD**
Patients that received CRT					
The TK model: Individual AIFs					
v_e (%)	ypT 0-2 versus 3-4	0.868	0.789	0.731	0.601
	TRG 0 versus 1-3	0.532	0.437	0.394	0.353
	ΔT 0-2 versus 3-4	0.318	0.285	0.227	0.494
The Brix model					
A_{Brix}	ypT 0-2 versus 3-4	0. 889	0.619	0.809	0.090
k_{ep} (min^{-1})	ΔT 0-2 versus 3-4	0.056	**0.016**	0.056	0.820

Table 4.5: Results of the Mann-Whitney U test for different endpoints on the histogram quantities kurtosis, RPH, skewness, and SD of the pretreatment model parameters. Emphasised in bold, p-values < 0.05 were considered statistically significant.

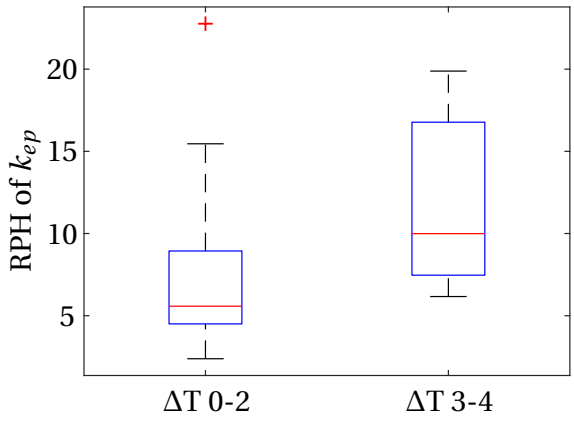

Figure 4.4: Box plots of the RPH of k_{ep} from the Brix model, for patients with ΔT 0-2 (poor treatment response) compared to patients with ΔT 3-4 (good treatment response). The central mark, bottom and top of the boxes respectively indicate the median, 25th and 75th percentile, and the whiskers indicate the most extreme values not considered outliers. Outliers are plotted individually using the '+' symbol. Patients that responded well to treatment generally had a high RPH of k_{ep}.

differentiated ΔT 3-4 (good treatment response) and ΔT 0-2 (poor treatment response). In figure 4.4, box plots illustrate the RPH values in the two groups, and show that the good responders generally had a higher RPH of k_{ep} than the poor responders.

In figure 4.5 the percentile p-values of v_e, from the TK model with individual AIFs, for ypT 0-2 versus ypT 3-4, TRG 0 versus TRG 1-3, and ΔT 0-2 versus ΔT 3-4 are shown. It can be seen that v_e seems to have the highest accuracy (lowest p-values) between the 80th and 95th percentile.

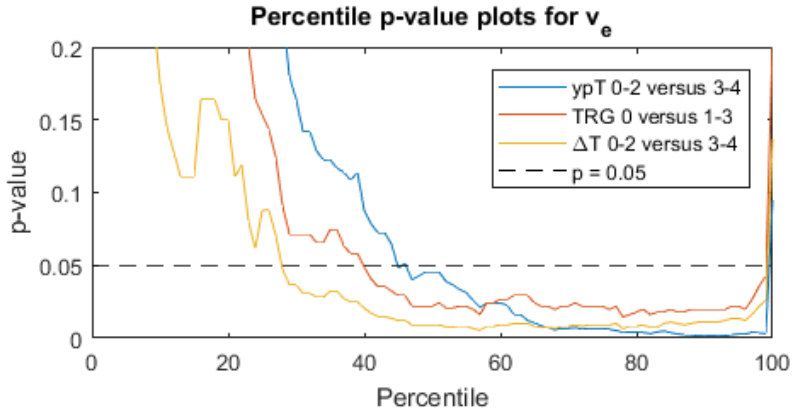

Figure 4.5: Individual AIF-based TK model p-values from the Mann-Whitney U test on the pre-treatment v_e percentiles for ypT 0-2 versus 3-4, TRG 0 versus TRG 1-3, and ΔT 0-2 versus ΔT 3-4.

The percentile plots for the Brix model p-values in figure 4.6, show that the p-value is fairly stable in the range from the 15th to the 50th percentile for A_{Brix} in ypT 0-2 versus 3-4. For k_{ep} in ΔT 0-2 versus 3-4, the lowest p-value is found in the 20th percentile.

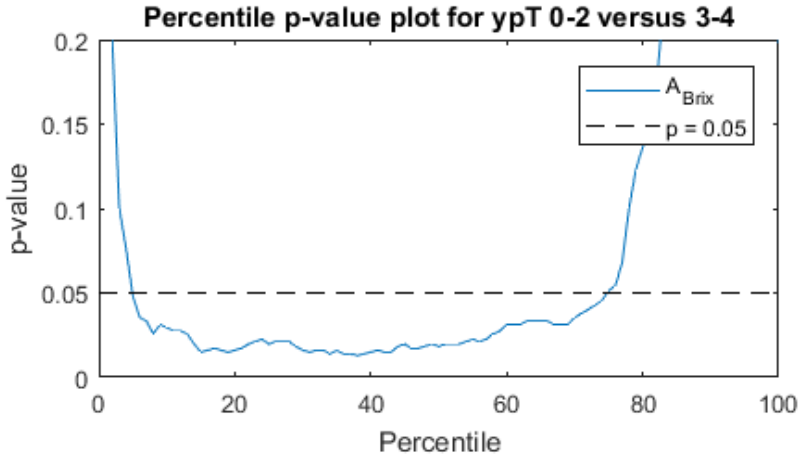

(a)

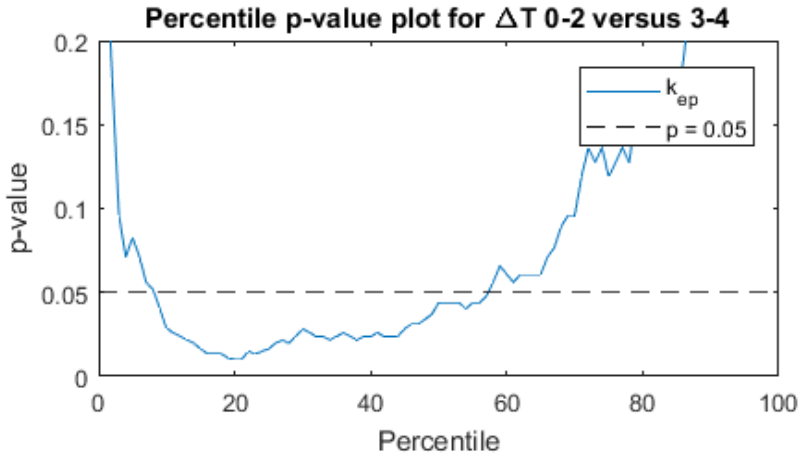

(b)

Figure 4.6: Brix model p-values from the Mann-Whitney U test on the pretreatment parameter percentiles for **a)** A_{Brix} in ypT 0-2 versus ypT 3-4, and **b)** k_{ep} in ΔT 0-2 versus ΔT 3-4.

4.3 Analysis of Post-CRT Data

For the 18 patients from which both pretreatment and post-CRT image data were available, the pretreatment, post-CRT, and change in parameter medians and ranges are displayed in table 4.6. The median parameters generally decreased in response to CRT, with exceptions for k_{ep} in both versions of the TK model, and A_{Brix} in the Brix model.

Parameter	**Median (range)**		Δ
	Pretreatment	**Post-CRT**	
The TK model: population based AIF			
K^{trans} (min^{-1})	0.49 (0.00 , 2.20)	0.01 (0.00 , 1.61)	-0.49
v_e (%)	44.10 (0.00 , 64.90)	0.42 (0.00 , 51.00)	-43.68
v_p (%)	0.40 (0.00 , 8.69)	0.01 (0.00 , 1.61)	-0.40
k_{ep} (min^{-1})	1.94 (0.82 , 15.17)	1.99 (0.61 , 11.78)	0.04
The TK Model: individual AIFs			
K^{trans} (min^{-1})	0.49 (0.11 , 2.00)	0.27 (0.00 , 1.61)	-0.22
v_e (%)	40.41 (12.97 , 65.98)	35.50 (0.00 , 59.51)	-4.91
v_p (%)	0.49 (0.00 , 5.79)	0.00 (0.00 , 8.35)	-0.49
k_{ep} (min^{-1})	1.78 (0.33 , 16.10)	1.97 (0.16 , 3.53)	0.19
The Brix Model			
A_{Brix}	1.51 (0.91 , 2.90)	1.60 (0.98 , 2.71)	0.09
k_{el} (min^{-1})	0.03 (0.00 , 1.57)	0.00 (0.00 , 0.04)	-0.03
k_{ep} (min^{-1})	5.05 (1.54 , 10.91)	3.48 (1.65 , 8.23)	-1.58

Table 4.6: The median and range of the estimated model parameters pre- and post-CRT treatment. The last column displays the difference in model median parameters from before to after the CRT regime. Negative values indicate a decrease in parameter value after CRT.

4.3.1 Post-CRT Medians

The results from the Mann-Whitney U test on the post-CRT median parameters from the TK model with the population-based AIF, along with parameter medians and ranges in the different endpoints, are presented in table 4.7. K^{trans} and v_p significantly differentiated good treatment response (TRG 0 and ΔT 3-4) from poor treatment response (TRG 1-3 and ΔT 0-2). The box plots in figure 4.7 show that K^{trans} and v_p were generally highest for the good responders.

Parameter	**Endpoint**	**Median (range)**		**p-value**
		Group 1	**Group 2**	
K^{trans}	ypT 0-2 versus 3-4	0.22 (0.00 , 1.61)	0.00 (0.00 , 0.29)	0.142
	ypN 0 versus 1-2	0.00 (0.00 , 1.61)	0.01 (0.00 , 0.29)	0.784
	TRG 0 versus TRG 1-3	0.96 (0.16 , 1.61)	0.00 (0.00 , 1.23)	**0.039**
	ΔT 0-2 versus 3-4	0.11 (-1.21 , 2.05)	0.96 (0.16 , 1.61)	**0.039**
	ΔN 0 versus 1-2	0.01 (0.00 , 0.25)	0.08 (0.00 , 1.23)	0.685
v_e (%)	ypT 0-2 versus 3-4	16.69 (0.00 , 51.00)	0.00 (0.00 , 37.59)	0.327
	ypN 0 versus 1-2	0.00 (0.00 , 51.00)	0.84 (0.00 , 26.57)	0.784
	TRG 0 versus TRG 1-3	20.04 (18.23 , 51.00)	0.00 (0.00 , 37.59)	0.056
	ΔT 0-2 versus 3-4	0.00 (0.00 , 37.59)	20.04 (18.23 , 51.00)	0.056
	ΔN 0 versus 1-2	0.84 (0.00 , 26.57)	7.58 (0.00 , 37.59)	0.926
v_p (%)	ypT 0-2 versus 3-4	0.00 (0.00 , 3.08)	0.00 (0.00 , 0.00)	0.173
	ypN 0 versus 1-2	0.00 (0.00 , 3.08)	0.00 (0.00 , 0.00)	0.710
	TRG 0 versus TRG 1-3	0.00 (0.00 , 3.08)	0.00 (0.00 , 2.22)	**0.027**
	ΔT 0-2 versus 3-4	0.00 (0.00 , 2.22)	0.00 (0.00 , 3.08)	**0.027**
	ΔN 0 versus 1-2	0.00 (0.00 , 0.00)	0.00 (0.00, 2.22)	0.685
k_{ep} (min^{-1})	ypT 0-2 versus 3-4	1.99 (0.75 , 4.90)	2.00 (0.61 , 11.78)	1.000
	ypN 0 versus 1-2	2.30 (0.92 , 4.90)	1.40 (0.61 , 11.78)	0.211
	TRG 0 versus TRG 1-3	3.28 (1.27 , 4.90)	1.96 (0.61 , 11.78)	0.426
	ΔT 0-2 versus 3-4	1.96 (0.61 , 11.78)	3.28 (1.27 , 4.90)	0.426
	ΔN 0 versus 1-2	1.32 (0.61 , 11.78)	1.93 (0.92 , 3.30)	0.435

Table 4.7: Results of the Mann-Whitney U test for different endpoints on the post-CRT median parameters of the TK model with a population-based AIF. Emphasised in bold, p-values < 0.05 were considered statistically significant. The groups are presented with median values and ranges of the median parameters for the different patients.

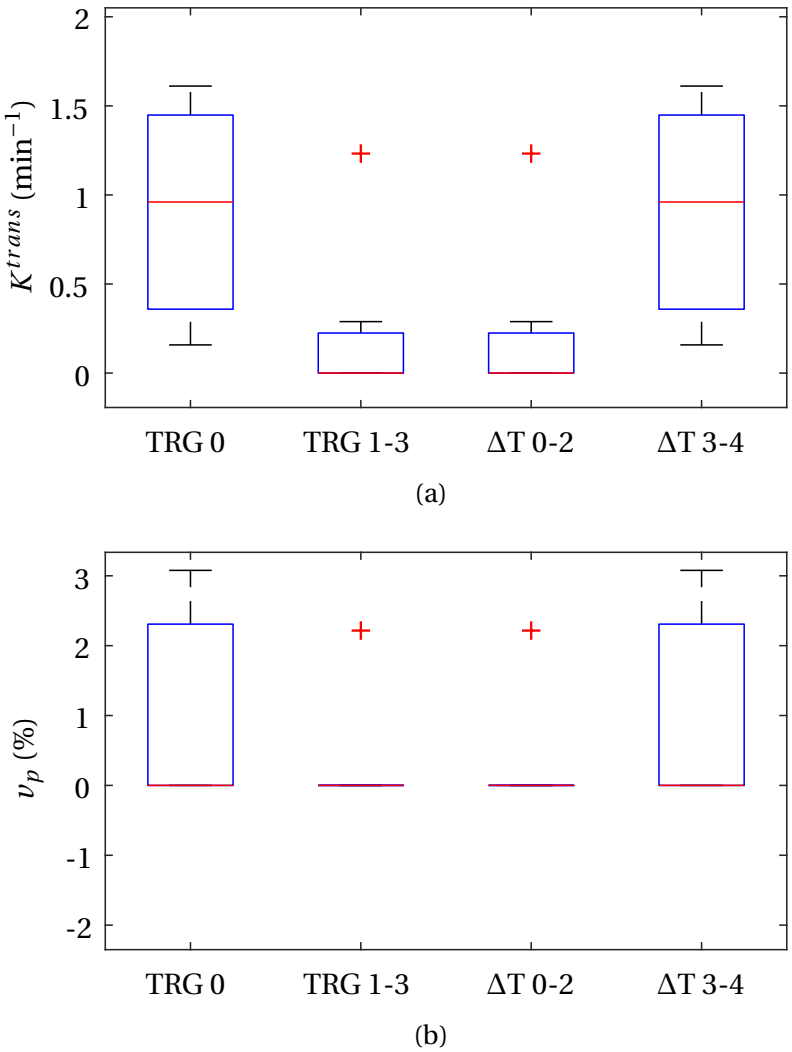

Figure 4.7: Box plots showing the post-CRT medians from the TK model with the population-based AIF, of (**a**) K^{trans} and (**b**) v_p for patients with good treatment response (TRG 0 and ΔT 3-4) and poor treatment response (TRG 1-3 and ΔT 0-2). The central mark, bottom and top of the boxes respectively indicate the median, 25th and 75th percentile, and the whiskers indicate the most extreme values not considered outliers. Outliers are plotted individually using the '+' symbol. Patients with good treatment response generally had a high K^{trans} and v_p.

The results from the Mann-Whitney U test on the post-CRT median parameters from the TK model with individual AIFs, along with parameter medians and ranges in the different end-points, are presented in table 4.8. Significant associations were found for K^{trans} between good

Parameter	Endpoint	Median (range)		p-value
		Group 1	Group 2	
K^{trans}	ypT 0-2 versus 3-4	0.37 (0.00 , 1.61)	0.26 (0.00 , 0.73)	0.554
	ypN 0 versus 1-2	0.08 (0.00 , 1.61)	0.27 (0.11 , 0.87)	0.405
	TRG 0 versus TRG 1-3	1.13 (0.48 , 1.61)	0.25 (0.00 , 0.87)	**0.017**
	ΔT 0-2 versus 3-4	0.25 (0.00 , 0.87)	1.13 (0.48 , 1.61)	**0.017**
	ΔN 0 versus 1-2	0.27 (0.11 , 0.47)	0.28 (0.00 , 0.87)	1.000
v_e (%)	ypT 0-2 versus 3-4	35.50 (0.00 , 59.51)	33.68 (0.00 , 59.20)	0.881
	ypN 0 versus 1-2	26.62 (0.00 , 59.51)	46.49 (20.06 , 59.20)	0.199
	TRG 0 versus TRG 1-3	51.00 (35.68 , 59.51)	26.62 (0.00 , 59.20)	0.076
	ΔT 0-2 versus 3-4	26.62 (0.00 , 59.20)	51.00 (35.68 , 59.51)	0.076
	ΔN 0 versus 1-2	46.49 (26.57 , 59.20)	23.34 (0.00 , 49.89)	0.124
v_p (%)	ypT 0-2 versus 3-4	0.00 (0.00 , 3.08)	1.30 (0.00 , 8.35)	0.302
	ypN 0 versus 1-2	0.00 (0.00 , 6.24)	2.52 (0.00 , 8.35)	**0.033**
	TRG 0 versus TRG 1-3	0.00 (0.00 , 3.08)	0.00 (0.00 , 8.35)	0.716
	ΔT 0-2 versus 3-4	0.00 (0.00 , 8.35)	0.00 (0.00 , 3.08)	0.716
	ΔN 0 versus 1-2	2.52 (0.00 , 8.35)	0.00 (0.00 , 6.24)	0.124
k_{ep} (min^{-1})	ypT 0-2 versus 3-4	1.99 (0.98 , 3.53)	1.20 (0.16 , 3.26)	0.146
	ypN 0 versus 1-2	2.30 (0.16 , 3.53)	1.05 (0.25 , 2.28)	**0.044**
	TRG 0 versus TRG 1-3	1.99 (1.93 , 3.28)	1.96 (0.16 , 3.53)	0.574
	ΔT 0-2 versus 3-4	1.96 (0.16 , 3.53)	1.99 (1.93 , 3.28)	0.426
	ΔN 0 versus 1-2	0.98 (0.25 , 1.32)	2.39 (0.16 , 3.53)	**0.030**

Table 4.8: Results of the Mann-Whitney U test for different endpoints on the post-CRT median parameters from the TK model with individual AIFs. Emphasised in bold, p-values < 0.05 were considered statistically significant. The groups are presented with median values and ranges of the median parameters for the different patients.

responders (TRG 0 and ΔT 3-4) and poor responders (TRG 1-3 and ΔT 0-2), for v_p between ypN 0 (good treatment response) and ypN 1-2 (poor treatment response), and for k_{ep} between good responders (ypN 0 and ΔN 1-2) and poor responders (ypN 1-2 and ΔN 0). In figure 4.8 box plots present the distribution of parameter medians in the different groups. The median K^{trans} and k_{ep} were highest for the good responders, while v_p was generally lowest for the good responders.

Finally, the results from the Mann-Whitney U test on the post-CRT median parameters from the Brix model, along with parameter medians and ranges in the different endpoints, are presented in table 4.9. The post-CRT median k_{ep} was found to significantly differentiate good (ΔN 1-2) and poor (ΔN 0) responders. Illustrated in figure 4.9, a high k_{ep} was associated with a good treatment response.

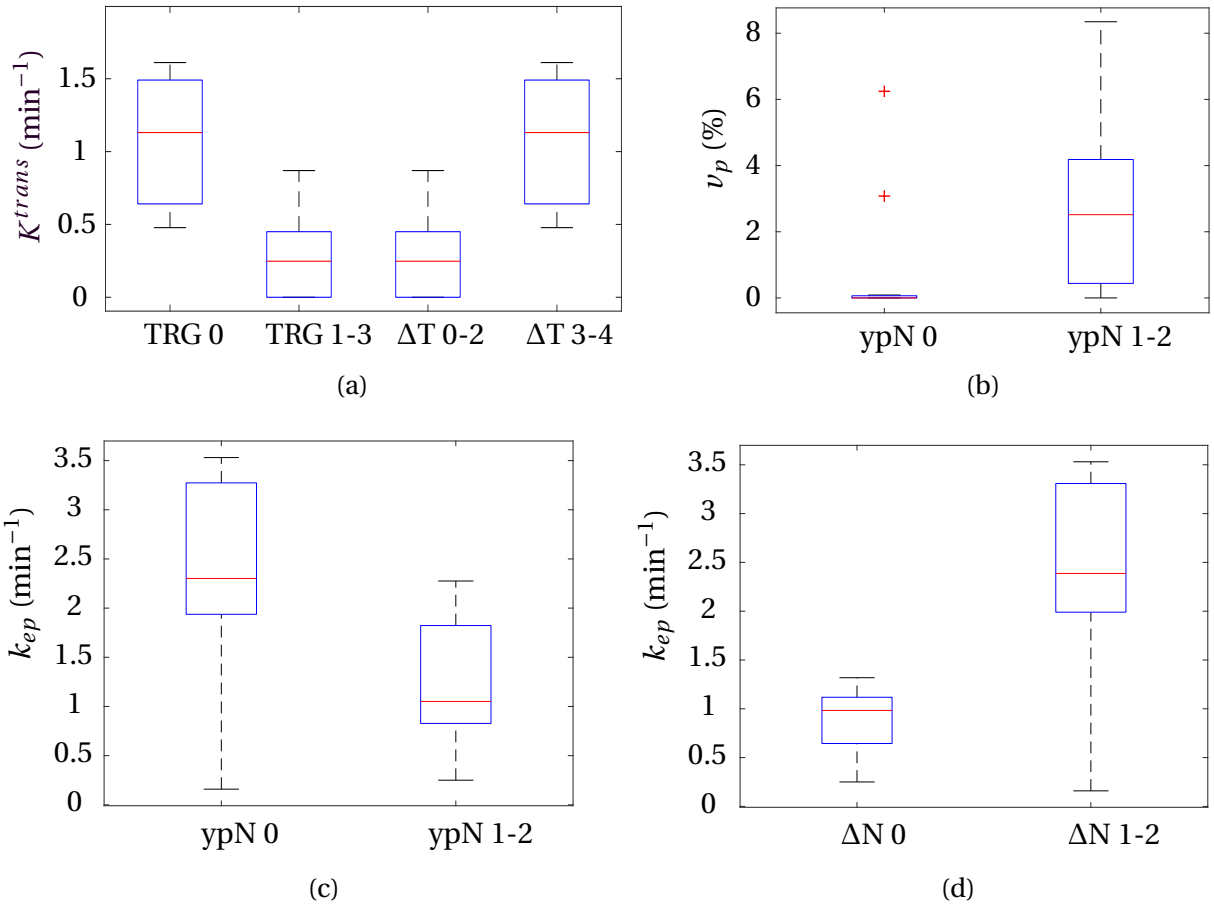

Figure 4.8: Box plots showing the post-CRT individual AIF-based TK model medians of **(a)** K^{trans} for patients with good treatment response (TRG 0 and ΔT 3-4) and poor treatment response (TRG 1-3 and ΔT 0-2), of **(b)** v_p for patients with good treatment response (ypN 0) and poor treatment response (ypN 1-2), and in **(c)** and **(d)** for k_{ep} for patients with good treatment response (ypN 0 and ΔN 1-2) and poor treatment response (ypN 1-2 and ΔN 0). The central mark, bottom and top of the boxes respectively indicate the median, 25th and 75th percentile, and the whiskers indicate the most extreme values not considered outliers. Outliers are plotted individually using the '+' symbol. Patients with good treatment response generally had a high K^{trans} and k_{ep} and a low v_p compared to the poor responders.

Parameter	Endpoint	Median (range)		p-value
		Group 1	Group 2	
A_{Brix}	ypT 0-2 versus 3-4	1.50 (0.98 , 2.71)	1.65 (1.29 , 2.26)	0.360
	ypN 0 versus 1-2	1.52 (0.98 , 2.71)	1.65 (1.25 , 2.10)	1.000
	TRG 0 versus TRG 1-3	1.48 (1.27 , 2.71)	1.65 (0.98 , 2.26)	0.912
	ΔT 0-2 versus 3-4	1.65 (0.98 , 2.26)	1.48 (1.27 , 2.71)	0.912
	ΔN 0 versus 1-2	1.65 (1.25 , 1.83)	1.72 (1.27 , 2.18)	0.354
k_{el} (min^{-1})	ypT 0-2 versus 3-4	0.00 (0.00 , 0.04)	0.01 (0.00 , 0.02)	0.829
	ypN 0 versus 1-2	0.00 (0.00 , 0.04)	0.00 (0.00 , 0.04)	0.659
	TRG 0 versus TRG 1-3	0.00 (0.00 , 0.01)	0.00 (0.00 , 0.04)	0.912
	ΔT 0-2 versus 3-4	0.00 (0.00 , 0.04)	0.00 (0.00 , 0.01)	0.912
	ΔN 0 versus 1-2	0.00 (0.00 , 0.01)	0.01 (0.00 , 0.04)	0.354
k_{ep} (min^{-1})	ypT 0-2 versus 3-4	3.57 (2.94 , 8.23)	3.48 (1.65 , 6.89)	0.573
	ypN 0 versus 1-2	3.76 (2.94 , 8.23)	2.79 (1.65 , 6.89)	0.069
	TRG 0 versus TRG 1-3	2.96 (2.94 , 3.79)	3.56 (1.65 , 8.23)	0.654
	ΔT 0-2 versus 3-4	3.56 (1.65 , 8.23)	2.96 (2.94 , 3.79)	0.654
	ΔN 0 versus 1-2	2.39 (1.65 , 3.20)	3.83 (2.94 , 8.23)	**0.003**

Table 4.9: Results of the Mann-Whitney U test for different endpoints on the post-CRT median Brix model parameters. Emphasised in bold, p-values < 0.05 were considered statistically significant. The groups are presented with median values and ranges of the median parameters for the different patients.

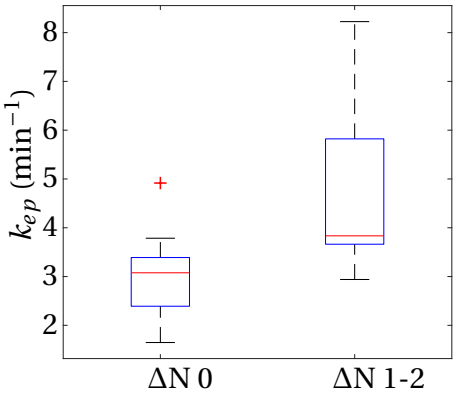

Figure 4.9: Box plots showing the post-CRT Brix model medians of k_{ep} for the groups of patients with ΔN 1-2 (good treatment response) and ΔN 0 (poor treatment response). The central mark, bottom and top of the boxes respectively indicate the median, 25th and 75th percentile, and the whiskers indicate the most extreme values not considered outliers. In general k_{ep} was higher for the patients with good treatment response than for the poor responders.

4.3.2 Change in Median Parameters from CRT

The results for the Mann-Whitney U test on the change in median parameter of the TK model with a population-based AIF, along with medians and ranges of parameter changes in the different endpoints, are shown in table 4.10. Δv_e significantly differentiated patients with good treatment response (TRG 0 and ΔT 3-4) and patients with poor treatment response (TRG 1-3 and ΔT 0-2). Illustrated in the box plots in figure 4.10, there was a significant decrease in v_e for poor responders.

Parameter	**Endpoint**	**Median (range)**		**p-value**
		Group 1	**Group 2**	
ΔK^{trans}	ypT 0-2 versus 3-4	0.35 (-1.21 , 2.05)	0.24 (0.00 , 1.29)	0.762
	ypN 0 versus 1-2	-0.23 (-2.05 , 1.21)	-0.37 (-0.89 , -0.01)	1.000
	TRG 0 versus TRG 1-3	-0.11 (-2.05 , 1.21)	-0.32 (-1.29, 0.00)	0.738
	ΔT 0-2 versus 3-4	-0.32 (-1.29 , 0.00)	-0.11 (-2.05 , 1.21)	0.738
	ΔN 0 versus 1-2	-0.25 (-0.49 , -0.01)	-0.35 (-2.05 , 0.00)	0.524
Δv_e (%)	ypT 0-2 versus 3-4	-22.17 (-50.37 , 3.64)	-23.79 (-62.96 , 0.00)	0.633
	ypN 0 versus 1-2	-20.27 (-62.96 , 3.64)	-28.89 (- 58.54 , -1.79)	0.536
	TRG 0 versus TRG 1-3	2.87 (-15.46 , 3.64)	-28.89 (-62.96 , 0.00)	**0.039**
	ΔT 0-2 versus 3-4	-28.89 (-62.96 , 0.00)	2.87 (-15.46 , 3.64)	**0.039**
	ΔN 0 versus 1-2	-12.99 (-53.72 , -1.79)	-28.10 (-58.54 , 3.64)	1.000
Δv_p (%)	ypT 0-2 versus 3-4	-0.18 (-3.81 , 3.08)	-0.22 (-8.69 , 0.00)	0.897
	ypN 0 versus 1-2	0.00 (-2.43 , 3.08)	-0.44 (8.69 , 0.00)	0.246
	TRG 0 versus TRG 1-3	-2.41 (-2.43 , 3.08)	-0.01 (-8.69 , 0.88)	0.912
	ΔT 0-2 versus 3-4	-0.01 (-8.69 , 0.88)	-2.41 (-2.43 , 3.08)	0.912
	ΔN 0 versus 1-2	-0.44 (-8.69 , 0.00)	-0.01 (-7.29 , 0.88)	0.622
Δk_{ep} (min^{-1})	ypT 0-2 versus 3-4	0.18 (-13.90 , 1.50)	-0.30 (-0.98 , 7.48)	0.515
	ypN 0 versus 1-2	0.33 (-13.90 , 1.50)	0.23 (-1.04 , 7.48)	0.724
	TRG 0 versus TRG 1-3	1.30 (-13.90 , 1.50)	0.23 (-1.04 , 7.48)	0.654
	ΔT 0-2 versus 3-4	0.23 (-1.04 , 7.48)	1.30 (-13.90 , 1.50)	0.654
	ΔN 0 versus 1-2	-0.44 (-1.04 , 7.48)	0.30 (-13.90 , 0.95)	0.622

Table 4.10: Results of the Mann-Whitney U test for different endpoints on the difference between pretreatment and post-CRT median parameters for the TK model with the population-based AIF. Emphasised in bold, p-values < 0.05 were considered statistically significant. The groups are presented with median values and ranges of the median parameter changes for the different patients.

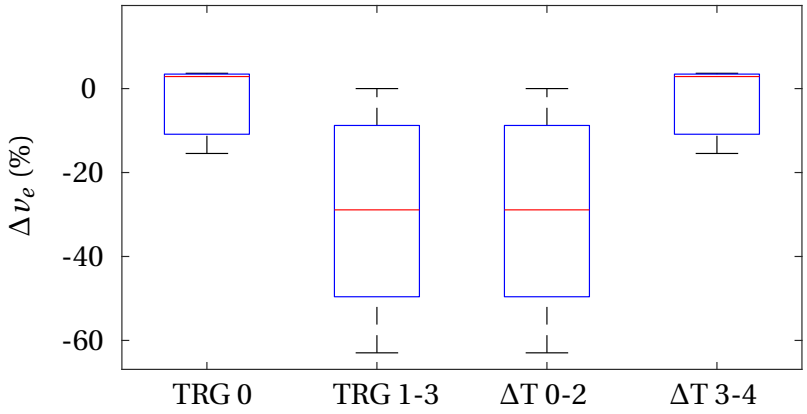

Figure 4.10: Box plots showing the median values of Δv_e from the TK model with the population based AIF, for patients with TRG 0 and Δ T 3-4 (good treatment response) and TRG 1-3 and Δ T 0-2 (poor treatment response). The central mark, bottom and top of the boxes respectively indicate the median, 25th and 75th percentile, and the whiskers indicate the most extreme values not considered outliers. In general there was a bigger reduction in v_e for the poor responders.

The results for the Mann-Whitney U test on the change in median parameter of the TK model with individual AIFs, along with the medians and ranges of parameter changes in the different endpoints, are shown in table 4.11. In figure 4.11 box plots present the distribution of parameter change in the different response groups. For v_e a net increase occurred for patients with good treatment response (TRG 0 and ΔT 3-4) and a net decrease occurred for patients with poor treatment response (TRG 1-3 and ΔT 0-2).

The results for the Mann-Whitney U tests on the change in median parameters of the Brix model, along with the medians and ranges of the parameter changes, are shown in table 4.12. In figure 4.12, box plots illustrate the variations in Δk_{ep} for the patients with good treatment response (ypN 0) and poor treatment response (ypN 1-2), and show that there was a larger decrease in k_{ep} for the poor responders than for the good responders.

Parameter	Endpoint	Median (range)		p-value
		Group 1	Group 2	
ΔK^{trans}	ypT 0-2 versus 3-4	-0.27 (-1.48 , 1.19)	-0.20 (-1.26 , 0.27)	1.000
	ypN 0 versus 1-2	-0.32 (-1.48 , 1.19)	-0.16 (-0.36 , 0.30)	0.246
	TRG 0 versus TRG 1-3	0.80 (-1.48 , 1.19)	-0.25 (-1.26 , 0.30)	0.426
	ΔT 0-2 versus 3-4	-0.25 (-1.26 , 0.30)	0.80 (-1.48 , 1.19)	0.426
	ΔN 0 versus 1-2	-0.16 (-0.25 , 0.06)	-0.58 (-1.48 , 0.30)	0.065
Δv_e (%)	ypT 0-2 versus 3-4	5.39 (-51.44 , 25.12)	-5.83 (-48.12 , 27.11)	0.762
	ypN 0 versus 1-2	-33.79 (-51.44 , 25.12)	1.32 (-29.99 , 27.11)	0.285
	TRG 0 versus TRG 1-3	22.82 (22.71 , 25.12)	-12.99 (-51.44 , 27.11)	**0.039**
	ΔT 0-2 versus 3-4	-12.99 (-51.44 , 27.11)	22.82 (22.71 , 25.12)	**0.039**
	ΔN 0 versus 1-2	1.32 (-12.99 , 27.11)	-34.67 (-51.44 , 24.02)	0.284
Δv_p (%)	ypT 0-2 versus 3-4	0.00 (-4.40 , 2.54)	-0.22 (-2.95 , 8.35)	0.633
	ypN 0 versus 1-2	0.00 (-4.40 , 6.24)	0.00 (-2.69 , 8.35)	0.479
	TRG 0 versus TRG 1-3	0.00 (-2.55 , 2.54)	0.00 (-4.40 , 8.35)	0.654
	ΔT 0-2 versus 3-4	0.00 (-4.40 , 8.35)	0.00 (-2.55 , 2.54)	0.654
	ΔN 0 versus 1-2	1.82 (-2.05 , 8.35)	0.00 (-4.40 , 6.24)	0.354
Δk_{ep} (min^{-1})	ypT 0-2 versus 3-4	0.36 (-14.11 , 2.53)	-0.06 (- 2.77 , 2.17)	0.829
	ypN 0 versus 1-2	0.94 (-14.11 , 2.53)	-0.52 (-1.98 , 0.49)	0.126
	TRG 0 versus TRG 1-3	0.94 (-14.11 , 1.75)	-0.14 (-2.77 , 2.53)	0.912
	ΔT 0-2 versus 3-4	-0.14 (-2.77 , 2.53)	0.94 (-14.11 , 1.75)	0.912
	ΔN 0 versus 1-2	-0.79 (-1.98 , -0.14)	0.26 (-14.11 , 2.53)	0.222

Table 4.11: Results of the Mann-Whitney U test for different endpoints on the difference between pretreatment and post-CRT median parameters for the TK model with individual AIFs. Emphasised in bold, p-values < 0.05 were considered statistically significant. The groups are presented with median values and ranges of the median parameter changes for the different patients.

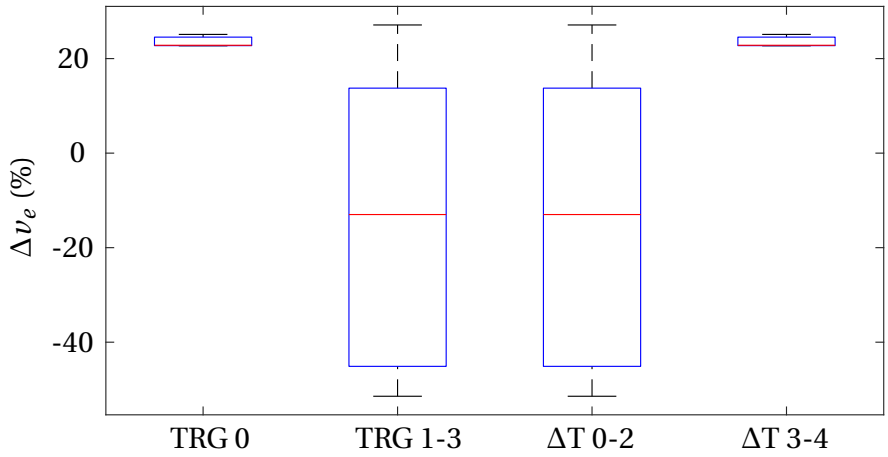

Figure 4.11: Box plots showing the individual AIF-based TK model median values of Δv_e for patients with good treatment response (TRG 0 and ΔT 3-4) and poor treatment response (TRG 1-3 and ΔT 0-2). The central mark, bottom and top of the boxes respectively indicate the median, 25th and 75th percentile, and the whiskers indicate the most extreme values not considered outliers. Outliers are plotted individually using the '+' symbol. v_e tended to increase for good responders and decrease for poor responders.

Parameter	**Endpoint**	**Median (range)**		**p-value**
		Group 1	**Group 2**	
ΔA_{Brix}	ypT 0-2 versus 3-4	0.23 (-1.63 , 1.22)	0.19 (-0.80 , 0.71)	1.000
	ypN 0 versus 1-2	0.12 (-1.63 , 1.22)	0.30 (-0.80 , 0.69)	0.860
	TRG 0 versus TRG 1-3	-0.13 (-1.63 , 1.22)	0.30 (-0.80 , 0.71)	0.654
	ΔT 0-2 versus 3-4	0.30 (-0.80 , 0.71)	-0.13 (-1.63 , 1.22)	0.654
	ΔN 0 versus 1-2	0.08 (-0.80 , 0.33)	0.45 (-1.63 , 0.69)	0.127
Δk_{el} (min^{-1})	ypT 0-2 versus 3-4	-0.03 (-1.57 , -0.01)	-0.01 (-0.03 , 0.00)	0.083
	ypN 0 versus 1-2	-0.01 (-1.57 , 0.00)	-0.01 (-0.05 , 0.00)	0.860
	TRG 0 versus TRG 1-3	-0.02 (-1.57 , -0.01)	-0.01 (-0.05 , 0.00)	0.301
	ΔT 0-2 versus 3-4	-0.01 (-0.05 , 0.00)	-0.02 (-1.57 , -0.01)	0.301
	ΔN 0 versus 1-2	-0.01 (-0.05 , 0.00)	-0.02 (-1.57 , 0.00)	0.833
Δk_{ep} (min^{-1})	ypT 0-2 versus 3-4	-1.22 (-7.71 , 1.13)	-1.20 (-4.52 , 2.23)	0.965
	ypN 0 versus 1-2	-0.17 (-3.65 , 2.23)	-3.36 (-7.71 , -0.62)	**0.006**
	TRG 0 versus TRG 1-3	-1.10 (-1.35 , 1.13)	-1.78 (-7.71 , 2.23)	0.426
	ΔT 0-2 versus 3-4	-1.78 (-7.71 , 2.23)	-1.10 (-1.35 , 1.13)	0.426
	ΔN 0 versus 1-2	-3.36 (-7.71 , -0.62)	-0.32 (-4.00 , 2.23)	0.065

Table 4.12: Results of the Mann-Whitney U test for different endpoints on the change in the median Brix model parameters from the image data acquired before and after CRT. Emphasised in bold, p-values < 0.05 were considered statistically significant. The groups are presented with median values and ranges of the median parameter changes for the different patients.

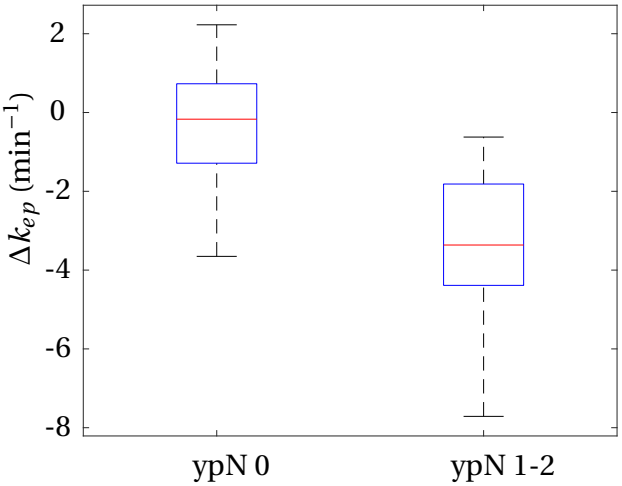

Figure 4.12: Box plots showing the median values of Δk_{ep} from the Brix model for the patients with ypN 0 (good treatment response) and ypN 1-2 (poor treatment response). The central mark, bottom and top of the boxes respectively indicate the median, 25th and 75th percentile, and the whiskers indicate the most extreme values not considered outliers. In general there was a bigger reduction in k_{ep} for the patients with poor treatment response.

Chapter 5

Discussion

5.1 Sources of Error

Milder CRT regimes were given to some of the patients, who were either too old or too sick to handle the standard treatment regime. This may have interfered with the results, if the patients responded differently to the received treatment than they would have to the standard regime. This was however only the case for a few patients, and the effect on the overall results when using groups to analyse them was therefore thought to be small.

5.1.1 AIF Estimation

The ROIs used for AIF measurements were generally drawn as large as possible. This may have resulted in some error, because the edge pixels close to the artery wall may partially or solely represent extravascular tissue, which will decrease the height of the AIF peak [29]. In some cases the cross sections were small or unclear, increasing the likelihood of this error. Attempting to draw the ROIs closer to the centre of the arteries could counter these effects. Doing this could lead to a higher mean contrast agent concentration, and thereby, as explained in section 2.4.1, increase the amount of potential errors in equation 2.14 if the T_1-relaxation time in the centre

pixels is short enough that the assumption $TR << T_1$ is no longer valid. Another option could be to have stricter requirements for determining which cross sections are eligible for AIF estimation. Having a requirement for goodness of fit for the fitted AIF could also have increased the accuracy, as in this study, all AIFs with visible peaks where the fitted curves did not obviously deviate from the data, were included.

5.1.2 Model Parameter Estimation

To avoid errors in the median parameters caused by poor curve fits, all parameters above a threshold determined for each parameter were removed prior to the analysis. This loss of pixels could be a potential source of error in the study. Another option could have been to restrict the limits for the different parameter values to the desired level during the curve fitting process as opposed to after. This would provide a larger amount of parameters from which to estimate the parameter medians for the different patients, but could potentially create additional uncertainty because the poorly estimated parameters may then become more difficult to detect.

5.2 Results

5.2.1 AIF Estimation

In figure 5.1 a series of AIFs are shown to illustrate how the measured data and fitted individual AIFs varied for different patients. Examples of measured AIFs where the second peak was and was not easily distinguishable can be seen in figures 5.1a and 5.1c. In figure 5.1a the fitted function is close to the data points, but the second peak seems to have lifted the estimated plateau slightly higher than the actual data points. In this case, it could have been advantageous to account for the second peak during the AIF estimation. In figure 5.1c the second peak is visible, but has been slightly mixed with the rest of the data points. This results in a more accurate fit to the plateau and the data points in general, supporting the findings of McGrath et al. which

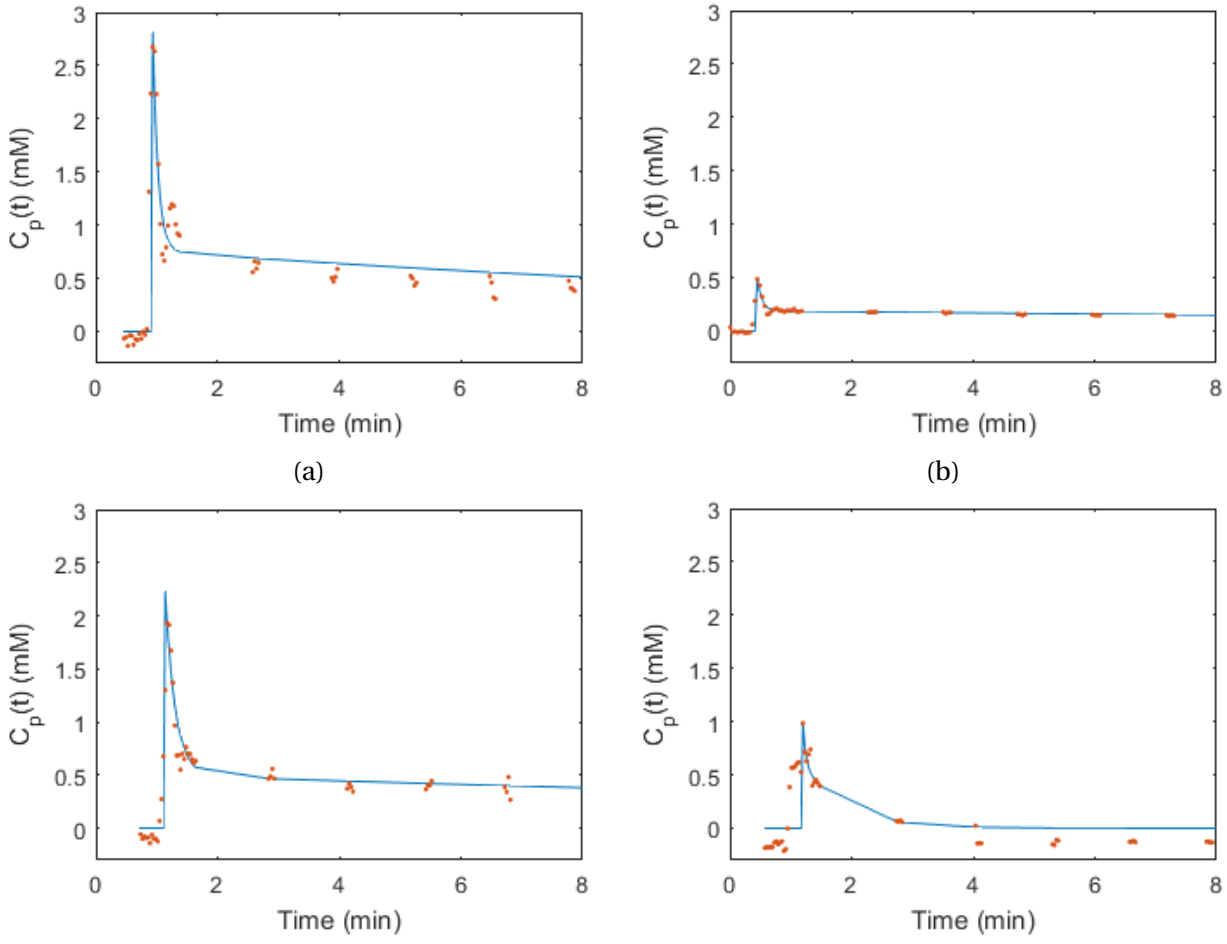

Figure 5.1: Examples of different variations for the measured and estimated AIFs that were included in the calculation of the population-based TK model and in the individual AIF-based TK model analysis. **a)** An AIF with a tall and sharp peak. The second peak is clearly visible from the measured data. **(b)** An AIF with a low peak height. The measured second peak can be seen, but is very small. **(c)** An AIF where the initial peak is high, but the second peak is not easily visible. Here the function has fitted to the outer data points of the second peak, so that the initial peak appears wider than it actually is. **(d)** A measured AIF where the initial and plateau contrast agent concentrations were below zero due to a low SNR, causing the fitted plateau to stabilise at zero.

indicated that for data with a certain amount of noise, using a bi-exponential function for the AIF was ideal [29]. However, the function seems to have fitted to the outer points of the second peak so that the estimated initial peak appears wider than that of figure 5.1a.

As seen in figure 5.1, there were significant variations in the height of both the peak and the plateau. This can among other things be caused by differences in blood flow velocity, which when high will result in a tall peak in the AIF [29] [30]. The differences were likely also caused by noise in the images in some cases, as abnormally low peak and even negative plateau heights occurred for some of the patients (figure 5.1d). As explained in section 2.4.1, a low SNR can lead to reduced and even negative values for the contrast agent concentration.

McGrath et al. explored the differences between different AIF models, and found that using a bi-exponential model, for example equation 2.17, for the TK model gave close fits to K^{trans} and v_e, but poorer fits for v_p, than models that account for the second peak (for example the model proposed by Parker et al. in [49]) [29]. They additionally found that the bi-exponential approach would give the most accurate fits for data with low SNR. Thus the choice of a bi-exponential model will contribute to closer fits for the noisy images, but the general increased accuracy may come at the cost of the validity of v_p.

The estimated individual AIF parameters deviated a lot from the mean parameters used for the population-based AIF. That the most significant outliers were not removed, could therefore make the population-based AIF prone to error. In 1997 Tofts et al. found $a_1 = 3.99\,\mathrm{kgl}^{-1}$, $a_2 = 4.78\,\mathrm{kgl}^{-1}$, $m_1 = 0.144\,\mathrm{min}^{-1}$ and $m_2 = 0.011\,\mathrm{min}^{-1}$ [34], significantly lower than what was found in this study. This inconsistency could potentially be caused by the high deviations for the individual AIFs. It is likely that either removing the more extreme outliers, or using the median AIF parameters for the population-based AIF, could have resulted in more accurate estimations.

5.2.2 Median Parameters of Pretreatment Images

From figure 4.2 it can be seen that the patients with poor treatment response generally had a higher v_e than the patients with good treatment response. Physiologically, this may be explained

by a decreased ability of cell-cell adhesion in the poor responders, which will increase the fraction of EES, and has been shown to be an important factor for both local tumour growth and distant metastases [13] [50]. Other possible physiological indications are high vascularities for good responders, if blood vessels occupy the tissue space in place of the EES, or possibly fibrous EES which the contrast agent is unable to leak into [32]. A high vascularity in a tumour is known to be associated with a lack of, or only small amounts of hypoxic tissue, which is associated with a good treatment response. Good oxygenation could thus be a contributor to good treatment response for these patients. It should be noted that there was no statistical significance for v_p that could indicate contributions from high vascularity, but considering the possible errors in estimation of v_p discussed in section 5.2.1, it should not be ruled out.

No associations with treatment response were found when using the population-based AIF in the TK model, indicating that the individual-AIF based TK model more accurately estimates model parameters. This suggests that the measured AIF-variations are caused by individual variations between the patients to a higher extent than from poor measurements or fits, noise and image artefacts. It should however be noted, that as discussed in section 5.2.1, the calculated population-based AIF deviated strongly from the previously estimated AIF. This is possibly why, contradicting previous studies, no associations were found between pretreatment K^{trans} and treatment response for the population-based AIF [26] [8] [10]. Large errors in the population-based AIF could contribute to the lack of statistical significance, and it is possible that performing some of the changes suggested, could improve the results of the TK model for the population-based AIF.

For the Brix model, figures 4.3a and 4.3b show that patients with good treatment response generally had a lower A_{Brix} and k_{ep} than patients with poor treatment response. This is in agreement with the results of Lollert et al. [11], who found that for rectal cancer a low A_{Brix} was associated with pN 0, and that patients with a low k_{ep} had better survival than patients with a high k_{ep}. It should however be noted that these results were found for patients that did not receive CRT.

Halle et al. [37] contrarily found that a low A_{Brix} indicated a poor treatment response and an upregulation of HIF-1α in cervix cancer. It is possible that the type of cancer examined is of

importance for the physiological meaning of Brix model parameters. Another cause could be differences in the settings of the MR experiment, as A_{Brix} in addition to tissue properties is sensitive to MRI input parameters. Lollert et al. suggested that, as A_{Brix} is dependent on the size of the EES, where an increase in A_{Brix} would indicate a bigger fraction of EES in the tissue, the results could imply that a large EES fraction relates to a poor treatment response [11]. This would be in agreement with the results for v_e found in the TK model, and the physiological reasoning behind them.

5.2.3 Heterogeneity

The percentile plots in figures 4.5 and 4.6 indicate that in general, the significant pretreatment results are credible, because there was not a lot of instability in the parameters causing the p-value to vary drastically. It can also be seen that for prediction of certain endpoints, the median may not be the optimal choice, instead other percentiles could be more accurate.

Seen in table 4.5 and figure 4.4, the RPH of k_{ep} in the Brix model was significantly larger for the patients with good treatment response (ΔT 3-4) than for the patients with poor treatment response (ΔT 0-2). This indicates that for patients with good treatment response, a larger amount of the estimated parameters gathered around a specific value of k_{ep} than for the patients with poor treatment response. This can be explained physiologically by the biology of a tumour. A high k_{ep} represents tumour angiogenesis and tissue permeability [38]. Aggressive tumours have larger fractions of hypoxic tissue, and higher extents of accelerated angiogenesis, leading to more leaky blood vessels [3]. It is likely that this will be well represented by k_{ep}, with a low k_{ep} in hypoxic tissue, and a high k_{ep} in highly vascularised tissue, leading to a high heterogeneity for k_{ep} in the tumour. On the other hand, less aggressive tumours will likely have a smaller fraction of hypoxic tissue, leading to a more stable and higher k_{ep}.

In 2014, Torheim et al. found that heterogeneity for the Brix model parameters was larger in patients with poor treatment response, and that k_{ep} was the most robust parameter for heterogeneity, coinciding with the findings in this study [38]. The results of Torheim et al. were

acquired using grey level co-occurrence analysis, which checks for repetition of pixel grey-level pairs, rather than histogram analysis, and thus better analyse spatial relations in the tumour. Possibly, this method is more effective, which could explain why of the parameters for which heterogeneity was tested in this study, the only statistically significant association was found for k_{ep}.

5.2.4 Post-CRT Parameter Medians

The post-CRT parameter medians were generally more effective for separating good and poor treatment responses than the pretreatment median parameters. A possible explanation for this is that for tumours of good treatment response, there will be an increase in fibrotic tissue due to tumour cell death, and a decrease in hypoxic tissue, which will affect the distribution of contrast agent [28].

In both versions of the TK model, a significantly higher K^{trans} was found for patients with good treatment response than for patients with poor treatment response. This is in agreement with several studies in pretreatment parameters [26] [8] [10]. For post-CRT parameters however, associations between K^{trans} and treatment response are uncommon [10] [9].

Further, a high v_p when using a population-based AIF in the TK model, and a high k_{ep} in the individual AIF-based TK model and Brix model identified good responders, which could be connected to the high K^{trans} of good responders. As discussed in section 2.4.2, physiologically, K^{trans} reflects tissue permeability and vascular leakiness, k_{ep} reflects vascular leakiness and v_p reflects vascularity. Low permeability and vascularity in tumour tissue is linked to hypoxia, and will thus, as described in section 2.1, lead to a poorer response to treatment. It is important to consider figure 4.7, as it can be seen that in the poor response groups the median v_p is equal to zero for all except one of the patients. Possibly, some instability for the population-based AIF in TK model cause problems with fitting v_p for certain types of tissue.

Contrarily, the individual AIF-based TK model indicated that a high v_p lead to a poor treatment response (ypN 1-2). A possible explanation is that the low v_p for the good treatment response

group in this case is caused by high amounts of fibrotic or healthy tissue in the tumour volume that the model struggled to fit. Figure 4.8 b) seems to support this, as in the good treatment response group the majority of median values of v_p seem to be equal to zero. It is possible that the previously discussed weakness for v_p when using a bi-exponential AIF model is the cause of the problems, and that the problems occur for different types of tissue depending on which type of AIF is used. This also appears to be a problem in other studies, as associations between v_p and treatment response are often not found [51] [52]. A low baseline v_p in metastatic sites was however found to predict progression free survival by Hahn et al. in renal cancer patients [53], indicating that some reliability is obtainable for the parameter. The v_p of a metastatic site is however unlikely to be physiologically comparable to the parameters of the primary tumour volumes examined in this study.

5.2.5 Difference in Pretreatment and Post-CRT Parameter Medians

For the TK model with individual AIFs in this study, an increase in v_e for patients with good treatment response was found, and a net decrease in v_e was associated with a poor treatment response in both versions of the TK model. Contrarily, Pickles et al. [54] found that v_e increased for patients with poor treatment response, and Tong et al. [10] found a significant decrease for patients with good treatment response. The results were however in agreement with the results of Chikui et al. on oral cancer, who found that an increase in v_e was associated with a good treatment response [55]. They concluded that an increase in EES volume due to tumour cell death caused the increase in v_e, which fits the results of this study. The different types of cancer and choices of models possibly cause the different results. For example, the model used by Pickles et al. was described as a modified version of the Brix model [54]. The results found for k_{ep} in the Brix model are however not in agreement with their results either, as they found a decrease in k_{ep} for good responders, while this study found the decrease in k_{ep} to be largest for the poor responders. A possible physiological explanation may be an increase in fraction of hypoxic tissue, which is known to be of low vascularity, for the poor responders.

The increase in v_e for patients with good treatment response in this study could thus possibly

be explained by an increased amount of permeable fibrotic tissue caused by cell death. That a larger decrease in v_e was found for the patients with poor treatment response could similarly indicate that the cellular density increased due to tumour growth.

5.3 Potential of Parametric Modelling

Based on the physiological meanings of the model parameters, tumours that are highly vascular (high v_p) and permeable (high k_{ep} and K^{trans}) seem to respond well to treatment, while tumours that are hypoxic, expressed through low vascularities (low v_p) and low permeabilities (low k_{ep} and K^{trans}) seem to respond poorly to treatment. Additionally, tumours of larger leakage spaces (high A_{Brix} and v_e) seem to respond poorly to treatment.

Generally, the individual AIF-based TK model seemed to most frequently differentiate good and poor treatment responses. For the pretreatment medians, both the individual AIF-based TK model and the Brix model separated good and poor treatment responses, whereas using the population-based AIF in the TK model gave no significant results. The lowest p-value was found for v_e in ΔT 0-2 versus 3-4 (p = 0.009), indicating an effective prediction of downstaging of T-stage. The pretreatment results thus indicate that in the TK model, individual AIFs should be used. This is in accordance with the findings of McGrath et al [29]. The Brix model gave the only statistically significant results for heterogeneity. Further testing on heterogeneity should be performed to assess if this could indicate that this model has a better potential in histogram analysis. Based on the pretreatment p-values found, the TK model seems to most effectively predict tumour regression, while the Brix model seems to most effectively identify the patients with poor treatment response.

When considering results from the post-CRT parameters and the differences between pretreatment and post-CRT parameters, the individual AIF and population-based AIF seem more similar in promise. There were still more statistically significant values when using individual AIFs, but the differences were not large. K^{trans} seems to be a robust parameter, as it was statistically significant in the same endpoints for both versions of the TK model for the post-CRT parame-

ters. The same can be said for v_e for the difference in median parameters before and after CRT. k_{ep} was a particularly good assessor of nodal involvement, with significant associations both for the post-CRT k_{ep} and Δk_{ep} in the Brix model, and for the post-CRT k_{ep} in the individual AIF-based TK model. The Brix model quantity wise provided fewer significant results, but also had the lowest p-value, for k_{ep} in ΔN 0 versus ΔN 1-2 ($p = 0.003$). The post-CRT results thus indicate that the TK model gives more accurate results for treatment response in terms of tumour regression, and based on the number of significant results, that individual AIFs worked better than a population-based AIF in the TK model. The Brix model on the other hand seems to be the most accurate with regard to N-stage.

Finally, no associations were found between tumour aggressiveness and model parameters for the patients that did not receive CRT. This indicates that while associations were found for the ypT-stage for patients that received CRT, these associations are related to the downstaging of the tumour in response to treatment, rather than to the T-stage of the tumour alone. This is further confirmed in the TK model by the fact that the associations with TRG and ΔT ($p = 0.022$ and $p = 0.009$) are stronger than the association with ypT ($p = 0.045$). This effect could be explained by the fact that while there is some association between tumour stage and aggressiveness, aggressiveness can also vary independently on the size of the tumour [3]. Thus, it strengthens the basis for using the TK model for prognostic endeavours, as it is able to predict treatment response in cases where TN-staging alone would provide less accurate results. The Brix model implies the opposite, with a stronger association with ypT-stage ($p = 0.018$) than with ΔT ($p = 0.044$), indicating a stronger influence from the initial size of the tumour.

For all of the results, it should be taken into consideration that, as previously discussed in section 5.2.1, the unusually high population-based AIF parameter values may be erroneous, and that thus, improvements in the population-based AIF estimation could lead to improved results for application of this AIF to the TK model. A second important consideration is that the settings for the experiment, the type of model used, and the type of cancer, all seem to have some effect on the estimated parameters and associations.

5.3.1 Clinical Potential

Parametric modelling in general improves the information acquired pretreatment and prior to surgery about the response to CRT. In comparison, the traditional morphological imaging mainly provides information on the size and TN-staging of the tumour. The advantage of the TK and Brix model is that they are quantitative: rather than only offering a visual evaluation, they provide measurable quantities of tumour characteristics important for treatment response and survival, that can be compared for different patients. The TK model predicts TRG 0 accurately, and for these patients, surgery could perhaps be avoided, providing a better quality of life for the patients. Similarly, the Brix model's ability to identify patients which will have ypN 0 prior to surgery might contribute to them receiving a less advanced surgery where less of the nearby lymph nodes are removed, thus providing a better quality of life. For patients where the Brix model predicts a ypT-stage of 3 or 4, it could potentially be useful to apply a more aggressive CRT regime prior to surgery. This might increase survival for this group of patients.

5.4 Further Work

It is likely that a more accurate population-based AIF will lead to more accurate curve fits and parameter estimations for the TK model. Adjustments should therefore be done to the population-based AIF so that it is less affected by outliers, as discussed in section 5.2.1. The TK model parameter estimations for the population-based AIF should then be performed again using the new population-based AIF.

Receiver operating characteristic analysis should be performed in order to determine the sensitivity and specificity of the parameters, and an optimal threshold for separating the good and poor responders. An analysis on progression free survival should also be performed, in order to uncover the long-term prognostic potential of the image parameters.

For the heterogeneity analysis, it would be interesting to test for all parameters and endpoints, rather than limiting this analysis to the cases where significant associations were found for the

pretreatment medians. Additionally it would be useful to perform a grey-level co-occurrence analysis, as this type of analysis gives information about spatial variations of the parameter values in the tumour, in addition to the general parameter variations investigated in this study [38].

Finally, while parametric modelling offers parameters that are physiologically significant, semi-quantitative analysis is simpler and less time consuming to perform. The models investigated in this study should therefore be compared to the potential of a semi-quantitative analysis, described in section 2.4.2, of the DCE-MRI data.

Chapter 6

Conclusion

Two compartmental models, the TK model and the Brix model, were investigated for their potential to predict aggressiveness and CRT response in rectal cancer. The significance of the AIF was investigated by applying both a population-based AIF and individual AIFs to the TK model, and the results were compared to those of the Brix model, which does not use an AIF.

Parametric modelling of DCE-MRI was found to effectively predict CRT response, but did not assess aggressiveness in patients that did not receive CRT. Using individual AIFs in the TK model was found to be a stronger predictor of treatment response than a population-based AIF, and they thus seem to have a lot of potential. The population-based AIF should however not be dismissed, as the calculated mean parameters in this study were likely affected by outliers. More accurate results may thus be achieved if this potential error is corrected. The significance of using a suitable AIF in the TK model has thus been shown to be large, and it could therefore be considered an advantage of the Brix model that it does not depend on an AIF.

As the Brix model and the TK model both provide significant results, the choice of model seems to be important with regard to what is to be examined, rather than to achieve accurate results. The Brix model gave somewhat fewer significant results than the TK model, but predicted lymph node involvement and poor treatment response more accurately than the TK model. The TK model on the other hand predicted complete histomorphological tumour response (TRG 0)

more accurately. Both models thus show potential for clinical use, where the TK model might distinguish patients who are not in need of surgery, while the Brix model might identify patients in need of less aggressive surgeries, based on the predicted nodal involvement, and patients in need of more aggressive CRT regimes, based on the predicted ypT-stage.

Now that the images of the Oxytarget study have been analysed, it is necessary to examine whether the results are reproducible. Studies should therefore be performed on different data, in order to determine if the results are clinically relevant.

Bibliography

[1] G. F. Weber, R. Rosenberg, J. E. Murphy, C. M. z. Büschenfelde, and H. Friess, "Multimodal treatment strategies for locally advanced rectal cancer," *Expert Review of Anticancer Therapy*, vol. 12, no. 4, pp. 481–494, 2012.

[2] Cancer Registry of Norway, "Cancer in Norway 2016 - Cancer incidence, mortality, survival and prevalence in Norway," *Oslo: Cancer Registry of Norway*, 2012.

[3] S. Meltzer, "Circulating markers of immunogenicity and metastasis in combined-modality treatment of rectal cancer," 2017. ISBN: 978-82-8377-144-2.

[4] E. Grøvik, "Multimodal dynamic MRI for structural and functional assessment of cancer," 2017. ISBN: 1501-7710.

[5] F. Khalifa, A. Soliman, A. El-Baz, M. Abou El-Ghar, T. El-Diasty, G. Gimel'farb, R. Ouseph, and A. C. Dwyer, "Models and methods for analyzing DCE-MRI: A review," *Medical Physics*, vol. 41, no. 12, 2014.

[6] P. S. Tofts and A. G. Kermode, "Measurement of the blood-brain barrier permeability and leakage space using dynamic MR imaging. 1. fundamental concepts," *Magnetic Resonance in Medicine*, vol. 17, no. 2, pp. 357–367, 1991.

[7] G. Brix, W. Semmler, R. Port, L. R. Schad, G. Layer, and W. J. Lorenz, "Pharmacokinetic parameters in CNS Gd-DTPA enhanced MR imaging.," *Journal of Computer Assisted Tomography*, vol. 15, no. 4, pp. 621–628, 1991.

[8] M. Gollub, K. Cao, D. Gultekin, D. Kuk, M. Gonen, M. Sohn, L. Schwartz, M. Weiser, L. Temple, G. Nash, *et al.*, "Prognostic aspects of DCE-MRI in recurrent rectal cancer," *European Radiology*, vol. 23, no. 12, pp. 3336–3344, 2013.

[9] M. Intven, O. Reerink, and M. E. Philippens, "Dynamic contrast enhanced MR imaging for rectal cancer response assessment after neo-adjuvant chemoradiation," *Journal of Magnetic Resonance Imaging*, vol. 41, no. 6, pp. 1646–1653, 2015.

[10] T. Tong, Y. Sun, M. J. Gollub, W. Peng, S. Cai, Z. Zhang, and Y. Gu, "Dynamic contrast-enhanced MRI: Use in predicting pathological complete response to neoadjuvant chemoradiation in locally advanced rectal cancer," *Journal of Magnetic Resonance Imaging*, vol. 42, no. 3, pp. 673–680, 2015.

[11] A. Lollert, T. Junginger, C. C. Schimanski, S. Biesterfeld, I. Gockel, C. Düber, and K. Oberholzer, "Rectal cancer: Dynamic contrast-enhanced mri correlates with lymph node status and epidermal growth factor receptor expression," *Journal of Magnetic Resonance Imaging*, vol. 39, no. 6, pp. 1436–1442, 2014.

[12] T. S. Evensen, "Analysis of DCE-MRI for chemoradiotherapy response prediction in rectal cancer," *Department of Physics*, vol. 254, no. 5028, pp. 43–50, 2017.

[13] D. Hanahan and R. A. Weinberg, "Hallmarks of cancer: the next generation," *Cell*, vol. 144, no. 5, pp. 646–674, 2011.

[14] E. J. Hall and A. J. Giaccia, *Radiobiology for the Radiologist*. Lippincott Williams & Wilkins, 7th ed., 2012.

[15] H. Kobayashi, R. Watanabe, and P. L. Choyke, "Improving conventional enhanced permeability and retention (EPR) effects; what is the appropriate target?," *Theranostics*, vol. 4, no. 1, p. 81, 2014.

[16] H. Harada, "How can we overcome tumor hypoxia in radiation therapy?," *Journal of Radiation Research*, vol. 52, no. 5, pp. 545–556, 2011.

[17] H. Maeda, J. Wu, T. Sawa, Y. Matsumura, and K. Hori, "Tumor vascular permeability and the EPR effect in macromolecular therapeutics: a review," *Journal of Controlled Release*, vol. 65, no. 1, pp. 271–284, 2000.

[18] G. E. Theodoropoulos, A. C. Lazaris, V. E. Theodoropoulos, K. Papatheodosiou, M. Gazouli, J. Bramis, E. Patsouris, and D. Panoussopoulos, "Hypoxia, angiogenesis and apoptosis markers in locally advanced rectal cancer," *International Journal of Colorectal Disease*, vol. 21, no. 3, pp. 248–257, 2006.

[19] Y. Toiyama, Y. Inoue, S. Saigusa, Y. Okugawa, T. Yokoe, K. Tanaka, C. Miki, and M. Kusunoki, "Gene expression profiles of epidermal growth factor receptor, vascular endothelial growth factor and hypoxia-inducible factor-1 with special reference to local responsiveness to neoadjuvant chemoradiotherapy and disease recurrence after rectal cancer surgery," *Clinical Oncology*, vol. 22, no. 4, pp. 272–280, 2010.

[20] X.-g. Lu, C.-g. Xing, Y.-z. Feng, J. Chen, and C. Deng, "Clinical significance of immunohistochemical expression of hypoxia-inducible factor–1α as a prognostic marker in rectal adenocarcinoma," *Clinical Colorectal Cancer*, vol. 5, no. 5, pp. 350–353, 2006.

[21] S. Edge, D. Byrd, C. Compton, A. Fritz, F. Greene, and A. Trotti, "American joint committee on cancer staging manual. 7," 2009.

[22] H. Bouzourene, F. T. Bosman, W. Seelentag, M. Matter, and P. Coucke, "Importance of tumor regression assessment in predicting the outcome in patients with locally advanced rectal carcinoma who are treated with preoperative radiotherapy," *Cancer*, vol. 94, no. 4, pp. 1121–1130, 2002.

[23] L. H. Tang, J. Berlin, P. Branton, L. J. Burgart, D. K. Carter, C. C. Compton, P. Fitzgibbons, W. L. Frankel, J. Jessup, S. Kakar, B. Minsky, R. Nakhleh, and K. Washington, "Protocol for the examination of specimens from patients with carcinoma of the stomach.." http://www.cap.org/ShowProperty?nodePath=/UCMCon/Contribution%20Folders/WebContent/pdf/cp-stomach14-protocol.pdf., 2014. Accessed: 2018-05-16.

[24] R. W. Brown, Y.-C. N. Cheng, E. M. Haacke, M. R. Thompson, and R. Venkatesan, *Magnetic Resonance Imaging: Physical Principles and Sequence Design*. Wiley-Blackwell, 2nd ed., 2014.

[25] C. Westbrook, C. K. Roth, and J. Talbot, *MRI in Practice*. Wiley-Blackwell, 4th ed., 2011.

[26] E. Grøvik, K. R. Redalen, T. H. Storås, A. Negård, S. H. Holmedal, A. H. Ree, S. Meltzer, A. Bjørnerud, and K.-I. Gjesdal, "Dynamic multi-echo DCE-and DSC-MRI in rectal cancer: Low primary tumor Ktrans and δr2* peak are significantly associated with lymph node metastasis," *Journal of Magnetic Resonance Imaging*, vol. 46, no. 1, pp. 194–206, 2017.

[27] M. K. Stehling, R. Turner, and P. Mansfield, "Echo-planar imaging: magnetic resonance imaging in a fraction of a second," *Science*, vol. 254, no. 5028, pp. 43–50, 1991.

[28] R. G. Beets-Tan and G. L. Beets, "MRI for assessing and predicting response to neoadjuvant treatment in rectal cancer," *Nature Reviews Gastroenterology & Hepatology*, vol. 11, no. 8, pp. 480–488, 2014.

[29] D. M. McGrath, D. P. Bradley, J. L. Tessier, T. Lacey, C. J. Taylor, and G. J. Parker, "Comparison of model-based arterial input functions for dynamic contrast-enhanced MRI in tumor bearing rats," *Magnetic Resonance in Medicine*, vol. 61, no. 5, pp. 1173–1184, 2009.

[30] M.-Y. Su, J.-C. Jao, and O. Nalcioglu, "Measurement of vascular volume fraction and blood-tissue permeability constants with a pharmacokinetic model: Studies in rat muscle tumors with dynamic Gd-DTPA enhanced MRI," *Magnetic Resonance in Medicine*, vol. 32, no. 6, pp. 714–724, 1994.

[31] S. I. Fox, *Human Physiology*. McGraw-Hill, 13th ed., 2013.

[32] P. S. Tofts, G. Brix, D. L. Buckley, J. L. Evelhoch, E. Henderson, M. V. Knopp, H. B. Larsson, T.-Y. Lee, N. A. Mayr, G. J. Parker, *et al.*, "Estimating kinetic parameters from dynamic contrast-enhanced T 1-weighted MRI of a diffusable tracer: standardized quantities and symbols," *Journal of Magnetic Resonance Imaging*, vol. 10, no. 3, pp. 223–232, 1999.

[33] I. Q. Løkken, "Classification of breast cancer based on DCE MRI," Master's thesis, NTNU, 2017.

[34] P. S. Tofts, "Modeling tracer kinetics in dynamic Gd-DTPA MR imaging," *Journal of Magnetic Resonance Imaging*, vol. 7, no. 1, pp. 91–101, 1997.

[35] U. Hoffmann, G. Brix, M. V. Knopp, T. Heβ, and W. J. Lorenz, "Pharmacokinetic mapping of the breast: a new method for dynamic MR mammography," *Magnetic Resonance in Medicine*, vol. 33, no. 4, pp. 506–514, 1995.

[36] A. Thukral, D. M. Thomasson, C. K. Chow, R. Eulate, S. B. Wedam, S. N. Gupta, B. J. Wise, S. M. Steinberg, D. J. Liewehr, P. L. Choyke, *et al.*, "Inflammatory breast cancer: dynamic contrast-enhanced MR in patients receiving bevacizumab—initial experience," *Radiology*, vol. 244, no. 3, pp. 727–735, 2007.

[37] C. Halle, E. Andersen, M. Lando, E.-K. Aarnes, G. Hasvold, M. Holden, R. G. Syljuåsen, K. Sundfør, G. B. Kristensen, R. Holm, *et al.*, "Hypoxia-induced gene expression in chemoradioresistant cervical cancer revealed by dynamic contrast-enhanced MRI," *Cancer Research*, vol. 72, no. 20, pp. 5285–5295, 2012.

[38] T. Torheim, E. Malinen, K. Kvaal, H. Lyng, U. G. Indahl, E. K. Andersen, and C. M. Futsaether, "Classification of dynamic contrast enhanced MR images of cervical cancers using texture analysis and support vector machines," *IEEE Transactions on Medical Imaging*, vol. 33, no. 8, pp. 1648–1656, 2014.

[39] "The Oxytarget Study." http://www.acredit.no/the-oxytarget-study/. Accessed: 2018-04-05.

[40] "Norsk legemiddelhåndbok." http://legemiddelhandboka.no/. Accessed: 2018-06-05.

[41] "fit." https://www.mathworks.com/help/curvefit/fit.html. Accessed: 2018-04-06.

[42] E. Grøvik, A. Bjørnerud, T. H. Storås, and K.-I. Gjesdal, "Split dynamic MRI: Single bolus high spatial–temporal resolution and multi contrast evaluation of breast lesions," *Journal of Magnetic Resonance Imaging*, vol. 39, no. 3, pp. 673–682, 2014.

[43] J. U. Harrer, G. J. Parker, H. A. Haroon, D. L. Buckley, K. Embelton, C. Roberts, D. Balériaux, and A. Jackson, "Comparative study of methods for determining vascular permeability and

blood volume in human gliomas," *Journal of Magnetic Resonance Imaging*, vol. 20, no. 5, pp. 748–757, 2004.

[44] P. L. Choyke, A. J. Dwyer, and M. V. Knopp, "Functional tumor imaging with dynamic contrast-enhanced magnetic resonance imaging," *Journal of Magnetic Resonance Imaging*, vol. 17, no. 5, pp. 509–520, 2003.

[45] H. B. Mann and D. R. Whitney, "On a test of whether one of two random variables is stochastically larger than the other," *The Annals of Mathematical Statistics*, pp. 50–60, 1947.

[46] "std." https://www.mathworks.com/help/matlab/ref/std.html. Accessed: 2018-06-08.

[47] "kurtosis." https://www.mathworks.com/help/stats/kurtosis.html. Accessed: 2018-06-08.

[48] "skewness." https://www.mathworks.com/help/stats/skewness.html. Accessed: 2018-06-08.

[49] G. J. Parker, C. Roberts, A. Macdonald, G. A. Buonaccorsi, S. Cheung, D. L. Buckley, A. Jackson, Y. Watson, K. Davies, and G. C. Jayson, "Experimentally-derived functional form for a population-averaged high-temporal-resolution arterial input function for dynamic contrast-enhanced MRI," *Magnetic Resonance in Medicine*, vol. 56, no. 5, pp. 993–1000, 2006.

[50] M. Herzig, F. Savarese, M. Novatchkova, H. Semb, and G. Christofori, "Tumor progression induced by the loss of E-cadherin independent of β-catenin/Tcf-mediated Wnt signaling," *Oncogene*, vol. 26, no. 16, p. 2290, 2007.

[51] A. Oto, C. Yang, A. Kayhan, M. Tretiakova, T. Antic, C. Schmid-Tannwald, S. Eggener, G. S. Karczmar, and W. M. Stadler, "Diffusion-weighted and dynamic contrast-enhanced MRI of prostate cancer: correlation of quantitative MR parameters with gleason score and tumor angiogenesis," *American Journal of Roentgenology*, vol. 197, no. 6, pp. 1382–1390, 2011.

[52] M. Bergamino, L. Saitta, L. Barletta, L. Bonzano, G. L. Mancardi, L. Castellan, J. L. Ravetti, and L. Roccatagliata, "Measurement of blood-brain barrier permeability with T 1-weighted dynamic contrast-enhanced MRI in brain tumors: A comparative study with two different algorithms," *ISRN Neuroscience*, vol. 2013, 2013.

[53] O. M. Hahn, C. Yang, M. Medved, G. Karczmar, E. Kistner, T. Karrison, E. Manchen, M. Mitchell, M. J. Ratain, and W. M. Stadler, "Dynamic contrast-enhanced magnetic resonance imaging pharmacodynamic biomarker study of sorafenib in metastatic renal carcinoma," *Journal of Clinical Oncology*, vol. 26, no. 28, p. 4572, 2008.

[54] M. D. Pickles, M. Lowry, D. J. Manton, P. Gibbs, and L. W. Turnbull, "Role of dynamic contrast enhanced MRI in monitoring early response of locally advanced breast cancer to neoadjuvant chemotherapy," *Breast Cancer Research and Treatment*, vol. 91, no. 1, pp. 1–10, 2005.

[55] T. Chikui, E. Kitamoto, S. Kawano, T. Sugiura, M. Obara, A. W. Simonetti, M. Hatakenaka, Y. Matsuo, S. Koga, M. Ohga, *et al.*, "Pharmacokinetic analysis based on dynamic contrast-enhanced MRI for evaluating tumor response to preoperative therapy for oral cancer," *Journal of Magnetic Resonance Imaging*, vol. 36, no. 3, pp. 589–597, 2012.

[56] "Tools for NIfTI and ANALYZE image." https://www.mathworks.com/matlabcentral/fileexchange/8797-tools-for-nifti-and-analyze-image. Accessed: 2017-12-11.

Appendix A

Matlab Scripts

A.1 Image Sorting

The following script sorts the dicom-images into a four-dimensional matrix, so that they are in the correct order according to slice location and time.

```
%This program sorts the dicom images into a 4D-matrix where the third
%dimension is slice and the fourth dimension is time.

filePath = 'C:\Users\Tina\Documents\Skole\Masteroppgave\Data\';

pList = [24 27 28 29 31 32 41 43 44 45 46 47 48 49 50 51 52 55 56 57 58 61 64
    65 67 72 73 74 75 77 78 79 80 83 85 87 88 89 90 92 94 96 98 103 105 106 108
     110 112 115 116 118 119 120 121 122 124 125 126 127 130 131 132 133 134
    138 143 144 146 147 149 150 151 152 153 154 156 157 160 162 164 165 166 169
     170 171 172 174 175 176 181];

n = length(pList);

for i = 1:n
    patient = pList(i);

```

```
13  imList = dir([filePath 'Oxytarget_' int2str(patient) ' PRE\M0\Im*']); %
    Lists all the images that will be sorted
14  nIm = length(imList);
15
16  info = dicominfo([filePath 'Oxytarget_' int2str(patient) ' PRE\M0\' imList
    (1).name]);
17  x= info.Rows; %Extract info from one image to obtain the dimensions of the
     images in the folder
18
19  aValue = zeros(nIm,1); %Initialise time vector
20  zValue = ones(nIm,1); %Initialise slice vector
21
22  im = zeros(x,x,nIm); %Initialise matrix containing all images
23
24  for iNo = 1:nIm
25      info = dicominfo([filePath 'Oxytarget_' int2str(patient) ' PRE\M0\'
    imList(iNo).name]);
26      im(:,:,iNo) = dicomread([filePath 'Oxytarget_' int2str(patient) ' PRE\
    M0\' imList(iNo).name]); %Read images into matrix
27
28      SeriesTime = info.SeriesTime; %Obtain the time at which the image
    sequence started.
29      AT = info.AcquisitionTime; %Obtain time where the image was acquired.
30
31      %Use these to calulate the acquisition time for the images:
32      hours = (str2double(AT(1:2))-str2double(SeriesTime(1:2)))*3600;
33      minutes = (str2double(AT(3:4))-str2double(SeriesTime(3:4)))*60;
34      seconds = str2double( AT(5:length(AT)))-str2double(SeriesTime(5:length
    (SeriesTime)));
35
36      aValue(iNo) = hours + minutes + seconds; %Calculated acquisition time
37
38      zValuetemp = info.ImagePositionPatient; %extract coordinates for image
39      zValue(iNo) = zValuetemp(3,1); %Extract slice coordinate
40  end
41
```

```
    %Sorts the slices so that they are in the correct order
    [zValue, indzSort] = sort(zValue);
    im = im(:,:,indzSort);
    aValue = aValue(indzSort);

    %Sorts so that the images are also chronological order
    [aValue, indaSort] = sort(aValue);
    im = im(:,:,indaSort);

    na = length(unique(aValue)); %Counts the amount of time points.
    nSlices = nIm/na; %Finds number of slices

    %Reshape the matrix so that it has one dimension for slice and one
    %dimension for time in addition to the x and y dimensions.
    im = reshape(im, [x, x, nSlices, na]);
    aValue = reshape(aValue, [nSlices,na]);
    aValue = aValue';
    zValue = reshape(zValue, [na, nSlices]);
    nz= length(zValue);
    signal = zeros(1,na);

    filename = [filePath 'PRE' num2str(patient) '_M0.mat'];
    save(filename,'im','aValue','zValue','nSlices','na'); %The matrix for each
    patient is saved

end
```

A.2 Image Analysis

A.2.1 AIF

The following script is used to draw an ROI around a blood vessel cross section, and then measures the signal intensity curves within this ROI.

```
clear all
filePath = 'C:\Users\Tina\Documents\Skole\Masteroppgave\Data\';

pList = [24 32 56 58 74 79 121]; %patient identification numbers for a
    selection of patients.
N_s0 = [11 10 14 14 21 14 8]; %time of CA injection
n = length(pList);
i = 1; %chooses which patient in the pList vector to measure the AIF for.
snitt = [9 10 11 5 2 10 4];% selects which image slice to attempt to extract
    an AIF from for the different patients.

peak = N_s0(i) + 5; %used to choose a slice where the contrast enhancement in
    the blood is large, to make the delineation of the ROI easier
j = snitt(i);
patient = pList(i);
current = load([filePath 'P' num2str(patient) '_M0.mat']); %uploads dicom
    images
im = current.im;
aValue = current.aValue;
zValue = current.zValue;
nSlices = current.nSlices;
na = current.na;

AIF = zeros(256,256,na); %initialises signal intensity matrix for the measured
     CA concentrations.
ROI = roipoly(current.im(:,:,j,peak)); %function used to draw the ROI
for x_i = 1:length(im)
    for y_i = 1: length(im)
        if ROI(x_i,y_i) == 1
            for t = 1:na
                AIF(x_i,y_i,t) = im(x_i,y_i,j,t); %saved signal intensities
    from the image into the AIF matrix
            end
        end
    end
end
```

```
31
32 filename = [filePath 'P' num2str(patient) '_M0.mat'];
33 save(filename,'im','aValue','zValue','nSlices','na', 'ROI', 'AIF'); %The
   matrix for each patient is saved)
```

The following script calculates the blood plasma contrast agent concentrations from the signal intensity curves within the AIF ROI.

```
1 %calculateAIF
2 clear all;
3 filePath = 'C:\Users\Tina\Documents\Skole\Masteroppgave\Data\';
4 pList = [24 32 56 58 74 79 121 130 131 138 146 150 153 162 166 169 175 181]; %
   patient identification numbers for a selection
5 N_s0 = [11 10 14 14 21 14 8 15 17 19 16 18 13 17 21 15 20 19]; %the time step
   where the contrast agent is injected
6 n = length(pList);
7 Gender = 'MKMKMKMKMMKMMMMMMK';%gender for the selection of patients
8 TR = 39; %(ms) Repetition time for the image sequence
9 T_10 = 1528; %ms. Initial T1-time. Measured by Groevik et al.
10 cosalpha = cosd(28); %flip angle of the image sequence
11 r1 = 3.6; %relaxivity of contrast agent
12 for i = 1:n
13     if Gender(i) == 'K'
14        Hct = 0.41; %decides the hematocrit value, dependant on the gender of
   the patient.
15     else
16         Hct = 0.47;
17     end
18     patient = pList(i);
19     %loads images with measured AIF signal intensity matrix, time vectors
20     %and slice locations
21     current = load([filePath 'P' num2str(patient) '_M0.mat']);
22     im = current.im;
23     aValue = current.aValue;
24     zValue = current.zValue;
25     nSlices = current.nSlices;
26     x = length(im);
```

```
    na = current.na;
    ROI = current.ROI;
    AIF = current.AIF;
    Cb = zeros(1,na); %initalises vector contrast agent concentration in the
   blood
    Cp = zeros(x,x,na); %initialises blood plasma contrast agent concentration
    matrix
 for x_i = 1:x
          for y_i = 1:x
              if ROI(x_i,y_i) == 1
                   signal = squeeze(AIF(x_i,y_i,:));
                   signal_0 = sum(signal(1:N_s0(i)))/N_s0(i);
                   Cb = (signal - signal_0)./(signal_0 *0.001*r1 * T_10); %
   calcucate contrast agent concentration in the blood.
                   for t = 1:na
                       Cp(x_i,y_i,t) = (Cb(t)/(1-Hct)); %calculates contrast
   agent concentrations in the blood plasma
                   end
              end
          end
 end
    filename = [filePath 'P' num2str(patient) '_M0.mat'];
    save(filename,'im','aValue','zValue','nSlices','na', 'ROI', 'AIF','Cp', '
   time','Cp_median'); %The matrix for each patient is saved)
end
```

This script fits the blood plasma concentrations ($C_p(t)$) to the AIF (equation 2.17), and calculates the median parameters.

```
clear all;
filePath = 'C:\Users\Tina\Documents\Skole\Masteroppgave\Data\';
pList = [24 32 56 58 74 79 121 130 131 138 146 150 153 162 166 169 175 181]; %
   patient identification numbers for a selection
N_s0 = [11 10 14 14 21 14 8 15 17 19 16 18 13 17 21 15 20 19]; %the time step
   where the contrast agent is injected

n = length(pList);
```

```
D_e = 0.1; %the contrast agent injection dose.
fo    =    fitoptions('Method','NonlinearLeastSquares','StartPoint',[ 3.99 0.144
     4.78 0.0111] ,'Algorithm','Levenberg-Marquardt','MaxFunEvals', 1000 ,'
    MaxIter',600);
f = fittype('0.1*(a1*exp(- m1 * x) + a2*exp(-m2*x))', 'options', fo);

for i = 1:n
    patient = pList(i);
    current = load([filePath 'POST' num2str(patient) '_M0.mat']); %loads AIF
    data
    im = current.im;
    zValue = current.zValue;
    nSlices = current.nSlices;
    na = current.na;
    ROI = current.ROI;
    Cp = current.Cp;
    time = current.time;
    savedir = [filePath 'slices\' num2str(patient)];
    x= length(im);
    %initalisation of marameter matrices
    D = zeros(x,x);
    a1 = zeros(x,x);
    a2 = zeros(x,x);
    m1 = zeros(x,x);
    m2 = zeros(x,x);
    t_c = time(N_s0(i)+1);
    time(1:(N_s0(i)))=[];
    time = time - t_c; %starts AIF fitting at the top of the measured peak

    for x_i = 1:x
        for y_i = 1:x
            if ROI(x_i, y_i) == 1
                total = total+1; %keeps track of the number of pixels within
    the ROI
                try
                [simpleAIF, gof , fitinfo] = fit(time, squeeze(Cp(x_i,y_i,N_s0
```

```
(i)+1:na)), f, 'Robust', 'LAR'); % fits the AIF to the measured contrast agent concentration data
            %saves the fitted parameters
            a1(x_i,y_i) = simpleAIF.a1;
            m1(x_i,y_i) = simpleAIF.m1;
            a2(x_i,y_i) = simpleAIF.a2;
            m2(x_i,y_i) = simpleAIF.m2;

            catch
                ROI(x_i,y_i)=0; % if fit is unsuccessful, the ROI for the pixel is set to 0.
            end
        end

    end
end
a1s = zeros(1,total);
m1s = zeros(1,total);
a2s = zeros(1,total);
m2s = zeros(1,total);
it= 0;
%save the parameters in vectors
for x_i = 1:x
    for y_i = 1:x
        if ROI(x_i,y_i) == 1
            it = it+1;
            a1s(it) = a1(x_i,y_i);
            m1s(it) = m1(x_i,y_i);
            a2s(it) = a2(x_i,y_i);
            m2s(it) = m2(x_i,y_i);
        end
    end
end
%calculates medians of the different parameters
a1_e = median(a1s);
a2_e = median(a2s);
```

```
    m1_e = median(m1s);
    m2_e = median(m2s);

    AIF_e = D_e.* (a1_e .* exp( - m1_e .* time) + a2_e .* exp (- m2_e .*time )
    );
    filename = [filePath 'Resultater\AIFS\POST' num2str(patient) '_AIF_e.mat'
    ];
    %saves the images and median AIF parameters for each patient.
    save(filename,'im','zValue','nSlices','na','Cp', 'time','AIF_e','D_e','
    m1_e', 'm2_e','a1_e','a2_e');
end
```

Finally, the following script calculates the mean parameters from the suitable AIFs, thus obtaining the population-based AIF.

```
%This script calculates the population-based AIF
filePath = 'C:\Users\Tina\Documents\Skole\Masteroppgave\Data\';
PREList = [131 73 44 92 77 122 24 27 28 29 31 32 41 43 45 47 48 49 50 51 52 55
    56 57 58 61 64 65 67 74 75 78 80 83 85 87 88 90 94 96 98 103 108 112 116
    118 124 126 127 130 132 133 134 138 143 144 146 147 150 151 152 153 154 156
    157 160 162 164 165 166 169 170 171 172 174 175 176]; %the patients where
    suitable AIFs were available from the pretreatment data
nPRE = length(pList); %amount of pretreatment AIFs available

D = 0.1; %contrast agent injection dose
%initialise median parameter vectors for the pretreatment data
a1PREs =  zeros(1,nPRE);
a2PREs = zeros(1,nPRE);
m1PREs = zeros(1,nPRE);
m2PREs = zeros(1,nPRE);
for i = 1:nPRE
    %extracts median AIF parameter for each patient
    patient = PREList(i);
    current = load([filePath 'Resultater\AIFS\P' num2str(patient) '_AIF_e.mat'
    ]);%loads individual AIFs
    m1PREs(i) = current.m1_e;
    m2PREs(i) = current.m2_e;
```

```
    a1PREs(i) = current.a1_e;
    a2PREs(i) = current.a2_e;
end

pList = [121 24 32 56 58 74 131 138 146 162 166 175 181]; %Patients for which
   suitable AIFs were available for post-CRT data
nPOST = length(pList);
%initialise post-CRT AIF parameters
a1POSTs =  zeros(1,nPOST);
a2POSTs = zeros(1,nPOST);
m1POSTs = zeros(1,nPOST);
m2POSTs = zeros(1,nPOST);

for i = 1:nPOST
    %extracts median AIF parameter for each patient
    patient = pList(i);
    current = load([filePath 'Resultater\AIFS\POST' num2str(patient) '_AIF_e.
   mat']);
    m1POSTs(i) = current.m1_e;
    m2POSTs(i) = current.m2_e;
    a1POSTs(i) = current.a1_e;
    a2POSTs(i) = current.a2_e;
end
n = nPRE + nPOST; %total number of AIFs
% gathers AIF parameters from the pretreatment and post-CRT data
a1s = [a1PREs a1POSTs];
a2s = [a2PREs a2POSTs];
m1s = [m1PREs m1POSTs];
m2s = [m2PREs m2POSTs];
%calculates mean, minimum and maximum median AIF parameters
m1st = [mean(m1s) min(m1s) max(m1s)];
m2st = [mean(m2s) min(m2s) max(m2s)];
a1st = [mean(a1s) min(a1s) max(a1s)];
a2st = [mean(a2s) min(a2s) max(a2s)];
%calculates the mean of the median AIF parameters
m1 = mean(m1s);
```

```
m2 = mean(m2s);
a1 = mean(a1s);
a2 = mean(a2s);
filename = [filePath 'Resultater\AIFS\AIFmain'];
save(filename,'D','m1','m2','a1','a2'); %saves the population-based AIF
```

A.2.2 The TK Model

The following script was used for data analysis using the TK model with individual AIFs. Because the only difference between the TK model analysis from population-based and individual AIFs was which AIF was included, only the script for analysis using the TK model with individual AIFs is included here.

```
% TK model
filePath = 'C:\Users\Tina\Documents\Skole\Masteroppgave\Data\';
pList = [56 58 74 131 138 146 162 166 175 181] %a selection of patients
N_s0 = [5 13 12 14 18 16 16 21 13 13]; %the measured time step where injection
    took place for a selection of patients.
n = length(pList);
T_10 = 1354; %(ms) initial T1-relaxation time, estimated by Groevik et al.
r1 = 3.6; %(1/(mM*s)) relaxivity of the contrast agent

for i = 1:n
    patient = pList(i);
    current = load([filePath 'Resultater\AIFS\POST' num2str(patient) '_AIF_e.
   mat']);%loads individual AIFs, in this analysis for the POST-data
    im = current.im;
    x= length(im);
    zValue = current.zValue;
    nSlices = current.nSlices;
    na = current.na;
    time = current.time;
    Cp_median = current.Cp_median;
    AIF_e = current.AIF_e;
    D_e = current.D_e;
```

```
21  m1_e = current.m1_e;
22  m2_e = current.m2_e;
23  a1_e = current.a1_e;
24  a2_e = current.a2_e;
25  AIF = [num2str(D_e) '*(' num2str(a1_e) '* exp (- ' num2str(m1_e) '*x) + '
    num2str(a2_e) '*exp(-' num2str(m2_e) '*x  )) ']; %creates the AIF function
26  %stepwise incorporation of the AIF into the equation for the TK model
27  A = ['K_trans * ' num2str(D_e) '* exp(-(K_trans/ve)*x)'];
28  b = [num2str(a1_e) '*(1-exp(-(' num2str(m1_e) '- K_trans/ve)*x))/ ('
    num2str(m1_e) '-K_trans/ve)'];
29  c = [num2str(a2_e) '*(1-exp(-(' num2str(m2_e) '- K_trans/ve)*x))/ ('
    num2str(m2_e) '-K_trans/ve)'];
30  Ctfit = ['vp *(' AIF ') + ' A '*(' b '+' c ')']; %the equation used for
    analysis with the TK model
31  problem = zeros(x,x,nSlices); %initialises a matrix used to save locations
     where fit problems occur
32  Brix = load([filePath 'Resultater\Brix\POST' num2str(patient) '_Brix.mat'
    ]);%loads the ROI where analysis will be performed
33  ROI = Brix.ROI;
34  fo   =   fitoptions('Method','NonlinearLeastSquares','StartPoint',[1.67
    0.3 37], 'Algorithm','Trust-Region','Lower',[0,0,0], 'Upper' , [10 1 1], '
    MaxFunEvals', 1000 ,'MaxIter',600);
35  f = fittype(Ctfit,'options', fo);  %initialises fit settings
36  %initialises parameter matrices. In addition to the parameters, maximum
37  %and minimum values, and information about the goodness of fit was
38  %saved
39  K_trans = zeros(x,x,nSlices);
40  K_trans_low = zeros(x,x,nSlices);
41  K_trans_high = zeros(x,x,nSlices);
42  ve = zeros(x,x,nSlices);
43  ve_low = zeros(x,x,nSlices);
44  ve_high = zeros(x,x,nSlices);
45  vp = zeros(x,x,nSlices);
46  vp_low = zeros(x,x,nSlices);
47  vp_high = zeros(x,x,nSlices);
48  rmse = zeros(x,x,nSlices);
```

```
49      rsquare = zeros(x,x,nSlices);
50      total = 0; %used to count number of pixels within the ROI
51      badfit = 0; %used to count the number of unsuccessful fits for the patient
        .
52      Ct = zeros(x,x,nSlices,na); %initalises contrast agent concentration
        matrix
53      t_c = time(N_s0(i)+1);
54      time(1:(N_s0(i)))=[]; %the fitting will be performed for the measured
        curve starting after the contrast agent is injected
55      time = time - t_c;
56      for j = 1:nSlices
57          fileID = fopen('C:\Users\Tina\Documents\Skole\Masteroppgave\Programmer
        \ongoings.txt','a'); %used to keep track of the progress of the analysis
58          fprintf(fileID,' Begin calculations on patient %1.0f, slice %1.0f ',
        patient, j);
59          fprintf(fileID, '\r\n');
60          fclose(fileID);
61          fprintf('\n Begin calculations on patient %1.0f, slice %1.0f \n',
        patient, j);
62          for x_i = 1:x
63              for y_i = 1:x
64                  if ROI(x_i,y_i,j) ~= 0
65                      signal = squeeze(im(x_i,y_i,j,:));
66                      signal_0 = sum(signal(1:N_s0(i)))/N_s0(i); %calculates the
         average signal intensity prior to CA injection
67                      total = total+1;
68                      Ct(x_i,y_i,j,:) = (signal - signal_0)./(signal_0 *0.001*r1
         * T_10);%calculates the contrast agent concentration from the signal
        intensity
69                      try
70                      Ctshort = squeeze(Ct(x_i,y_i,j,N_s0(i)+1:na));
71                      [Tofts_e, gof , fitinfo] = fit(time, Ctshort , f, 'Robust'
        , 'LAR'); %fits the contrast agent concentration curves to the TK model
72                      %saves the parameters
73                      K_trans(x_i,y_i,j) = Tofts_e.K_trans;
```

```
74                  ve(x_i,y_i,j) = 100*Tofts_e.ve; %multiplies with 100 to
    get the unit %
75                  vp(x_i,y_i,j) = 100*Tofts_e.vp; %Multiplies with 100 to
    get the unit %
76                  rmse(x_i,y_i,j) = gof.rmse;
77                  rsquare(x_i,y_i,j) = gof.rsquare;
78                  inter = confint(Tofts_e);
79                  K_trans_low(x_i,y_i,j) = inter(1,1);
80                  K_trans_high (x_i,y_i,j) = inter(2,1);
81                  ve_low(x_i,y_i,j) = inter(1,2);
82                  ve_high(x_i,y_i,j) = inter(2,2);
83                  vp_low(x_i,y_i,j) = inter(1,3);
84                  vp_high(x_i,y_i,j) = inter(2,3);
85                  if rem(x_i,2) == 0
86                 figure,  plot(Tofts_e,time,Ctshort);
87                  end
88                  catch %prevents the program from stopping if an error
    occurs in a fit, and saves the location of the error
89                      badfit = badfit+1;
90                      problem(x_i,y_i,j) = 1000;
91                  end
92              end
93          end
94
95      end
96   end
97   total = total-badfit; %finds number length of the vectors used for the
    parameters
98   %intialises vectors where all parameters are gathered
99   K_transes = zeros(1,total);
100  ves = zeros(1,total);
101  vps = zeros(1,total);
102  rmses = zeros(1,total);
103  rsquares = zeros(1,total);
104  it = 0;
105  for j = 1:nSlices
```

```
106         for x_i = 1:x
107             for y_i = 1:x
108                 if ROI(x_i,y_i,j) ~= 0 %here the parameters are gatered into
    one vector each
109                     it = it+1;
110                     K_transes(it) = K_trans(x_i,y_i,j);
111                     ves(it) = ve(x_i,y_i,j);
112                     vps(it) = vp(x_i,y_i,j);
113                     rmses(it) = rmse(x_i,y_i,j);
114                     rsquares(it) = rsquare(x_i,y_i,j);
115                 end
116
117             end
118         end
119     end
120     Ct_median = zeros(1,60);
121     for k = 1:60
122         pixels = zeros(1,total);
123         totn =0;
124         for x_i = 1: x
125             for y_i =1:x
126                 if ROI(x_i,y_i) == 1
127                     totn = totn+1;
128                     pixels(totn) = Ct(x_i,y_i,k);
129                 end
130             end
131         end
132         Ct_median(k) = median(pixels); %saves the median values of the
    contrast agent concentrations within the tumour at the different time
    points.
133     end
134 time_whole = current.time;
135 beforecontrast = zeros(1,N_s0(i));
136 %saves the TK model parameters
137 filename = [filePath 'Resultater\Tofts\POST' num2str(patient) '_Tofts_e.mat'];
```

```
parsaveTofts(filename,K_trans_low,K_trans,K_trans_high,K_transes,ve,ve_low,
    ve_high,ves,vp,vp_low,vp_high,vps,rsquare,rsquares,rmse,rmses,time,
    time_whole,Ct_median);
end
```

A.2.3 The Brix Model

The following script was used for data analysis using the Brix model.

```
clear all
filePath = 'C:\Users\Tina\Documents\Skole\Masteroppgave\';
addpath('C:\Users\Tina\Documents\Skole\Prosjekt\NIFTI'); %Include functions
    for opening niftifiles.
addpath('C:\Users\Tina\Documents\Skole\Prosjekt');

pList = [56 58 74 131 138 146 162 166 175 181] %a selection of patients
N_s0 = [5 13 12 14 18 16 16 21 13 13]; %the measured time step where injection
     took place for a selection of patients.
n = length(pList);

for i = 1:n
    S_ligning = ['A * k_ep /(k_ep-k_el) * (exp(-k_el*x) - exp(-k_ep*x))']; %
    the model equation the data is to be fitted to
    %intialise curve fit settings
    fo = fitoptions('Method','NonlinearLeastSquares','StartPoint',[0.21 0.17
    15], 'Algorithm','Trust-Region', 'MaxFunEvals', 1000, 'MaxIter',600);
    f = fittype(S_ligning,'options',fo);

    filename = ['P' num2str(pList(i)) '_M0.mat'];
    S = load([filePath 'Data\' filename]); %Loads information from
    SortPatients.m
    aValue = S.aValue; %time values
    im = S.im; %image matrix
    nSlices = S.nSlices; %number of slices for patient
    na = S.na; %number of elements in time vector
```

```
22    zValue = S.zValue; %slice location vector
23
24    x=length(im); %determine size dimension of image
25    patient = pList(i);
26
27     radiologist = 'shh';
28    if patient == 58
29       radiologist = 'an'; %for some patients, the tumour ROIs created by SHH
      were not available, and the ROIs by AN was used instead
30    end
31    [ROI,T2Values,roiz] = niftiresize(x,nSlices,zValue,patient,radiologist); %
      obtains resized ROI from nifti-file. T2values are the original slice
      locations for the ROI, and roiz gives the selected slices closest to those
      of the DCE-MR images.
32    %initialise matrices
33    A_brix = zeros(x,x,nSlices);
34    A_brix_low = zeros(x,x,nSlices);
35    A_brix_high = zeros(x,x,nSlices);
36    k_el_brix = zeros(x,x,nSlices);
37    k_el_brix_low = zeros(x,x,nSlices);
38    k_el_brix_high = zeros(x,x,nSlices);
39    k_ep_brix = zeros(x,x,nSlices);
40    k_ep_brix_low = zeros(x,x,nSlices);
41    k_ep_brix_high = zeros(x,x,nSlices);
42    rmse = zeros(x,x,nSlices);
43    s0juster = zeros(x,x,nSlices);
44    signal = zeros(1,na);
45
46    for j = 1:nSlices
47        %below, the progress in the analysis is exported to a text file in
48        %order for it to be easier to keep track of.
49        fileID = fopen('C:\Users\Tina\Documents\Skole\Masteroppgave\Programmer
      \ongoings.txt','a');
50        fprintf(fileID,' Begin calculations on patient %1.0f, slice %1.0f ',
      patient, j);
51       fprintf(fileID, '\r\n');
```

```
52      fclose(fileID);
53      fprintf('\n Begin calculations on patient %1.0f, slice %1.0f \n',
    patient, j);
54      feil = 0;
55      for x_i = 1:x
56          for y_i = 1:x
57               if ROI(x_i,y_i,j) ~= 0
58                  for k = 1:na
59                      signal(k) = im(x_i,y_i,j,k); %signal intensity
    variation in one pixel is extracted
60                  end
61              time = aValue(:,j);
62              signal_0 = sum(signal(1:N_s0(i)))/N_s0(i); %the average signal
     intensity prior to CA injection is calculated
63              RSI = zeros(1,na);
64              if signal_0 == 0
65                  nullvar =N_s0(i);
66                  while signal_0 == 0 && nullvar < length(signal)
67                      nullvar = nullvar+1;
68                      signal_0 = sum(signal(1:nullvar))/nullvar;
69                  end
70                  s0juster(x_i,y_i,j) = nullvar; %in some cases signal_0 was
     0. Then a few more time steps were included to avoid an error. But the
    pixels this happened for were deleted prior to further analysis.
71              end
72                  for it = 1:length(signal)
73                      RSI(it) = (signal(it)-signal_0)/signal_0; %the
    relative signal intensity is calculated
74                  end
75                  RSI = RSI(N_s0(i)+1:length(RSI));
76                  t0 = time(N_s0(i));
77                  time = time(N_s0(i)+1:length(time)); %fitting to the Brix
    model starts at time of contrast agent injection
78                  for tidsi = 1:length(time)
79                  time(tidsi) = (time(tidsi)-t0)/60;
80                  end
```

```
81                    try %here the relative signal intensity curves are fitted
   to the Brix model.
82                        [fit1,gof,fitinfo] = fit(time,RSI',f,'Robust','LAR', '
   Lower', [0 0 0],'Upper',[500 500 500]);
83                        A_brix(x_i,y_i,j) = fit1.A;
84                        inter = confint(fit1);
85                        A_brix_low(x_i,y_i,j) = inter(1,1);
86                        A_brix_high(x_i,y_i,j) = inter(2,1);
87                        k_el_brix(x_i,y_i,j) = fit1.k_el;
88                        k_el_brix_low(x_i,y_i,j) = inter(1,2);
89                        k_el_brix_high(x_i,y_i,j)=inter(2,2);
90                        k_ep_brix(x_i,y_i,j) = fit1.k_ep;
91                        k_ep_brix_low(x_i,y_i,j) = inter(1,3);
92                        k_ep_brix_high(x_i,y_i,j)=inter(2,3);
93                        rmse(x_i,y_i,j) = gof.rmse;
94                    catch %in cases where errors occured for the fitting, the
   locations were saved by setting the parameter pixels = -1, and were not
   included in further analysis.
95                        feil =feil+1; %counts number of failed curve fits for
   each patient.
96                        A_brix(x_i,y_i,j) = -1;
97                        k_el_brix(x_i,y_i,j) = -1;
98                        k_ep_brix(x_i,y_i,j) = -1;
99                    end
100               end
101           end
102       end
103    end
104       resultater = [filePath 'Data\Resultater\Brix\PRE' num2str(pList(i)) '
   _Brix.mat'];  %the fitted parameters are saved
105       parsave(resultater,A_brix,A_brix_high,A_brix_low,ROI,feil,k_el_brix,
   k_el_brix_high,k_el_brix_low,k_ep_brix,k_ep_brix_high,k_ep_brix_low,rmse,
   s0juster);
106 end
```

A.3 Statistical Analysis

The scripts analysing the Brix and TK model parameters were almost identical. Therefore only the script used for the Brix model parameters is included. Below, the script from the pretreatment analysis is found.

```
%This script test analyses the pretreatment parameters from the Brix
%model. Medians are calculated from the parameter percentiles, and
%additionally analysis on heterogeneity is performed.
filePath = 'C:\Users\Tina\Documents\Skole\Masteroppgave\Data\';
%patients were loaded in groups based on what was tested for. Now the
%patients who received CRT are active
%patients who did not receive CRT:
%pList = [28 29 31 45 46 48 57 61 64 65 72 73 75 77 78 83 85 88 92 94 98 103
    105 106 108 110 112 115 118 122 124 127 133 134 143 144 147 149 151 152 157
     160 164 165 171 172 174 176];
%patients that received CRT
pList = [24 27 32 41 43 44 47 49 50 51 52 55 56 58 67 74 79 80 87 89 90 96 116
     119 120 121 125 126 130 131 132 138 146 150 153 154 156 162 166 169 170
    175 181];
%pList = [27 32 44 51 89 96 116 119 121 131 132 146 162 170 175 181 24 43 49
    50 55 58 67 74 79 120 156 166 169 90];% patients with mrN 1 or 2
n = length(pList);
N = 101; %length of percentile matrix: percentiles 0-100
M = 100; %number of histogram slots
%initalises percentile matrices and heterogeneity matrices
A_perc = zeros(n,N);
el_perc = zeros(n,N);
ep_perc = zeros(n,N);
skew = zeros(3,n);
rel = zeros(3,n);
kurt = zeros(3,n);
stds = zeros(3,n);

for i = 1:n
    hists = zeros(3,M);%initialise histogram matrix for all parameters
```

```
patient = pList(i);
S = load([filePath 'Resultater\Brix\PRE' num2str(patient) '_Brix.mat']); % loads Brix model parameters for a patient
lengde = 0;
dims = size(S.A_brix); %finds dimension of the images
nSlices = dims(3);
x= dims(1);
ROI = S.ROI; %loads the region of interest
for j = 1:nSlices
    for x_i = 1:x
        for y_i = 1:x
            if S.A_brix(x_i,y_i,j) < 0 || S.A_brix(x_i,y_i,j) > 7 || S.k_el_brix(x_i,y_i,j) > 2 || S.k_ep_brix(x_i,y_i,j) > 40%|| Here, pixels of unsuccessful fits are removed (A_brix = -1). In addition nonphysiological values are removed. Upper limits for the TK model parameters were set to 3 for Ktrans, 80 for ve, and 20 for vp.
                ROI(x_i,y_i,j)=0;
            end
            if S.s0juster(x_i,y_i,j)~=0 %remove poor signal curves found in the Brix script
                ROI(x_i,y_i,j) = 0;
            end
            if ROI(x_i,y_i,j) ~= 0
               lengde = lengde +1;  %find length of vectors containing the fitted parameters.
            end
        end
    end
end
%initalise vectors where all parameters are gathered.
A_verdier = zeros(1,lengde);
k_el_verdier = zeros(1,lengde);
k_ep_verdier = zeros(1,lengde);
nr = 0;
for j = 1:nSlices
    for x_i = 1:x
```

```
            for y_i = 1:x
                if ROI(x_i,y_i,j) ~= 0
                   %Here the parameters from within the ROI are saved in
   different vectors
                   nr=nr+1;
                   A_verdier(nr)= S.A_brix(x_i,y_i,j);
                   k_el_verdier(nr) = S.k_el_brix(x_i,y_i,j);
                   k_ep_verdier(nr) = S.k_ep_brix(x_i,y_i,j);
                end
            end
        end
    end
    %the first slots in the percentile matrices are set to the minimum value
   of
    %the parameters
   A_perc(i,1) = min(A_verdier);
   el_perc(i,1) = min(k_el_verdier);
   ep_perc(i,1) = min(k_ep_verdier);
   %the remaining percentiles are calulated
 for k = 2:N
     A_perc(i,k) = prctile(A_verdier,k-1);
      el_perc(i,k) = prctile(k_el_verdier,k-1);
       ep_perc(i,k) = prctile(k_ep_verdier,k-1);
 end
 %histogram vectors are calculated.
 hists(1,:) = histcounts(A_verdier,100);
 hists(2,:) = histcounts(k_el_verdier,100);
 hists(3,:) = histcounts(k_ep_verdier,100);
%histogram quantities are saved for each patient.
 for m = 1:3
 skew(m,i) = skewness(hists(m,:));
rel(m,i) = max(hists(m,:))/mean(hists(m,:));
kurt(m,i) = kurtosis(hists(m,:));
stds(m,i) = std(hists(m,:));
 end
end
```

```
%%
p_A = ones(N,1); %percentile p-values are initialised
p_el = ones(N,1);
p_ep = ones(N,1);
%Here the noCRT patients are assigned a group number based on the endpoints
T02vs34 = [1 1 2 2 2 1 1 2 2 2 1 1 1 1 2 2 2 1 1 1 1 2 1 2 2 1 2 2 2 1 2 2 2 2
    1 1 1 1 2 1 1 2 2 1 1 1 2 2]; %ypT 0-2 vs 3-4
N0vs12 = [2 1 2 1 2 1 2 1 2 1 1 1 1 1 1 2 2 1 1 1 1 2 1 2 2 1 1 1 2 1 2 1 1 1
   1 1 1 2 2 2 1 2 1 2 1 1 2 2] %ypN 0 vs 1-2

%Here the CRT patients are assigned a group number based on the endpoints
CT0234 = [2 2 2 1 1 2 2 2 2 1 2 1 1 2 2 2 2 2 1 2 2 2 2 1 2 1 2 2 2 1 1 2 1 1
   1 2 2 2 1 2 2 2 1]; %ypT 0-2 vs 3-4
CN012 = [2 2 2 1 2 2 1 2 1 1 1 2 1 2 2 2 2 2 1 1 2 1 1 2 1 1 1 1 1 1 1 1 1 1
    2 2 1 2 1 1 1 2]; %ypN 0 vs 1-2
TRG013= [2 2 2 2 2 2 2 2 2 2 2 2 1 2 2 2 2 2 1 2 2 2 2 2 2 2 2 2 1 1 2 2 1 2
    2 2 2 2 2 2 2 2]; %TRG 0 vs 1-3
dT0234 = [1 1 1 1 1 1 1 1 1 2 1 1 2 1 1 1 1 1 2 1 1 1 1 1 1 1 1 1 2 2 1 1 2
   1 1 1 1 1 1 1 1 1]; %deltaT 0-2 vs 3-4
%group numbers for the patients with mrN 1-2 who received CRT
dN = [1 1 1 2 2 2 2 1 2 2 2 2 2 2 2 1 1 2 1 2 2 2 1 1 1 2 2 2 2 2]; %deltaN 0
   vs 1-2
threshold = zeros(1,N); %used to intialise a 0.05 vector used in the
   percentile plots.
G = CT0234 %endpoint is selected
%matrices that will contain the median, minimum and maximum median values
%of the different groups is created
G1_median = zeros(3,3);
G2_median = zeros(3,3);
for j = 1:N %calculates p-values for the different percentiles
   A_brix = A_perc(:,j);
   k_el = el_perc(:,j);
   k_ep = ep_perc(:,j);

[G1A,G2A] = makegroups(A_brix,G); %the function divides the parameters into
   groups. It is displayed later in the appendix.
```

```
p_A(j) = ranksum(G1A,G2A);
if j == 51 %this is the median
    G1_median(1,1) = median(G1A);
    G1_median(1,2) = min(G1A);
    G1_median(1,3) = max(G1A);
    G2_median(1,1) = median(G2A);
    G2_median(1,2) = min(G2A);
    G2_median(1,3) = max(G2A);
end

[G1el,G2el] = makegroups(k_el,G);
p_el(j) = ranksum(G1el,G2el);
if j == 51
    G1_median(2,1) = median(G1el);
    G1_median(2,2) = min(G1el);
    G1_median(2,3) = max(G1el);
    G2_median(2,1) = median(G2el);
    G2_median(2,2) = min(G2el);
    G2_median(2,3) = max(G2el);
end

[G1ep,G2ep] = makegroups(k_ep,G);
p_ep(j) = ranksum(G1ep,G2ep);
if j == 51
    G1_median(3,1) = median(G1ep);
    G1_median(3,2) = min(G1ep);
    G1_median(3,3) = max(G1ep);
    G2_median(3,1) = median(G2ep);
    G2_median(3,2) = min(G2ep);
    G2_median(3,3) = max(G2ep);
end
threshold(j)=0.05; %threshold used in percentile plot set to 0.05
end
p = [0:1:100];
%percentile plot is created
```

```
figure; plot(p,p_ep,p,threshold,'k--'), legend('k_{ep}', 'p = 0.05'),  ylim([0
    0.2]), ylabel('p-value'), xlabel('Percentile') ,title('Percentile p-value
   plot for \DeltaT 0-2 versus 3-4')

Amedians = A_perc(:,51); %saves the parameter medians for the different
   patients. These are used to make the box plots.
k_elmedians = el_perc(:,51);
k_epmedians = ep_perc(:,51);
p_median = [ p_A(51) ; p_el(51) ; p_ep(51) ]'; %the median p-values

p_skew= zeros(3,1)'; %histogram p-value matrices are intialised.
p_rel =zeros(3,1)';
p_kurt = zeros(3,1)';
p_std = zeros(3,1)';
for i =1:3 %for the different parameters, histogram quantity p-values are
   calculated saved to one matrix each.
[G1A,G2A] = makegroups(skew(i,:),G);
p_skew(i) = ranksum(G1A,G2A);
[G1A,G2A] = makegroups(rel(i,:),G);
p_rel(i) = ranksum(G1A,G2A);
[G1A,G2A] = makegroups(kurt(i,:),G);
p_kurt(i) = ranksum(G1A,G2A);
[G1A,G2A] = makegroups(stds(i,:),G);
p_std(i) = ranksum(G1A,G2A);
end
figure, boxplot(Amedians,G,'Labels',{'ypT 0-2', 'ypT 3-4'}), ylabel('$A_{Brix}
   $'); %A box plot is made for the A_brixmedians in ypT 0-2 vs 3-4
```

The script used for analysis of post-CRT medians and changes from pretreatment to post-CRT medians is showed below.

```
% In this script the post-CRT parameter medians and change in medians from
% pretreatment to post-CRT are tested againtst different endpoints.
clear all
pList = [24 32 56 58 74 79 121 130 131 138 146 150 153 162 166 169 175 181]; %
   all 18 post-CRT patients
%pList = [32 121 131 146 162 175 181 24 58 74 79 166 169] %the post-CRT
```

```
%patients that had mrN 1-2. Used for det delta N 0 vs 1-2 endpoint.
filePath = 'C:\Users\Tina\Documents\Skole\Masteroppgave\Data\';
n = length(pList);
PAR_PRE = zeros(3,n); %initialise matrix: medians for pretreatment parameters
    of the different patients
PAR_POST = zeros(3,n);%initialise matrix: medians for post-CRT parameters of
    the different patients
deltaPAR = zeros(3,n);%initialise matrix: change in median parameters of the
    different patients
for i = 1:n
    patient = pList(i);
    SPRE = load([filePath 'Resultater\Brix\PRE' num2str(patient) '_Brix.mat'])
    ; %load pretreatment parameters
    SPOST = load([filePath 'Resultater\Brix\POST' num2str(patient) '_Brix.mat'
    ]); %load post-CRT parameters
    lengdePRE = 0; %later set to the amount of pixels within the pretreatment
    ROI
    lengdePOST = 0; %later set to the amount of pixels within the post-CRT ROI
    dimsPRE = size(SPRE.A_brix); %dimensions of the images
    dimsPOST = size(SPOST.A_brix);
    nSlicesPRE = dimsPRE(3); %slices of the images
    nSlicesPOST = dimsPOST(3);
    xPRE= dimsPRE(1); %dimensions of the images
    xPOST = dimsPOST(1);
    ROIPRE = SPRE.ROI; %pretreatment ROI
    ROIPOST = SPOST.ROI; %post-CRT ROI
    for j = 1:nSlicesPRE
        for x_i = 1:xPRE
            for y_i = 1:xPRE
                if SPRE.A_brix(x_i,y_i,j) < 0 || SPRE.A_brix(x_i,y_i,j) > 7 ||
     SPRE.k_el_brix(x_i,y_i,j) > 2 || SPRE.k_ep_brix(x_i,y_i,j) > 40 %
    unsuccessful fits are removed (A = -1). Nonphysiological parameters are
    removed. For the TK model the upper limits for the parameters were 3 for
    Ktrans, 80 for ve, and 20 for vp.
                    ROIPRE(x_i,y_i,j)=0;
                end
```

```
32              if SPRE.s0juster(x_i,y_i,j)~=0 %remove poor signal curves
    found in Brixfit.m
33                  ROIPRE(x_i,y_i,j) = 0;
34              end
35              if ROIPRE(x_i,y_i,j) ~= 0
36                 lengdePRE = lengdePRE +1;  %find length of vectors
    containing the fitted parameters.
37              end
38          end
39      end
40  end
41  for j = 1:nSlicesPOST
42      for x_i = 1:xPOST
43          for y_i = 1:xPOST
44              if SPOST.A_brix(x_i,y_i,j) < 0 || SPOST.A_brix(x_i,y_i,j) > 7
    || SPOST.k_el_brix(x_i,y_i,j) > 2 || SPOST.k_ep_brix(x_i,y_i,j) > 40%
    removal of nonphysiological parameters and unsuccessful fits repeated for
    the post-CRT data
45                  ROIPOST(x_i,y_i,j)=0;
46              end
47              if SPOST.s0juster(x_i,y_i,j)~=0 %remove poor signal curves
    found in Brixfit.m
48                  ROIPOST(x_i,y_i,j) = 0;
49              end
50              if ROIPOST(x_i,y_i,j) ~= 0
51                 lengdePOST = lengdePOST +1;  %find length of vectors
    containing the fitted parameters.
52              end
53          end
54      end
55  end
56  A_verdier_PRE = zeros(1,lengdePRE); %intialise parameter vectors
57  k_el_verdier_PRE = zeros(1,lengdePRE);
58  k_ep_verdier_PRE = zeros(1,lengdePRE);
59  A_verdier_POST = zeros(1,lengdePOST);
60  k_el_verdier_POST = zeros(1,lengdePOST);
```

```
    k_ep_verdier_POST = zeros(1,lengdePOST);
    nrPRE = 0;
    nrPOST = 0;
    for j = 1:nSlicesPRE %here the pretreatment parameters are saved to
   vectors
        for x_i = 1:xPRE
            for y_i = 1:xPRE
                if ROIPRE(x_i,y_i,j) ~= 0
                   nrPRE=nrPRE+1;
                   A_verdier_PRE(nrPRE)= SPRE.A_brix(x_i,y_i,j);
                   k_el_verdier_PRE(nrPRE) = SPRE.k_el_brix(x_i,y_i,j);
                   k_ep_verdier_PRE(nrPRE) = SPRE.k_ep_brix(x_i,y_i,j);
                end
            end
        end
    end
%medians for the pretreatment parameters are saved for each patient
    PAR_PRE(1,i) = median(A_verdier_PRE);
    PAR_PRE(2,i) = median(k_el_verdier_PRE);
    PAR_PRE(3,i) = median(k_ep_verdier_PRE);

    for j = 1:nSlicesPOST %here the post-CRT parameters are saved to vectors
        for x_i = 1:xPOST
            for y_i = 1:xPOST
                if ROIPOST(x_i,y_i,j) ~= 0
                   nrPOST=nrPOST+1;
                   A_verdier_POST(nrPOST)= SPOST.A_brix(x_i,y_i,j);
                   k_el_verdier_POST(nrPOST) = SPOST.k_el_brix(x_i,y_i,j);
                   k_ep_verdier_POST(nrPOST) = SPOST.k_ep_brix(x_i,y_i,j);
                end
            end
        end
    end
%medians for the post-CRT parameters are saved for each patient
    PAR_POST(1,i) = median(A_verdier_POST);
    PAR_POST(2,i) = median(k_el_verdier_POST);
```

```
    PAR_POST(3,i) = median(k_ep_verdier_POST);
    %difference between the parameters pretreatment and post-CRT is
    %calculated
    for j = 1:3
        deltaPAR(j,i) =  PAR_POST(j,i)-PAR_PRE(j,i);
    end

end

%%
%Here the patients are assigned a group number based on the endpoint
T0234 = [2 2 1 2 2 2 1 2 1 2 1 1 1 2 1 2 2 1]; %ypT 0-2 vs 3-4
N012 = [2 2 1 2 2 2 1 1 1 1 1 1 1 2 1 1 2]; %ypN 0 vs 1-2
TRG013 = [2 2 1 2 2 2 2 2 1 2 2 1 2 2 2 2 2 2]; % TRG 0 vs 1-3
dT0234 = [1 1 2 1 1 1 1 1 2 1 1 2 1 1 1 1 1 1]; %deltaT 0-2 vs 3-4
dN = [1 2 2 2 2 2 1 1 2 1 1 2 2]; % deltaN 0 vs 1-2. Only patients with mrN
    1-2 included.
G = T0234 %chooses the endpoint to analyse
pPOST = zeros(1,3); %initialise postCRT-pvalues
G1_POST = zeros(3,3); % initialise matrix for parameter medians, minimums and
    maximums for the two groups
G2_POST = zeros(3,3);%
%Abrix:
[G1A,G2A] = makegroups(PAR_POST(1,:),G); %divides the parameters into two
    vectors prior to the ranksum test
pPOST(1) = ranksum(G1A,G2A); %ranksum test on post parameters, then saves
    medians, maximum and minimum for the two groups.
    G1_POST(1,1) = median(G1A);
    G1_POST(1,2) = min(G1A);
    G1_POST(1,3) = max(G1A);
    G2_POST(1,1) = median(G2A);
    G2_POST(1,2) = min(G2A);
    G2_POST(1,3) = max(G2A);
%k_el;
[G1el,G2el] = makegroups(PAR_POST(2,:),G);
pPOST(2) = ranksum(G1el,G2el);
```

```
    G1_POST(2,1) = median(G1el);
    G1_POST(2,2) = min(G1el);
    G1_POST(2,3) = max(G1el);
    G2_POST(2,1) = median(G2el);
    G2_POST(2,2) = min(G2el);
    G2_POST(2,3) = max(G2el);
%k_ep:
[G1ep,G2ep] = makegroups(PAR_POST(3,:),G);
pPOST(3) = ranksum(G1ep,G2ep);
    G1_POST(3,1) = median(G1ep);
    G1_POST(3,2) = min(G1ep);
    G1_POST(3,3) = max(G1ep);
    G2_POST(3,1) = median(G2ep);
    G2_POST(3,2) = min(G2ep);
    G2_POST(3,3) = max(G2ep);

    pdelta = zeros(1,3);
    G1_d = zeros(3,3);
    G2_d = zeros(3,3);
%A_brix:
[G1Ad,G2Ad] = makegroups(deltaPAR(1,:),G); %divides the parameters into two
   vectors prior to the ranksum test
pdelta(1) = ranksum(G1Ad,G2Ad);  %ranksum test on post parameters, then saves
   medians, maximum and minimum for the two groups.
    G1_d(1,1) = median(G1Ad);
    G1_d(1,2) = min(G1Ad);
    G1_d(1,3) = max(G1Ad);
    G2_d(1,1) = median(G2Ad);
    G2_d(1,2) = min(G2Ad);
    G2_d(1,3) = max(G2Ad);
%k_el:
[G1eld,G2eld] = makegroups(deltaPAR(2,:),G);
pdelta(2) = ranksum(G1eld,G2eld);
    G1_d(2,1) = median(G1eld);
    G1_d(2,2) = min(G1eld);
    G1_d(2,3) = max(G1eld);
```

```
    G2_d(2,1) = median(G2eld);
    G2_d(2,2) = min(G2eld);
    G2_d(2,3) = max(G2eld);
%k_ep:
[G1epd,G2epd] = makegroups(deltaPAR(3,:),G);
pdelta(3) = ranksum(G1epd,G2epd);
    G1_d(3,1) = median(G1epd);
    G1_d(3,2) = min(G1epd);
    G1_d(3,3) = max(G1epd);
    G2_d(3,1) = median(G2epd);
    G2_d(3,2) = min(G2epd);
    G2_d(3,3) = max(G2epd);
%Creates a boxplot:
figure, boxplot(deltaPAR(3,:),N012,'Labels',{'ypN 0', 'ypN 1-2'});
```

A.4 Additional Scripts

The function used to load and resize ROIs is shown below. A function from the MathWorks package *Tools for NIfTI and ANALYZE image* was used to load the nifti-files and transform them into Matlab matrices [56].

```
%This function calculates a ROI,
function [roi,T2Values,roiz] = niftiresize(imSize,slice_number,zValue,patient,
    radiologist)
%roi: resised region of interest
%T2Values: slice locations for the ROI and the high resolution T2-weigthed
%images
%roiz: the slices from T2Values closest to the slices in the dynamic images
%radiologist: determines which ROI to load, the one drawn by SHH or the one
%drawn by AN
filePath = ['C:\Users\Tina\Documents\Skole\Masteroppgave\Data\'];
imList = dir([filePath 'Oxytarget_' int2str(patient) ' PRE\T2\Im*']);
tempSlices = length(imList); %number of slices in ROI, found from the high
    resolution T2-weighted images
```

```
T2Values = zeros(1,tempSlices);

for i = 1:tempSlices
    info = dicominfo([filePath 'Oxytarget_' int2str(patient) ' PRE\T2\' imList
    (i).name]);
    T2Slice = info.ImagePositionPatient;
    T2Values(i) = T2Slice(3,1); %Find the slice locations of the ROI
end
 %load the ROI struct
nifti = load_untouch_nii([filePath 'Oxytarget_' int2str(patient) ' PRE\binary\
    ' radiologist '\tumour.nii']);
temproi = nifti.img;                %Extract the ROI matrix

temproi = permute(temproi, [2 1 3]); %Adjust the geometry og the axes so that
    they match the images.
if patient == 115
   temproi = flip(temproi,3);
end
roi = zeros(imSize,imSize,slice_number) ; %initialise ROI matrix with desired
    dimensions.
tempLength= length(temproi);           %Find the dimension of the ROI
scale = tempLength/imSize              %How much smaller I want the xy-
    dimensions of the ROI to be

temproi2 = zeros(tempLength,tempLength,slice_number); %initialise matrix where
     only the slice dimensions has been reduced.

zValue = zValue(1,:); %Dynamic image slice locations
T2lengde = length(T2Values); %Number of slices in original roi.
roiz = zeros(1,slice_number); %Initialize vetor that will contain the slice
    locations from the original ROI closest to the slice locations of the
    dynamic images.

for j = 1:slice_number %In this loop the number of slices is reduces to the
    desired number.
    temproi2(:,:,j) = temproi(:,:,1);
```

```
    temp = abs(zValue(j)-T2Values(1));
    roiz(j) = T2Values(1);
    for k = 1:T2lengde
        diff =abs(zValue(j) - T2Values(k));
        if  diff <= temp
            temp = diff;
            temproi2(:,:,j) = temproi(:,:,k);
            roiz(j)=T2Values(k); %The slices of the ROI closest to those of the dynamic image are chosen for the new ROI.
        end
    end
end

for j = 1:slice_number %Here the dimensions in the image is reduced to the desired dimensions.
        for i = 2:2:tempLength
            for k = 2:2:tempLength
                    if temproi2(i-1,k-1,j) ~= 0 || temproi2(i,k-1,j) ~=0 || temproi2(i-1,k,j) ~= 0 || temproi2(i,k,j) ~= 0
                        is = round(i/scale);
                        ks = round(k/scale);
                        roi(is,ks,j) = 1; %A pixel is of the ROI is set to true if at least one of the neigbours of the original ROI are true.
                    else
                        is = round(i/scale);
                        ks = round(k/scale);
                        roi(is,ks,j) = 0;
                    end

            end

        end
end
end
```

The following script divided a vector into two groups based on a group vector where two num-

bers determined which group the index belonged to.

```
%This function sorts values in a vector into two new vectors according to
%groups defined by the group. The lowest value in group, defines group x.
function [x,y] = makegroups(vector,group)
n = length(vector);
var = min(group);
n1=0; %define the lengths of the vectors.
n2=0;
for i = 1:n
    if group(i) == var
        n1 = n1+1; %count number to be sorted into x
    else
        n2 = n2+1; %number of values to be sorted into y
    end
end
x= zeros(1,n1); %initialise new vectors
y=zeros(1,n2);
x_i=0;
y_i=0;
for i = 1:n %sort values into the correct vectors.
    if group(i) == var
        x_i = x_i+1;
        x(x_i) = vector(i);
    else
        y_i = y_i+1;
        y(y_i) = vector(i);
    end
end
```

Finally, variations of the following script were used to save parameters within a parfor loop, as the parfor loop initially does not allow for this.

```
function parsaveTofts(fname,K_trans_low,K_trans,K_trans_high,K_transes,ve,
    ve_low,ve_high,ves,vp,vp_low,vp_high,vps,rsquare,rsquares,rmse,rmses,time,
    time_whole,Ct_median)

```

```
save(fname,'K_trans_low','K_trans','K_trans_high','K_transes','ve','ve_low','
    ve_high','ves','vp','vp_low','vp_high','vps','rsquare','rsquares','rmse','
    rmses','time','time_whole','Ct_median');
end
```